Changes in Cortical Connectivity and Gene Expression of the Rostral Forelimb Area After Ischemic Infarct in Motor Cortex in the Rat

By

Edward T.R. Urban III

B.F.A Texas Christian University, 1998
B.S. University of Kansas, 2005

Submitted to the graduate degree program in Molecular and Integrative Physiology and the Graduate Faculty of the University of Kansas in partial fulfillment of the requirements for the degree of Doctor of Philosophy.

_____
Randolph J. Nudo, Ph.D., Chairman

_____
Michael W. Wolfe, Ph.D.

_____
Paul D. Cheney, Ph.D.

_____
Peter G. Smith, Ph.D.

_____
Brenda Rongish, Ph.D.

Date Defended: June 11, 2013

The Dissertation Committee for Edward T.R. Urban III
certifies that this is the approved version of the following dissertation:

Changes in Cortical Connectivity and Gene Expression of Rostral Forelimb Area After Ischemic Infarct in Motor Cortex in the Rat

_____
Randolph J. Nudo, Ph.D., Chairman

Date approved: June 11, 2013

Abstract

Stroke is a large and growing problem in the United States. There are 795,000 incidences each year, and most are new incidences. Survivors are left with lasting functional deficits, and therefore stroke is one of the leading causes of adult disability in humans. Some function is regained that was lost to stroke, and this recovery is correlated to physiological reorganization. That is to say, after stroke the brain functions differently. The physiological reorganization may be based on anatomical reorganization. If this is true, the brain acts differently, because it is wired differently after stroke. The anatomical reorganization may be based on expression differences; thus, leading to the conclusion that the brain is wired differently because genes were expressed in different ways after the stroke. The series of studies within this dissertation lead the reader down this train of thought and show evidence for it by using adult rats in a model of ischemic injury to the cortex, and compare the connectivity and gene expression patterns of lesioned brains to non-lesioned brains.

Dedication

I dedicate this to my family.

Acknowledgements

I thank my mentor, committee and lab members. They taught me, assisted me and helped me during this long journey of research. I would also like to thank Billie Byerley for her work with data collection.

Table of contents

List of Abbreviations

Rat Brain Regions

ALBSF	Anterolateral Barrel Subfield of S1
Aud	Auditory Cortex
CFA	Caudal Forelimb Area of the Rat is the primary motor area controlling the forelimb in the rat
CFAOv	Caudal Forelimb Area Overlap Zone with S1
CFAR	Caudal Forelimb Area, Rostral Portion
FIA	Forelimb ICMS Area
FR	Frontal Cortical Areas
FRO	Frontal Cortical Areas Not Otherwise Delineated
ICMSR	S1 Zone Responsive to Intracortical Microstimulation
IN	Insular Area
IZ	Intercalated Zone of S1
IZO	Intercalated Zone of S1 Not Otherwise Delineated
GZ	Granular Zone of S1
GZO	Granular Zone of S1 Not Otherwise Delineated
M1	Primary Motor Area
PirOl	Piriform and Olfactory Cortex
PL	Parietal Lateral Area
PM	Parietal Medial Area
PMBSF	Posteriomedial Barrel Subfield of S1
PR	Parietal Rhinal Cortex
PRH	Peri-rhinal Cortex
PV	Parietal Ventral Area
RFA	Rostral Forelimb Area of the Rat is the non-primary motor area controlling the forelimb in the rat
RS	Retrosplenial Area
S1	Primary Somatosensory Area
S1H	Hand Area of S1
S1HO	Hand Area of S1 Not Otherwise Delineated
S2	Secondary Somatosensory Area
TP	Temporal Posterior Cortex
VIS	Visual Cortex

Primate Motor Regions

M1	Primary Motor Area
PMv	Ventral Premotor Area

Technical Abbreviations

BDA10k	biotinylated dextran amine of 10,000 MW, anterograde tracer.
CTB488	Cholera toxin, beta subunit conjugated to AlexaFluor 488, retrograde tracer
CTB647	Cholera toxin, beta subunit conjugated to AlexaFluor 647, retrograde tracer
DBA	Diaminobenzadine, chromagen
ET-1	Endothelin 1, vasoconstrictor
ICMS	Intracortical Microstimulation, physiological method for defining cortical motor areas
IM	Intramuscular
IP	Intraperitoneal
IPA	Ingenuity Pathway Analysis
IVT	In Vitro Transcription
LCM	Laser Capture Microdissection
NeuN	Neuronal Nuclei
RIN	RNA Integrity Number
RMA	Robust Multi-array Averaging

Chapter 1

Background

Overview

Stroke (or ischemic infarct in animal models) is caused by loss of blood flow to the central nervous system leading to cell death. Once the nervous tissue dies, it does not regenerate, and any function the tissue was responsible for is lost. Stroke happens to around 800,000 Americans a year and leaves a large percentage with lasting deficits. This tragedy is tainted with a glimmer of hope, because some recovery does occur. The major theory behind this recovery, vicariation, is that spared regions can take over for the lost tissue after the infarct. The mechanism behind vicarious take over of function during recovery seems to hinge on anatomical reorganization of neuronal structures. To this end, a model of anatomical reorganization was studied.

Evidence exists that the premotor area is important to recovery of function after primary motor lesion with the primary somatosensory area (S1) hand area as the target of premotor reorganization. The current work adds to this evidence, first by showing neuroanatomical reorganization of the premotor area after infarct of the primary motor area, and second, by elucidating the gene expression changes in the premotor area after infarct of the primary motor area that may be the basis for the neuroanatomical changes.

The current ischemic model involves 3 areas concerned with forearm movement in the rat cortex: primary motor area (CFA, caudal forelimb area), pre-motor area (RFA, rostral forelimb area), and the forelimb region of the primary

somatosensory cortex (S1). Both of the motor areas can activate motor movement though cortical-spinal connections, and are heavily interconnected through corticocortical connections between each other as well as the primary somatosensory area. Corticocortical connections deal with communication between cortical areas. Since integration of sensory and motor information is necessary for motor movement and connections are lost due to infarct, it is reasonable to study these areas. Also in the squirrel monkey, which has similar areas, the premotor ventral area sent novel projections to the S1 hand area, which suggests an attempt to reintegrate itself into a pre-infarct way, as it had lost the normal connections.

Why study stroke?

Each year about 795,000 people experience a new or recurrent stroke. About 600,000 of these are first attacks, and 185,000 are recurrent attacks (Kissela, et al. 2001, NINDS.nih.gov, NHLBI.nih.gov). On average, someone in the United States has a stroke every 40 seconds. Each year, about 55,000 more women than men have a stroke (Kissela, et al. 2001, NINDS.nih.gov, heart.org) and 10% of stroke survivors recover almost completely, 25% recover with minor impairments, 40% experience moderate to severe impairments requiring special care, 10% require care in a nursing home or other long-term care facility, 15% die shortly after the stroke, and 6 million

survivors are living in the United States (stroke.org). It is easy to see that stroke in humans comes at a high cost.

Functional Recovery After Stroke

Some recovery of function happens after stroke but the mechanisms for recovery are still unclear. Some increase in function after stroke may be related to the resolution of an injury state caused by ischemic infarct called diaschisis. The theory instigated in 1914 by von Monakow (Wiesendanger M 2006), states that cortical infarct causes a disturbance in connected regions even some distance from each other. The dysfunction is not related to cell death caused by ischemic injury but an injury state that can resolve, and with its resolution, a return to function. Both contralesional cortex and ipsilesional cortex can be involved in this reaction. Modern techniques have shown these suppositions to be correct in part. Connected regions display hypometabolism that may or may not coincide with hypoperfusion. Using [18F]fluorodeoxyglucose small-animal positron emission tomography for glucose utilization and [14C]iodoantipyrine for cerebral blood flow, adult rats displayed regions of hypoperfusion at 1 day post-infarct but hypometabolism persisted for 8 days. Although the hypoperfusion existed in the infarct core, the hypometabolism was also in areas heavily interconnected to the infarct zone and some areas were later found to be areas of anatomical reorganization (Carmichael ST et al. 2004). Some deficits are

related to brain regions functioning incorrectly during this period of hypometabolism, which is resolved once the metabolism returns to normal. Resolution of diaschisis cannot account for any late gain of function, as it is an acute process.

Two major theories of functional recovery exist. One posits that new neurons are generated and can assume functions lost by ischemic damage. The other asserts that uninjured neurons in parts of the brain that survived assume the functions lost by ischemia. Surviving cortex can be in the same hemisphere as the lesion (ipsilesional) (Brown CE et al. 2009a), either immediately around the lesion (perilesional) (Nishibe M et al. 2010) or far removed from it (distant) (Dancause N et al. 2006b), or it can be on the opposite hemisphere (contralesional) (Zai L et al. 2009). Several models have been developed to study all three locations for expanded function, though the authors study the ipsilesional cortical tissue that is related in function to the lesioned tissue.

Neuron generation, migration and integration was found to exist in mammals. The subventricular zone in adult brain continuously produces new neurons that migrate to the olfactory bulb. After stroke in rat cortex, these new neurons can migrate to the site of injury and differentiate into the kind of neurons that were destroyed in the stroke (Arvidsson A et al. 2002). Though subventricular zone cell proliferation was found in adult humans (Bernier PJ et al. 2000), and increased proliferation after ischemia was maintained in older adults, there were low amounts of neurogenesis (Macas J et al. 2006). Therefore,

although originally thought to be a target for stroke recovery, neurogenesis is not seen as a significant contributor to stroke recovery in humans (Macas J *et al.* 2006). As the ultimate goal of the current line of study is to have some relevance to human stroke, such models, which are more likely to be relevant to humans were studied.

Vicariation is one such model that appears to contribute to stroke recovery in humans and other mammals. In this model, some other part of the brain takes over the function that was lost. Non-invasive imaging studies in humans confirms the reorganization of brain after cortical stroke. In such studies, humans after stroke use different regions of their brain to accomplish tasks than non-injured brains would. Although involvement of the contralateral cortex was also reported, evidence is mounting that greater activation of the ipsilesional cortex is correlated to better motor recovery after stroke (Calautti C and JC Baron 2003). In other words, although the cortex on the uninjured hemisphere is activated differently after stroke, those individuals experiencing better recovery are activating brain regions on the same side as the injury and in a pattern closer to normal activation. Activation of different regions than normal after stroke is the definition of vicariation. Therefore, vicariation may be a worthwhile model of study, and regions on the ipsilesional hemisphere may be the best targets of study.

Reorganization

If regions of the brain take over function from an injured part, how do they accomplish it? Each brain region has its own set of connections that allow for certain tasks to be accomplished. The primary somatosensory cortex receives peripheral sensory information from specialized neurons and interacts with multiple secondary somatosensory regions in interpreting it. The primary motor system receives input from the secondary motor regions and sends signals to periphery through specialized neurons. The information received through the sensory system is used to constantly adjust the movements produced. The network of connections is extensive, and not always redundant. It would be reasonable to think that any region taking up the function of another region would require some form of change in connectivity or reorganization to accomplish the task.

Several animal models of reorganization have been described and may be related to functional recovery. In vivo, voltage sensitive dye can be taken up and observed in firing cortical neurons. After cortical infarct, sensory neurons in the cortex were shown to respond to stimulation of different parts of the body after stroke than they did before injury to an adjacent brain region (Brown CE *et al.* 2009a). Single neurons responding differently before and after ischemic infarct is an example of vicariation through physiological reorganization. It shows that given the right circumstances a neuron can switch its function to a function lost with injury.

The motor cortex is also capable of reorganization. A model of motor cortex reorganization has been described in non-human primates after ischemic infarct. In this model, ischemic infarct destroys the primary motor area and the premotor area ventral (PMv) changes its connectivity pattern (Dancause N *et al.* 2006b). PMv neuronal projections increased to the somatosensory cortex. The PMv does not normally project to the hand area of the primary somatosensory cortex, but M1 does (Dancause N et al. 2006a). The new projection seemed to reintegrate the PMv into circuitry lost by the injury.

There are hints that the same is true for the rat. The rostral forelimb area (RFA), first described by Neafsey and Sievert using intracortical microstimulation (ICMS) (Neafsey EJ and C Sievert 1982), fulfills both requirements for premotor designation used in primates (Dum RP and PL Strick 2002). The RFA was also shown to be important to functional recovery after motor cortex lesion (Conner JM et al. 2005). Further, sensorimotor cortex caudal to the CFA has been shown to be important in behavioral recovery. After bilateral ablation, ventral tegmental stimulation during training and recovery, a novel ICMS area, which could activate forelimb movements appeared caudal to the normal location of CFA (Castro-Alamancos MA and J Borrel 1995). Deficits were reinstated with ablation of the novel area.

Reorganization in the Uninjured Brain

Cortical reorganization does not only occur after lesion, it also occurs in the uninjured state during learning. Uninjured adult owl and squirrel monkeys had increased areal representations of sensory areas related to learning a skilled reach task, with increased sensitivity of digits used in the task itself (i.e. the cutaneous receptive fields of digits became smaller suggesting increased cutaneous acuity) (Xerri C et al. 1998). Also, young Long-Evans rats exposed to enriched environments for 80-115 days experienced increased areal representation of forelimb sensory areas and increased discrimination while a deprived environment had the opposite affect. This effect was the same for adult rats with an immobilized limb, the areal representation shrank with either 7 or 15 days of restriction (Xerri C et al. 1996). Similar dopaminergic projections exist in the primate, and although there are differences in number and location (Gaspar P et al. 1992), they would presumably serve a similar function.

Motor learning and plasticity is dependent on protein synthesis during the learning process. Inhibition of protein synthesis, by intracortical injection of anisomycin, during the learning phase of a skilled reaching task inhibited the learning, but did not block performance once the task was already learned, nor did injection into the cerebellum block learning (Luft 2004). Motor skill learning induces synaptic strengthening and modification in rat M1 horizontal fibers. Horizontal fibers of rat cortical layer II/III in M1 show learning induced synaptic strengthening after 3-5 days of skilled reach training (Rioult-Pedotti MS et al.

1998). This strengthening was later shown more definitively to be due to long term potentiation (LTP) (Rioult-Pedotti M-S et al. 2000).

A similar process seems to be occurring after stroke. Chronic cortical stimulation after sensorimotor lesion increased efficacious axodendritic synapses in the ipsilesional cortex and was correlated with increased functional recovery in moderately impaired rats (Adkins DL et al. 2008). The chronic stimulation mimics the activity of learning, though not as neuron specific as the actual learning process.

Process of Ischemic Damage

Ischemic infarct, as can occur in stroke, progresses from a lack of blood flow to cell death. Lack of blood flow results in oxygen depletion, and depletion of adenosine triphosphate, the cells energy source. Neurons can no longer maintain electrolyte balance without ATP, and cells begin to swell, and malfunction. During ischemia, there is a threshold of blood flow for electrical activity cessation and a lower threshold for ion dysregulation. Cessation of electrical activity is not necessarily linked to cell death, but dysregulation of ion homeostasis is a harbinger of cell death (Astrup J et al. 1981). In baboon neocortex, lowering cerebral blood flow below the higher threshold leads to cessation of EEG activity, while a lowering below the lower threshold leads to an increase in extracellular K+. EEG and K+ levels could be restored to normal

values with the increase of cerebral blood flow to normal levels (Astrup J et al. 1977).

Anoxic depolarizations contribute to the final volume of ischemic lesion within the central nervous system. Anoxic depolarizations occur as the electrolyte imbalance leads to an increase in intracellular calcium and signal transduction. In adult rat hippocampal slices, inhibiting Na/K ATPase with Ouabain, delays anoxic depolarization 2 fold, while increasing osmolarity of extracellular space (to delay swelling) delays anoxic depolarization by 25%. This suggests ATP depletion leads to failure of the NA/K ATPase followed by swelling, which leads to anoxic depolarization (Balestrino M 1995). The authors bring up stretch related channels, but offer no proof of their existence. It is interesting that the swelling itself is related to the depolarizations, because one would think increases in Na would be sufficient to open voltage gated Na channels to initiate depolarization along with intracellular calcium and neurotransmitter release. These depolarizations further injure the neuron, as they use up any remaining ATP, possibly turning a survivable hypoxia into permanent cell damage. NMDA and non-NMDA antagonists can stop this progression, suggesting increased activity is part of the progression (Back T 1998). As depolarizations continue, the ischemic core of cell death expands into the penumbra until it relegates the penumbra to the edge of the ischemic territory.

Reorganization After Injury

The brain does not just die off in response to injury. It is actively changing. Organisms can upregulate various kinds of gene expression that may be helpful or hurtful to their eventual recovery. Cortical infarct in the rat induces an array of gene expression with increases and decreases in both growth promoting and growth inhibiting genes. The peri-infarct region has been studied extensively by the Carmichael lab. The peri-infarct cortex (a region that displays increased neuroanatomical reorganization) has a general decrease in extracellular matrix and increase in growth promoting gene expression after infarct (Carmichael ST et al. 2005). The pattern seems to include a trigger of sprouting consisting of synchronous neuronal activity. By exploiting differences in lesion type, synchronous activity between areas of sprouting was found to be an important trigger for reorganization (Carmichael ST and MF Chesselet 2002). After this synchronous activity was blocked, the reorganization did not occur. Following the trigger phase, there is an initiation and maintenance phase from 7-14 days post-infarct and a return to baseline by 28 days. The pattern of expression is not completely intuitive, as neurocan, as well as known developmental growth inhibitors ephrin-A5, ephB1, semaphorin IIIa, and neuropilin 1 were increased in the same place and during the same time as otherwise growth promoting gene expression.

Intrinsic vs Extrinsic Determinants of Reorganization

Neurons in adult animals have varying ability to instigate axonal reorganization after an injury. The ability to reorganize can be divided into intrinsic (the cells own ability) and extrinsic (the environment in which the cell is located) factors (Rossi F et al. 2007). Some neurons need nothing to regenerate axons after lesion, some can be manipulated to do so if external forces are removed, while still others will not reorganize, regardless of attempts to mitigate external inhibition or increase external instigation on the neuron (Rossi F et al. 1997).

Intrinsic ability difference begins with the most basic of divisions within the nervous system. While most neurons within the peripheral nervous system will undergo some form of reorganization (sometimes of limited extent), only some of the central nervous system neurons will undergo reorganization without overt manipulation (Jones LL et al. 2003). In adult animals, the intrinsic ability of neurons to reorganize axons can depend on the type of the neuron and the distance from the lesion. Cerebrospinal nuclei neurons will respond differently depending on the distance of the spinal cord lesion in adult zebrafish. Some neurons will only reorganize with proximal lesions, while others have an intrinsic difference that allows them to differentially express genes for reorganization with both proximal or distal placement of the lesion. Although the neuronal cell adhesion molecule L1.1 was upregulated in both kinds of neurons when regeneration was successfully launched, those neurons unable to regenerate with a distal lesion were unable to upregulated L1.1 (Becker T et al. 1998).

Development stage also plays a role in intrinsic ability. Embryonic day 16 frontal and occipital lobe cortex transplanted into newborn rat occipital lobe developed thalamic connections appropriate for their site of origin (Frappé I et al. 1999). This suggests specific factors arise in development.

Summary

The series of experiments within this dissertation study the connectivity of the Premotor region in the rat, and the changes it undergoes after ischemic infarct of a connected region of the cortex. First, Chapter 2 describes the connectivity pattern of RFA throughout the cortex of the rat. Second, Chapter 3 describes the changes of connectivity pattern of RFA after infarct of the primary motor cortex. Third, Chapter 4 discusses the gene expression changes in RFA neurons after primary motor cortex, and how they relate to the connectivity changes described in Chapter 3.

Chapter 2

Premotor Connectivity

Abstract

The rostral forelimb area (RFA) in the rat is considered a premotor cortical region based on its prominent efferent connections with the primary motor cortex, also known as the caudal forelimb area (CFA). In the present study, the RFA of adult male Long-Evans rats (n=6) was eletrophysiologically identified using intracortical microstimulation techniques and injected with the tract tracer, biotinylated dextran amine (BDA). The post-mortem cortical tissue was flattened and sectioned tangential to the surface. Somatosensory areas were delineated with the aid of cytochrome oxidase staining. The locations of 100 μm square voxels containing BDA-labeled boutons were projected to the surface, plotted, and tallied across the entire section. BDA-labeled neuronal somata were plotted and counted in a similar manner. Voxel and soma counts were normalized to the area of each region of interest and defined as containing dense, moderate, sparse and negligible connectivity. The results demonstrate that the RFA sends dense to moderate projections to CFA (including the overlap zone with the somatosensory hand area), widespread regions of the frontal cortex medial and lateral to RFA, the second somatosensory area (S2), the parietal ventral area (PV) and the parietal rhinal area (PR), and the intercalated zone of S1. By contrast, projections to the majority of the primary somatosensory cortex are relatively sparse. The distribution of retrogradely-labeled somata roughly paralleled that of labeled boutons, suggesting that connections with cortical

regions are largely reciprocal. Cortical connections of RFA in rat are strikingly similar to cortical connections of the ventral premotor cortex in non-human primates, suggesting that these areas share similar functions.

Introduction

The motor areas of the cerebral cortex of mammals have generally been divided into primary motor cortex and various premotor areas. By definition, premotor areas provide direct input into the primary motor cortex (Dum RP and PL Strick 2002). While several premotor areas have been identified in non-human primates, the status of premotor cortex in rodent species is still unclear. Rodents are used increasingly in studies focused on understanding the cortical control of movement, and the role of premotor areas in recovery after cortical injury. Therefore, it is important to understand the relationship of premotor areas in rodents and primates, and the similarity of their anatomical connectivity with other cortical areas justifies further exploration.

Functionally, the primary motor cortex is thought to be in direct control of motor movements, while the non-primary motor cortex is thought to be involved with higher order processing, which affects motor movement by instructing the primary motor cortex. Numerous interconnections between the two cortices could relay movement selection of the non-primary motor cortex into the primary motor cortex, which activates movement through corticospinal connections and

other descending pathways. In rat, both primary and non-primary cortices have corticospinal connections, which terminate in the intermediate zone and ventral horn of the spinal cord (Rouiller EM et al. 1993). This holds true for non-human primates, as well.

The areal extent of both primary motor and premotor areas can be defined neurophysiologically using low threshold intracortical microstimulation (ICMS). The non-primary motor cortex controlling forelimb movements (rostral forelimb area, RFA) is a well-studied region of the non-primary motor cortex in rats. On the basis of ICMS results, this area is separated from the primary motor area controlling the forelimb (CFA) by a thin strip of cortex where ICMS elicits neck movements.

Although other studies (Neafsey EJ et al. 1986; Li X-G et al. 1990) report possible connections to hind limb movements, this study will focus on the fully documented RFA function. As an entire body representation is not present in the rat non-primary motor area, it is essential to assess the forelimb region of the non-primary motor area. Information regarding the connectivity of the forelimb area is a useful surrogate for the entire non-primary motor area. Therefore, this study will focus on the connectivity of the RFA, in lieu of the entire non-primary motor area.

While there are many similarities in anatomy and physiology, the homology of rat and primate non-primary areas are still debated. Premotor areas in the primate are classically defined as regions of the frontal cortex with

corticospinal projecting neurons that are connected to the primary motor area (Dum RP and PL Strick 2002). The primate's frontal cortex houses the primary motor cortex and at least six premotor regions. The premotor ventral and dorsal areas (PMv and PMd) of the primate have a similar orientation and numerous interconnections with the M1, as RFA does to CFA. The areas combined (premotor, PM) make a logical first choice to compare homology. However, there are up to four other premotor areas of the primate, confusing any homology that could be derived. Further, the isolation of the premotor areas is different. If the Brecht model is used (Brecht M et al. 2004), the non-primary motor area of the rat is fully within M1, while each premotor and motor area is separated by several millimeters in the primate. Also, an area within the rat cortex, termed the sensorimotor overlap, has properties of both the motor and sensory cortex. This sensorimotor overlap does not exist in the primate, as it does in the rat.

Another similarity between the RFA and PMv is the incomplete cortical representation of body movements. A full body representation is difficult to delineate in the non-primary motor cortex. Hind limb, trunk and face representations have been reported to exist within the non-primary motor cortex, and some report corticospinal projections to the lumbar enlargement originating from close proximity to RFA (Li X-G *et al.* 1990), but few studies report eliciting hindlimb movements using ICMS (Neafsey EJ 1990). Also, RFA is surrounded by face, neck and trunk representations confusing the delineation between ICMS responses of these movements belonging to primary and non-primary motor

areas. In this sense, RFA is similar to the PMv of primates, as the hindlimb is also not observed in PMv during ICMS.

Due to this problem of homology, past studies in the rat have sought to define the connectivity of the motor cortices, in particular, with other cortical areas. As a first step in delineating the hierarchy of RFA, Rouiller determined the anterograde and retrograde connectivity of RFA and CFA (Rouiller EM *et al.* 1993). That study identified cortico-cortical projections from RFA to the ipsilateral CFA (all layers), S1, S2, AGm, anterior cingulate (AC) and insular cortex. Based on connectivity alone, those authors could not firmly conclude whether the RFA corresponds to the supplementary motor area (SMA) or premotor (PM) of the primate, though it had aspects of both. They did establish that the cortex controlling the forelimb, described as two regions by Neafsey (Neafsey EJ and C Sievert 1982), was in fact two distinct regions with different connectivity patterns, and that the CFA was akin to M1 of primates, while RFA shared similarities of both the supplementary motor area (SMA) and premotor area (PM).

In some ways the homology between primates and rats is clear. The fact that the RFA lacks sensory input, while CFA neurons respond to sensory stimulation, is consistent with RFA's role as a supplementary motor area (Sievert CF and EJ Neafsey 1986). The comparison is complicated because primate premotor areas each have connectivity patterns that are only partially similar to rat non-primary motor area. In the primate, both SMA and PM connect to the insular cortex (Jurgens U 1984; Matelli M et al. 1986) as does the RFA. This fact

helps separate out the RFA from CFA, but does not distinguish its homology to either.

While the basic connectivity of RFA has been described in a qualitative way, tract-tracing studies are quite scarce, and many more details are needed to resolve RFA's connectivity relationship with primate premotor cortex. For example, in the Rouiller study, the injection placement within the RFA was centered around stereotaxic coordinates and one ICMS site (Rouiller EM *et al.* 1993). While stereotaxic coordinates are valid for general placement, they cannot be precisely located within the RFA. This leaves some question as to how much of the RFA was labeled and how much tract tracer could have expanded into other cortical areas. Also, the injections of anterograde tracers themselves were variable and relatively large (3 μL per site for dextran amine), and thus, the tracer may have leaked beyond the confines of the RFA. Lastly, although the laminar distribution of connectivity to/from RFA was described in detail, coronal sectioning does not afford the same description of the topographic relationships of terminal fields as tangential sectioning allows. The current study employed ICMS, small injections (100 nL of biotinylated dextran amine, BDA), and tangential sectioning to understand the anterograde and retrograde connectivity of a limited cortical volume within RFA.

The result of the current study provides a description of the terminal fields of connectivity. Using tangential sectioning and a specific injection of small volumes of tracer within the physiologically defined borders of RFA, we confirm

that the ipsilateral corticocortical connectivity of RFA is not diffuse throughout the cortex, but has clusters of connectivity with a preference for motor regions and higher order processing areas. Further, by using the semiquantitative approach, we were able to rank order the density of connections, providing further documentation of the corticocortical hierarchy. Connections suggest important roles for these areas in the normal function of movement coordination of the forelimb. Although previous studies are largely consistent with our findings, we add the description of the connectivity to the parietal medial (PM), parietal lateral (PL) and accessory areas in the caudal (CAS) brain. The RFA sends few projections to the primary somatosensory area or areas associated with the special senses of taste, vision or hearing. The retrograde labeling follows this pattern, and hints that reciprocal connectivity may be important in the function of the RFA.

Materials and Methods

Male Long-Evans hooded rats (n=8; 370-450 g; 3-5 months of age Harlan, Indianapolis, IN) were singly-housed with a 12 hr:12 hr light:dark cycle. Food and water were provided *ad libitum*. The Institutional Animal Care and Use Committee of the University of Kansas Medical Center approved all animal use.

Surgical Procedure

Isoflurane sedation was followed by ketamine [100-80 mg/kg, intramuscularly (IM)] and xylazine [30 mg/kg, intraperitoneal (IP)] anesthesia. Supplemental doses of ketamine (20 mg/kg IM) were provided throughout the procedure as needed to maintain stable anesthetic depth. After the rat was secured in a stereotaxic frame, Bupivacaine (2.5 mg, local anesthetic) was applied to the scalp. A homeothermic blanket system maintained physiological body temperature. The scalp was incised and reflected, and muscles attached to the temporal and occipital ridges were released. The cisterna magna was opened to relieve cerebrospinal fluid, and a craniotomy performed from +5 anterior to and -4 mm posterior to Bregma, and from +1 mm lateral to the midline to the temporal ridge. The dura was reflected and warm sterile silicone oil applied to the cortex.

Motor areas were identified by intracortical microstimulation methods (Urban ET, 3rd et al. 2012). Briefly, a digital photomicrograph of the cortical surface vasculature was taken through the surgical microscope and overlaid with a grid pattern (250 μm) in image software (Canvas, Deneba Software, Miami, FL). A tapered and beveled glass electrode (20 μm outside diameter) filled with concentrated saline solution (3.5 M), was inserted 1725 μm below the cortical surface at every other grid intersection to give a resolution of 500 μm. A stimulation pulse train (40 msec duration) of 13 monophasic cathodal pulses (200 μsec duration, 350 Hz) was delivered each second from an electrically isolated,

charge-balanced, constant-current stimulation circuit (BSI-2, Bak Electronics Inc, Mount Airy, MD). The current was increased from 0 μA until a movement was visible, then reduced until the movement was no longer visible. Stimulation of "nonresponsive" sites did not elicit movements at the maximum current level of 80μA.

The size and shape of the electrically excitable and ICMS identifiable cortex, the RFA and FIA (CFA of others), are consistent with previous reports from this lab and others (Neafsey EJ and C Sievert 1982; Nishibe M *et al.* 2010). RFA was located between +3.7 and +2.7 mm anterior to Bregma and 2 to 4 mm lateral of the sagittal suture (Fig. 1A). FIA was located between +2.7 anterior and -1 mm posterior to Bregma and 2 to 4.5 mm lateral of the sagittal suture. The name of CFA was changed to FIA (Forelimb ICMS Area), because this ICMS responsive region overlapped the caudal part of IZ, which is outside the classically defined sensorimotor overlap zone, and the new name is reflective of that.

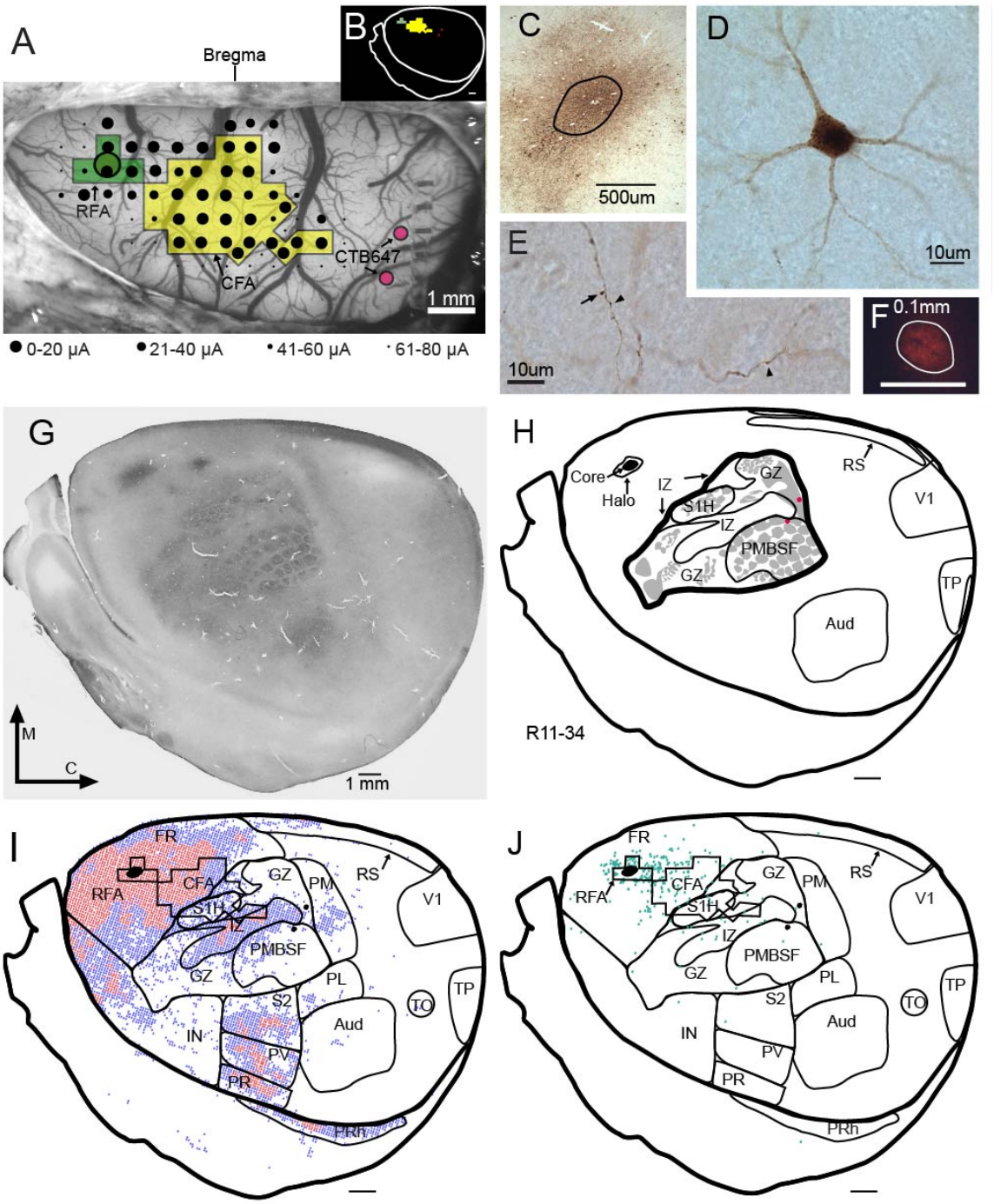
A
Bregma
B
RFA
CFA
CTB647
1 mm
0-20 µA
21-40 µA
41-60 µA
61-80 µA
C
500um
D
10um
E
10um
F
0.1mm
G
M
C
1 mm
H
Core
Halo
IZ
GZ
S1H
PMBSF
RS
V1
TP
Aud
R11-34
I
FR
RFA
CFA
GZ
PM
RS
V1
S1H
IZ
PMBSF
PL
S2
TO
TP
Aud
IN
PV
PR
PRh
J
FR
RFA
CFA
GZ
PM
RS
V1
S1H
IZ
PMBSF
PL
S2
TO
TP
Aud
IN
PV
PR
PRh

Fig. 1 Experimental overview, section alignment and voxel distribution of case R11-34. **A**. Location and border of RFA (green) and FIA (yellow) for rat R11-34. Photomicrograph of the cortex surface vasculature after craniotomy was taken through surgical microscope. A 250 μm grid was overlaid (removed for clarity), and stimulating electrode lowered to 1725μm sub-pial depth at every other grid intersection. Stimulation was increased from 0 to 80 μA until movement was elicited, and then decreased until movement was no longer visible (threshold). Black dots indicate site of stimulation while size is inverse to the threshold in 20 μA steps (largest is 0-20 μA, second largest is 21-40 μA, second smallest is 41-60 μA, and smallest is 61-80 μA). Anterograde tracer, biotinylated dextran amine with 10,000 molecular weight (BDA10kDa, black circle) was injected within RFA's center. Fiducial marker, cholera toxin B subunit conjugated to AlexaFluor 647 (CTB647, red dots) was injected 1mm caudal to the caudal extent of the CFA in two spots. Bregma (vertical line) is indicated. Scale bar is 1 mm, and is the same for B and G-J. **B**. Areas of pane A are overlaid on section outline (white line) of flattened cortex to show position. **C**. On the flattened cortex, the BDA10kDa injection core (black line) was drawn around the area of dark speckling with little identifiable cellular structure. Larger area of dark color is abundance of stained axons immediately around core. Scale bar is 500 μm. **D**. BDA10kDa is predominantly an anterograde tracer, retrogradely labeled neuronal somata (brown) are present. Scale bar is 10 μm. **E**. Axons labeled with BDA10kDa appear as lines with boutons (arrow heads). A bouton is a dark, round object about twice as big as the thin fiber on either side of it, or at the end of a thin projection off the main axon (arrow). Scale bar is 10 μm. **G**. Sensory cortex appears as dark cytochrome oxidase (CO) rich areas. Arrows point in medial (M) and caudal (C) directions, (directions same for all panes). **H**. Section in G is shown here with CO-rich areas outlined and identified. The granular zone of S1 (light grey areas) is further divided into S1H, GZ, and PMBSF. CTB647 (red dots) and BDA10kDa (black dot). **I**. Outline from H is overlaid with voxel counts. A 100 μm square grid was overlaid on the flattened cortex with a computerized microscope and stereology software (StereoInvestigator). Boutons were counted and recorded semi-quantitatively within each grid, or voxel: voxels of 2-30 boutons are shown as blue dots, and voxels of >30 boutons are shown as red dots. The cluster of voxels aided in the identification of PM, PL, PM, S2, PV, PR, and PRh. CTB647 (red dots) and BDA10kDa (black dot) served as fiducial markers to align CO sections with those used to count boutons. **J**. Same section as in I. Retrogradely labeled neurons (green dots) were overlaid on the section outline.

After defining the borders of RFA, a micropipette containing the neuronal tract tracer, biotinylated dextran amine, 10,000 MW (BDA10kDa, 10% w/v in 0.9% sterile saline) was placed at approximately the center of RFA. The injection needle included a tapered glass micropipette cut to 60μm outside diameter and was attached with beeswax to a 1μL Hamilton syringe (30100, Hamilton Company, Reno, NV). It was actuated by a microinjector (Micro4, World Precision Instruments, Sarasota, FL). Injection depth was controlled by a hydraulic Microdrive (650 Micropositioner, David Kopf Instruments, Tujunga, CA) on a stereotaxic arm. BDA10kDa was pressure injected in 3 boluses of 33.3nL (100nL total) at 1500, 1250 and 1000μm below the cortical surface, and CTB-647 injections were delivered in 2 boluses of 75nL (150nL total) at 1500 and 1000μm below the cortical surface. The fiducial marker cholera toxin beta subunit conjugated to AlexaFluor 647 (CTB647, 5 μg/μL in 0.9% sterile saline, C34778, Invitrogen, Grand Island, NY) was injected (with the same configuration and outside diameter as BDA10kDa) at 2 sites that were each roughly 1mm caudal to the caudal border of FIA as defined by ICMS.

The cortical surface was rinsed with warm sterile saline (0.9%) and covered with a silicone sheet (Invotec International Inc, Jacksonville, FL), gel foam, (Surgifoam, Ethicon, Sommerville NJ) and dental acrylic and resin (Lang Dental Mfg Co Inc, Wheeling, IL) to form a protective cap over the craniotomy. The skin was sutured, penicillin injected (45,000 U, SQ) into the nape of the neck and local anesthetic (Bupivicaine, 2.5mg, APP Pharmaceuticals, Schaumburg,

IL) and topical antibiotic (Vetropolylycine gel, Dechra Veterinary Products, OP, KS) applied. Buprenorphine (0.05 mg/kg SQ, Reckitt Benckiser Pharmaceuticals Inc, Richmond, VA) and acetaminophen (40 mg/kg oral) were given after the surgery for pain management. The rat was allowed to recover on the heating pad until it was alert and moving spontaneously, and then returned to its home cage. Three additional doses of buprenorphine and acetaminophen were given during the subsequent 48 hours.

Histology

Tissue Harvest

Seven days after the surgical procedure, rats were sedated with isoflurane, and euthanized with Beuthenasia-D (390mg pentobarbital, 50mg phenytoin sodium IP, Shering Plough Animal Health, Union, NJ). After rib cage reflection, heparin sodium (500 USP Units, Hospira Inc, IL) was injected into the left ventricle, and exsanguination was achieved through transcardial perfusion of saline solution [0.9% saline in distilled water, heparin sodium (1,000 USP Units, APP Pharmaceuticals, Schaumburg, IL) and lidocaine HCl (20 mg, APP Pharmaceuticals, Lake Forest, IL)] followed by 3% paraformaldehyde in 0.9% saline. The brain was extracted, both hemispheres of cortex were separated from the underlying structures, and flattened between glass slides. The flattened cortices were exposed to 4% paraformaldehyde-20% glycerol in 0.9% saline (2

hr), 20% glycerol-2% dimethylsulfoxide in 0.9% saline (overnight), and 20% glycerol in 0.9% saline (24 hr). Each flattened cortex was sectioned at 50 μm thickness on a freezing microtome chilled with dry ice. Individual sections were placed in 0.1 M PBS solution and kept at 4°C.

Cytochrome Oxidase Staining

Sections were placed in 0.1 M PBS solution and allowed to float. Then, sections were inspected with the unaided eye for the S1 representation, which is visible as several slightly opaque white areas within the translucent section. Sections with the most complete representations (3 to 4 sections/cortex) were chosen for cytochrome oxidase (CO) staining. After rinsing (2 x 10 min in 0.1 M PBS), floating sections were reacted with CO solution at 37°C containing cytochrome c oxidase (20 mg, Sigma, #C2506-500MG), sucrose (4 g, Fisher Scientific), and DAB (50 mg) per 100 mL of 0.1 M phosphate buffered distilled water (pH 7.4). Sections were allowed to react for ~2-3 hr until dark CO-rich areas were easily detectable against the lighter background. The sections were then rinsed (2 x 10 min) in 0.1 M PBS.

BDA10kDa Visualization

All sections underwent a standard staining procedure using Avidin-Biotin Complex (ABC) linked to peroxidase with 3,3' Diaminobenzidine (DAB, MP Biomedicals, Solon, OH, #980681) reaction product as the chromogen. Sections

were rinsed in 0.1 M PBS (2 x 10 min with agitation), then exposed to 0.4% Triton X-100 (Sigma, #X100-500ML) in 0.05 M PBS (1 hr with agitation). Sections were rinsed in 0.1 M PBS (3 x 10 min, with agitation). Sections were incubated overnight in 0.1 M PBS with reagents "A" and "B" added according to Vectastain Elite Kit (Vector Laboratories, Burlingame, CA, #PK6100). Then, sections were rinsed (4 x 10 min, 0.1 M PBS), and exposed to DAB solution (0.05% w/v DAB and 0.01% v/v H_2O_2 in 0.1 M PBS). Sections were wet mounted in 0.05 M PBS onto subbed slides and allowed to dry overnight.

BDA10kDa Signal Intensification

Sections on slides were dehydrated in ascending alcohol concentrations (50%, 70%, 95% and 100% for 5 min each), cleared with xylene (5 min), then rehydrated by reverse order of alcohol concentrations. Sections were exposed to 1.42% silver nitrate in distilled water (55°C, 1 hr), rinsed (15 min, distilled water), exposed to 0.2% gold chloride (10 min), rinsed (15 min, distilled water), exposed to sodium thiosulfate (5 min), and rinsed (15 min, distilled water). Finally, sections were dehydrated again, as described above, cleared in xylene, and coverslipped with DPX mounting medium (Sigma, #44581-500ML).

Bouton and Neuronal Soma Quantification

Section outlines were traced with the aid of a computerized microscope (Axiophot 2, Zeiss) and stereology program (Stereoinvestigator, Microbrightfield). A 100 μm square grid was overlaid on the flattened cortical outline. As the section thickness was 50 μm, voxels with dimensions 100 x 100 x 50 μm were examined systematically throughout the section. Voxels containing BDA-labeled boutons were coded as either "Red" ($\geq$ 30 boutons per voxel) or "Blue" (2-29 boutons per voxel).

Axons labeled with BDA10kDa appear as dark lines with varicosities or boutons (Fig. 1E). A bouton was defined as a dark (chromogen dense), round object about twice as wide as the thin dark fiber on either side of it (en passant bouton), or at the end of a thin projection off the main axon (terminal bouton). Boutons were counted and recorded semi-quantitatively within each 100 μm x 100 μm x 50 μm (section thickness) voxel. Voxels containing 2-30 boutons were marked with a blue dot (Fig. 1I), and voxel containing greater than 30 boutons were marked with a red dot (Fig. 1I).

Although BDA10kDa is an effective anterograde tract tracer, retrograde labeling occurs as well. BDA-labeled somata were plotted and counted on the same section as boutons. A neuronal soma was taken as a confluently dark, smooth-edged shape with evidence of at least one thin projection emanating out of it (Dancause N *et al.* 2006b) (Fig 1D). These BDA-labeled somata were marked with a green dot (Fig 1J).

Within a given region, the density of boutons was greatest in deeper cortical laminae and least in superficial laminae. However, the distribution of BDA-labeled boutons and somata was similar throughout cortical depths, similar to descriptions in previous connectivity studies in rat (Reep RL et al. 1987; Rouiller EM *et al.* 1993). The current experiment uses a superficial layer section in order to more easily delineate between regions of interest, as deep layers have a larger more diffuse projection pattern. Thus, although variations in overall density exist from superficial to deep laminae, it was deemed that a single section was representative of a particular animal's connectivity patterns. Due to the extensive amount of time required to plot BDA-labeling in each section, this was the most feasible approach to describing consistent connectivity patterns in the sample of rats.

Alignment Procedure

Fiducial markers were used to align the ICMS map from the surgical procedure with the section outlines, voxel counts, neuronal soma counts, and CO-rich zones drawn in StereoInvestigator. The location of 2 injections of CTB647 and 1 injection of BDA10kDa injection cores were marked on all ICMS maps and section outlines. Section outlines and ICMS maps were overlaid in Photoshop, and the ICMS map was scaled and rotated until the 3 injection cores were in register. Numerous symbols used to designate voxels (red and blue

dots) were present in the region of RFA and FIA. Careful attention was paid to the relationship of the borders of RFA and FIA to the symbols, which helped maintain correct proportion while transferring the RFA and FIA outlines into StereoInvestigator.

Calculation of Cortical Surface Area for each Region of Interest

The areal representations of the regions of interest (as determined by alignment of CO stained sections, ICMS maps and voxel clusters) were outlined in StereoInvestigator, and imported into a graphics software program (Illustrator, Adobe). The area (mm^2) of each region was then measured with another software program (Image J, NIH).

Statistical Analysis

Both voxel counts and soma counts were normalized to the surface area of the region of interest. These values (voxels/mm^2, somata/mm^2) were examined using a statistical program (JMP v10, SAS Institute). Since the variance in the different regions was determined to be unequal (O'Brien test, $F = 4.34$; $p < 0.0001$), a nonparametric analysis, Wilcoxon Rank-Sum test, was used to compare values in the different regions. Z-scores generated by the Wilcoxon test

were then used to define cutoff levels for dense, moderate, sparse and negligible connectivity.

Region Nomenclature and Identification

The nomenclature, location and description of the regions of interest utilized in this study are derived from various sources in order to achieve the most accurate and reliable description. Regions were identified using a variety of criteria including, response to ICMS, CO staining, obvious clustering of voxels, or spatial relationship to other regions, and are consistent with previously reported nomenclature. If regions were indistinguishable using the methods of the current study, they were pooled together.

Regions Identified as Cytochrome Oxidase Dense Zones

Cytochrome oxidase staining reveals dark zones within granular cortex of flattened sections (Fig. 1H or G). These CO-rich zones were useful in identifying the S1, VIS, RS, TP and Aud cortex. CO dense zones are widely accepted as the histological representation of the sensory cortex (Li H and MC Crair 2011). S1 is positioned in the middle of the flattened cortex with the ratunculus (body representation of the rat) in upside-down orientation facing rostral. The hindlimb representation is furthest medial, while the head, upper lip, and barrel field

representations are furthest lateral. The trunk area comprises the caudo-medial border, while the caudal end of the PMBSF comprises the caudal-lateral border. S1 is wider at its caudal than at its rostral aspect. It is consistent with Remple (Remple MS et al. 2003) Chapin and Lin (Chapin JK and C-S Lin 1984), and incorporates the IZ of Krubitzer (Krubitzer L et al. 2011).

VIS and TP are CO-dense regions coursing from the caudal edge of the cortex in a wide triangular shape. Both regions are thinnest at the rostral vertex. VIS is consistent with the Oc1M and Oc1B of Zilles (Zilles KJ 1985) pooled together. TP is the smaller triangular region directly lateral to and separated from VIS by a CO-sparse strip of cortex, consistent with Krubitzer (Krubitzer L *et al.* 2011). Aud is a large circular CO-dense region lateral and caudal to the S1. Our Aud is consistent with Aud of Remple (Remple MS *et al.* 2003), and the 5 auditory fields of Polley (Polley DB et al. 2007).

RS contains both a thin CO-dense region coursing along the medial edge of the caudal half of the flattened cortex (Harley CA and CH Bielajew 1992). The rostral aspect of RS stops at the caudal border of Fr; the lateral border is concurrent with the CAS, the caudal aspect ends 1-2 mm from VIS, and the medial border extends to the medial border of the cortex.

Regions Identified by Topographic Relationships to Other Identified Regions

After aligning CO-rich section tracings, voxel and neuronal maps, some regions were identifiable by their spatial relationship to other regions. Fr and IN were largely identified by their relationship to S1. S1 is useful because it is large, easily identifiable and shares large sections of borders with Fr to the rostral edge, and IN on the lateral edge. Fr occupies the rostral half of the medial cortex as well as the frontal pole, it borders S1 along its lateral caudal aspect. Fr, and IN cortex follow Zilles (Zilles KJ 1985) with some modification. All of the Frontal regions (Fr1, Fr2, and Fr3, and Cingulate cortex) were pooled into one region. Fr. Zilles' Insular cortex AID and AIV were pooled with the rostral half of Vi to form our IN. IN occupies the lateral aspect of the cortex and is bordered by Fr and S1 at its medial aspect, shares its caudal border with S2, PV and PR, and the rhinal fissure laterally. According to the Zilles terminology, the caudal half of Vi is our PV, and AIP is our PR. The border between IN and FR was drawn from the mediorostral edge of S1 to a small consistent area of dense axons and boutons in the rostral pole. The area has not previously been identified in connectivity experiments, and its identity is unknown.

A large portion of the caudal cortex is named CAS, which borders FRO, PM, PL, Aud, PV, and PR on the rostral edge, the rhinal fissure on the lateral edge, TP and VIS on the caudal edge, and RS at the medial edge. Because this cortex in the caudal half of the flattened cortex has neither dense CO staining (i.e., VIS) or readily identifiable clusters of voxels (i.e., S2), the CAS is a catchall term for the areas in the occipital and temporal lobes that have indeterminate

borders with the current methods. The name was chosen to reflect the nature of the association areas that make up the CAS: Oc2MM, Oc2ML, Oc2L, Te2, and Te3.

The piriform and olefactory bulb were not removed during sectioning and were included in the analysis for completeness sake. There is no connectivity to these areas, so the areas lateral to the rhinal fissure along its entire length are pooled together as PirOl, excluding the PRh.

Results

Of the eight animals that underwent surgical procedures, six were used for quantification. One animal died at the end of the surgical procedure. In another animal, the CO staining procedure failed to reveal the S1 representation.

In each of the six animals used for analysis, BDA-labeling of boutons and neuronal somata was clearly visible in various regions of the cortex. In the sections that follow, first the regions of interest are defined. Then, the relationship of the size of the BDA injection core to the physiologically defined RFA borders is described. Finally, the analysis of the relative density of BDA-labeled boutons (voxels) and neuronal somata is described.

Regions Based on ICMS Responsiveness and CO Histology

The regions of ICMS and CO staining were located as described in the Materials and Methods section above. Region location was in agreement with other published reports.

Regions Identified by Clustering of BDA-Labeling

Discrete clusters of voxels on section outlines led to the identification of some areas. Our S2, PV, PM, PR and PL are in accordance with Remple (Remple MS *et al.* 2003), and Fabri and Burton (Fabri M and H Burton 1991). Like Fabri and Burton, discrete dense clusters of connectivity were identifiable lateral to the S1, which spanned the caudal half of ALBSF and rostral half of PMBSF. Proceeding from medial to lateral, respectively, S2, PV and PR occupy the cortex lateral to S1, medial to the rhinal fissure, rostral to Aud and caudal to IN. These three areas are strips of cortex which generally share the same dimensions, 1-3 mm in the mediolateral and 2-3 mm in the rostrocaudal directions. The extent of the regions was determined by the largest extent of the cluster of voxels.

PM and PL were identified by small clusters of voxels, which were located caudal to and caudolateral to S1, respectively. PM shares the caudal border with S1 and is the width of the bouton clusters it surrounds, (~1.2 mm anterior-posterior). PL shares a border with PM and S1 medially, S2 rostrally, Aud laterally and ends caudally the same level as PM. This distribution pattern is

similar to those reported in other published reports (Fabri M and H Burton 1991; Reep RL and JV Corwin 2009).

The TO is an area that has a small cluster of sparse voxels between or within one or both of the Oc2L and Te2 of Zilles (Zilles KJ 1985). The TO has not been reported previously to our knowledge and is drawn as a circle of 1mm diameter, which is centered between TP and Aud with the medial tip of TO circle in a line with the medial tip of TP.

Regions of Physiological Overlap

Some regions were identified through the overlapping of ICMS regions with histological regions. These overlapping sections were treated as separate regions to avoid confusion in nomenclature and double-counting voxels during analysis. Also, in an effort to capture any connectivity differences in closely adjacent regions that might have existed because of the nature of the cortex overlap (sensory, motor, or sensorimotor overlap), closely adjacent regions were distinguished with different names. In the case of IZ, pieces of the rostral part of IZ were included in the overlap zone of CFAR, so non-overlapping IZ was renamed IZO (Fig 2). As the physiologically defined FIA was found to overlap the histologically defined IZ, S1H and GZ, additional terminology is introduced here: The cortex was overlapped by FIA and the rostral portion of IZ is included in CFAR along with the FIA, which was overlapped with FR. The cortex, which was

overlapped with FIA and S1H or GZ, became CFAOv, while non-overlapped S1H became S1HO and non-overlapped GZ became GZO. The cortex overlapped by FIA and the caudal portion of IZ is the ICMSR, while non-overlapped IZ is IZO. The issue of FIA overlap is further discussed below (see Discussion).

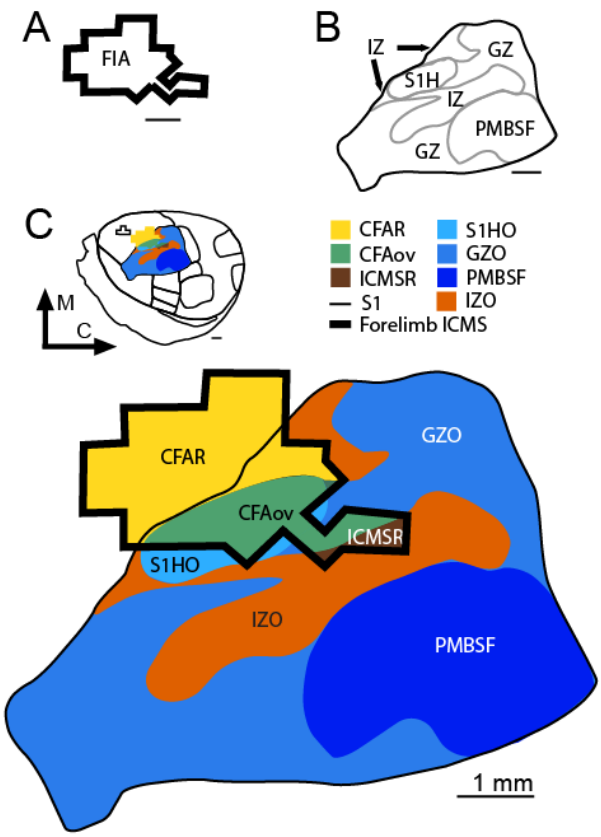
A
FIA
B
IZ
GZ
S1H
IZ
PMBSF
GZ
C
M
C
CFAR
CFAov
ICMSR
S1
Forelimb ICMS
S1HO
GZO
PMBSF
IZO
CFAR
GZO
CFAov
ICMSR
S1HO
IZO
PMBSF
1 mm

Fig. 2 Section outline from Fig.1H, overlaid with the subdivisions of FIA and S1 overlap to give overview of position of regions of interest. The FIA (**A**, thick line), based on its overlap with S1 (**B**, black line) and its subdivisions (grey lines, GZ, S1H, IZ and PMBSF), was subdivided (**C**) into CFAR (yellow), CFAOv (green) and ICMSR (brown). CFAR includes the FIA outside of S1 and the intersection between the FIA and the rostral parts of IZ, which have a larger cortical layer V than the caudal parts. CFAOv includes the overlap between FIA and S1H and some of GZ. ICMSR includes the overlap between FIA and the caudal parts of IZ, which are more dysgranular in nature, but without the motor-cortex-like layer V of the rostral half. PMBSF (dark blue) stays the same throughout. The parts of S1H, GZ and IZ that were not otherwise delineated by FIA overlap were renamed S1HO (light blue), GZO (medium blue), and IZO (Orange), respectively, to reflect this new stature. Arrows point in medial (M) and caudal (C) directions, and scale bar is 1 mm (same for **A**-**C**).

The last naming convention relates to subregional nomenclature. Larger regions were also given the extra designation of “O” for “not otherwise delineated.” In the case of FR, RFA resides fully within the borders of FR. RFA and CFAR became separate regions, while FR became FRO.

Although size and location of FIA was fairly consistent, each FIA did have variability when overlapped with S1 to create CFAR, CFAOv and ICMSR. While the more frequently reported sensorimotor overlap (our CFAR and CFAOv) are in all six animals (Fig. 3A and D), the new designation of ICMSR exists in four out of six animals (Fig. 3B, C, E, and F). The CFAR, which exists in the rostral half of FIA, forms a rostrolateral border with S1 at the hand and wrist representation, extends rostrally 2 mm from the S1 border, and is up to 2mm mediolateral. The CFAOv exists in the middle of or the caudal half of FIA. CFAOv covers the S1H in all animals, and some parts of the wrist and forearm representation in others. It runs in an oblique angle along the rostral aspect of S1, and is up to 2mm wide and 3mm long. The ICMSR, when present, is a thin strip of caudal FIA that overlaps exclusively with the caudal sections of IZ, also called the DZ by Chapin and Lin (Chapin JK and C-S Lin 1984). The ICMSR region extends up to 1.5 mm in an anteroposterior direction and up to 1 mm in a mediolateral direction and can encompass one to four ICMS stimulation sites.

Specificity of BDA Injections

In the flattened, tangentially-sectioned cortex, the BDA injection core was defined as the area of dark, uniformly-speckled staining with little identifiable cellular structure. The halo was identified as a larger area of dark staining extending beyond the core at low magnification; however, at higher magnification, it contains a large number of labeled axons immediately around the injection core (Fig. 1C). After visual inspection of the sectioned tissue, sections 8-24 were determined to be consistently intact among all animals and were used for further analysis. Every other section (nine sections per animal) was used for determining BDA injection core size. Both BDA and CTB647 (Fig. 1F) injection cores were outlined on sections. The section outlines and the ICMS maps were aligned using these cores as fiducial markers. The BDA injection core from each of the nine sections was within the borders of RFA as defined by ICMS (Fig. 4).

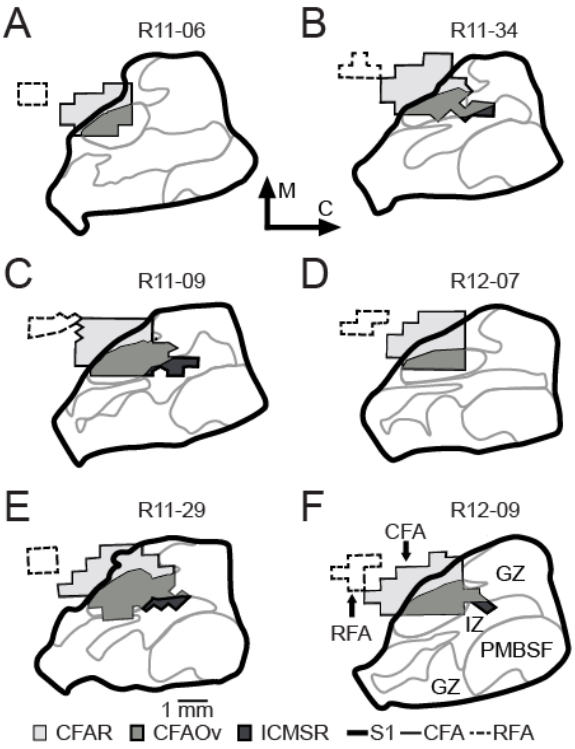
A
R11-06
B
R11-34
M
C
C
R11-09
D
R12-07
E
R11-29
F
R12-09
CFA
GZ
RFA
IZ
PMBSF
GZ
1 mm
CFAR
CFAOv
ICMSR
S1
CFA
RFA

Fig. 3 Overlap of specific cases. **A-F.** The animal identifier is immediately above its outline. RFA (dotted line) is rostral. Although size and location of FIA is fairly consistent, each FIA (thin line) overlaps with S1 (thick line) to create CFAR (light grey), CFAOv (medium grey) and ICMSR (dark grey) do have variability in shape. Arrows point in medial (M) and caudal (C) directions, and scale bar is 1 mm (same for all panes). **F**. RFA and RIA are labeled, as well as GZ, IZ, and PMBSF within their respective grey lines (same for **A-F**).

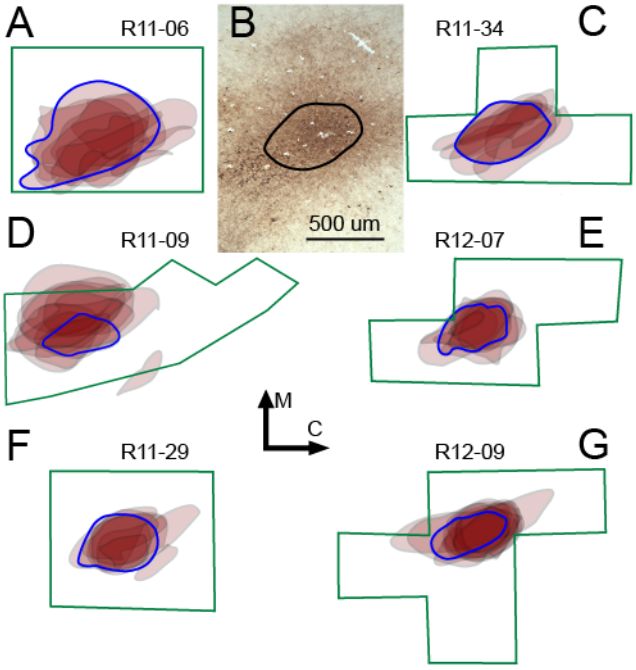
A
R11-06
B
R11-34
C
500 um
D
R11-09
R12-07
E
M
C
F
R11-29
R12-09
G

Fig. 4 A, C-G. In order to show that connectivity is specific to RFA, BDA10kDa injection cores from all nine sections (pink with grey outline) from each animal were outlined and aligned with each other and the ICMS map from that animal. Each RFA (green line, as determined by ICMS) encompasses the injection core with little spread past its borders. The injection core outline from the section used for bouton counting is outlined in blue. The animal identifier is immediately above its outline. **B**. The BDA10kDa injection core (black line) was identified as the diaminobenzadine (DAB) dense, pixelated area with little neuronal morphology visible. The area outside of the injection core has abundant labeled axonal projections and appears dark. Arrows point in medial (M) and caudal (C) directions, and scale bar is 0.5 mm (same for **A-G**).

Qualitative Description of Anterograde Corticocortical Connectivity

The connections of two animals R11-29 (Fig. 5A-B), which had the least total voxels with labeled boutons (4,129), and R11-09 (Fig. 5C-D), which had the most total voxels with labeled boutons (5,513), are displayed in Fig. 5. The regions of interest outlines (grey lines) are surrounded by the section outline (thick black lines). Regardless of differences in total number, the relative connectivity is similar between the two animals. FRO, RFA, CFAR, and CFAOv are almost confluent with both red (≥ 30 boutons/voxel) and blue (< 30 boutons/voxel) voxels with the frontal pole receiving mostly red voxels. GZO, S1HO and PMBSF) has small amounts of dispersed voxels throughout. Voxels present within the granular S1 are confined to the rostral border centered around CFAOv. The dysgranular cortex of IZ, is almost confluent with both red and blue voxels. The IN has many voxels in the rostral half of the region but has only a few scattered voxels in the lateral and caudal half. S2, PV, and PR have a dense cluster of both red and blue voxels within the center of each region, wherein the center of each of the clusters is made up of a group of red voxels. PM has a cluster of mostly blue voxels in the center of the mediolateral and rostrocaudal axis, although the center of the cluster of voxels is red. PL has a cluster of voxels in the rostral edge of the region, which may or may not have red voxels in the center. PRh has many blue and red voxels along the entire length of the region; the red voxels may or may not be in the center of the region. TO is a

region drawn between Aud and TP centered around a variably small cluster of blue voxels. Aud, PirOl, VIS, TP, CAS and RS have few dispersed blue voxels within the regions.

In the current study, the caudal half of the IZ was coextensive with an area of confluent voxels within the center of S1. The rest of S1 had few connections to RFA, as denoted by few voxels in the areas of GZO, PMBSF and S1HO. Before the aligning procedure, it was easy to guess where the CO-rich regions of S1H, PMBSF and GZ would rest after alignment by looking at the voxel section. The zones with no voxels formed a negative image for the GZ, S1H and PMBSF to fit into. This pattern holds true in all rats tested.

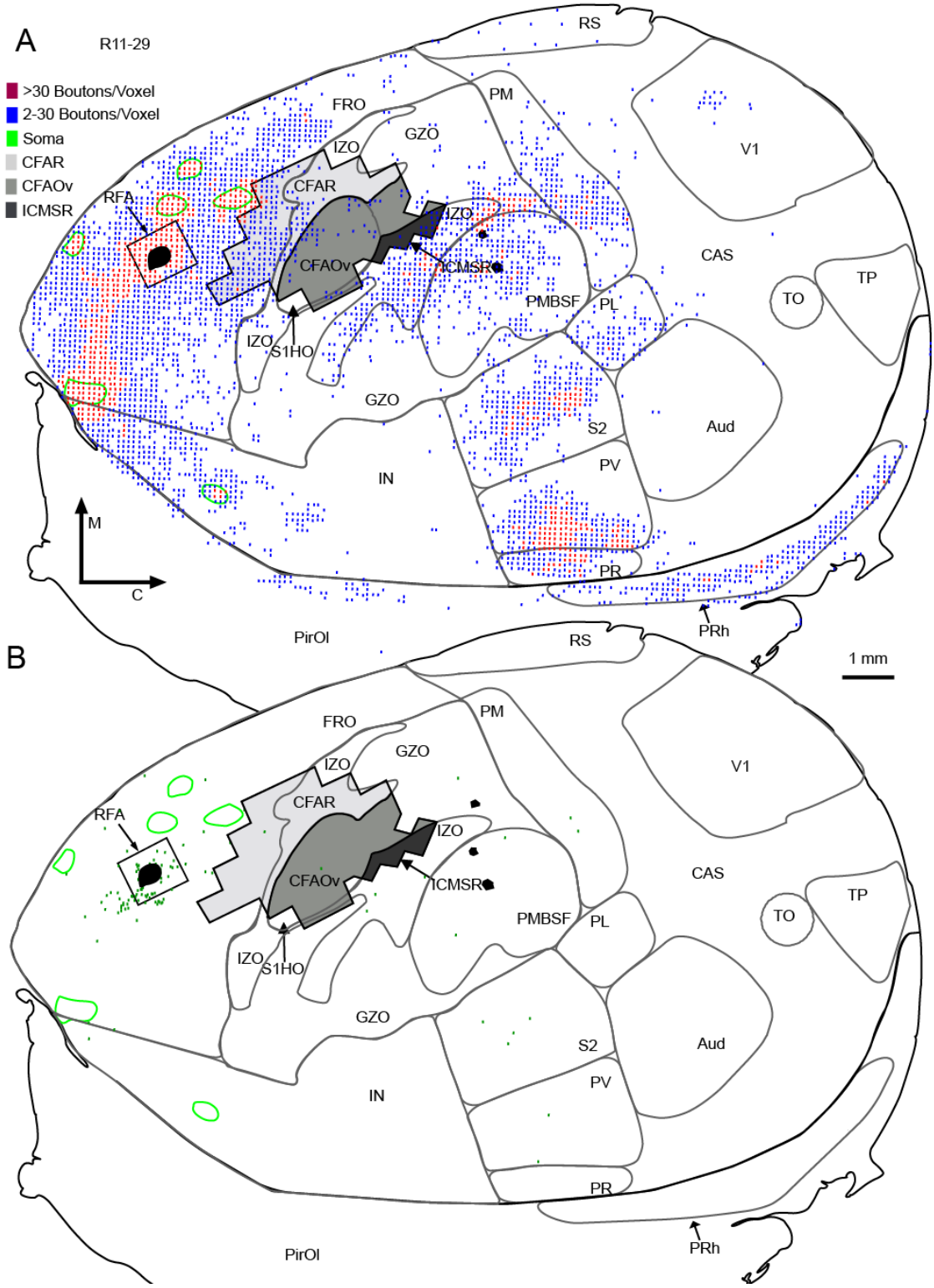
A
R11-29
>30 Boutons/Voxel
2-30 Boutons/Voxel
Soma
CFAR
CFAOv
ICMSR
RS
PM
FRO
GZO
IZO
V1
CFAR
RFA
IZO
CFAOv
ICMSR
CAS
TP
TO
PMBSF
PL
IZO
S1HO
GZO
S2
Aud
PV
IN
M
C
PR
PirOl
PRh
B
RS
1 mm
FRO
PM
GZO
IZO
V1
CFAR
RFA
IZO
CFAOv
ICMSR
CAS
TP
TO
PMBSF
PL
IZO
S1HO
GZO
S2
Aud
PV
IN
PR
PirOl
PRh

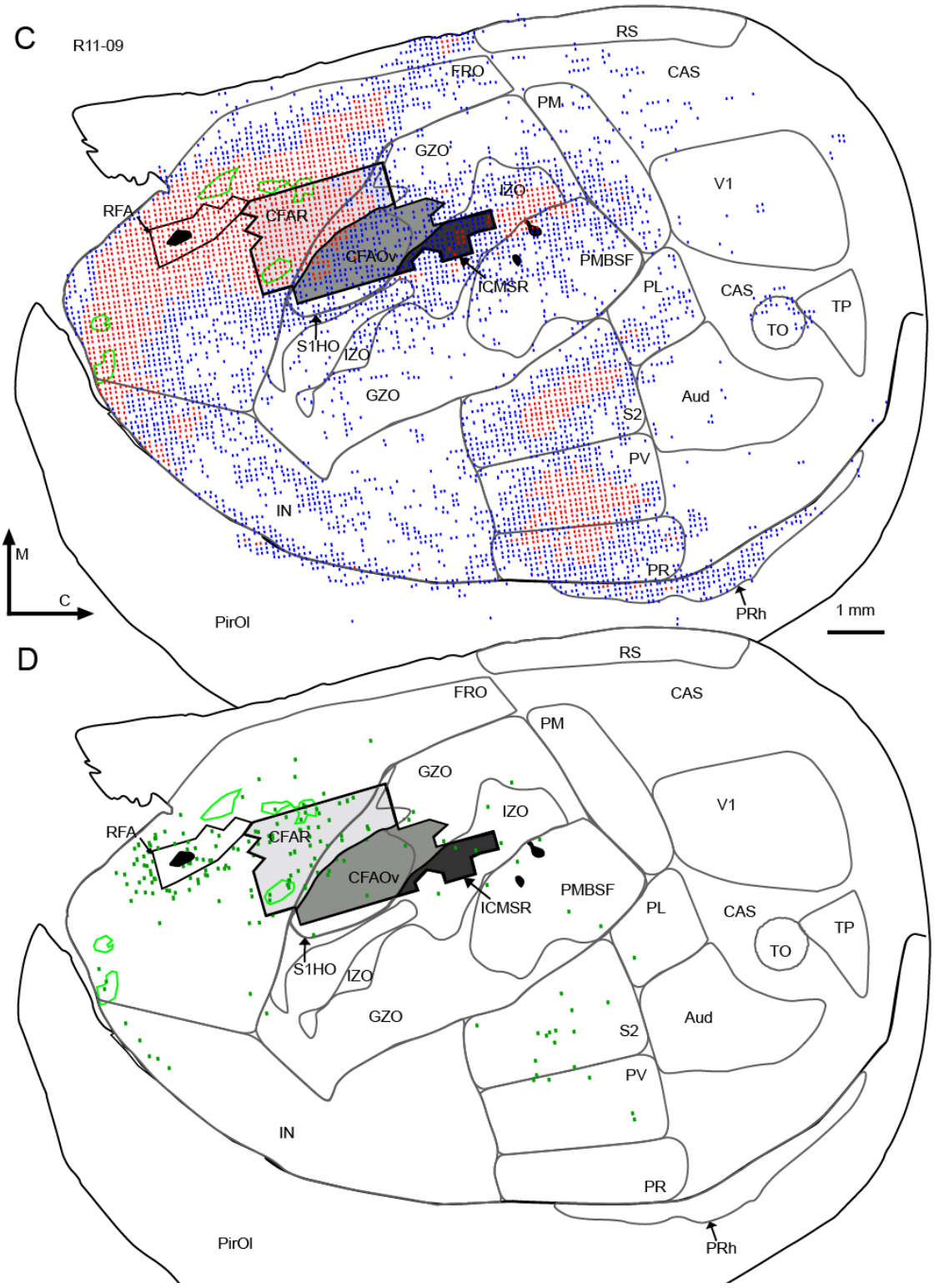
C
R11-09
RS
FRO
CAS
PM
GZO
V1
IZO
RFA
CFAR
CFAOv
PMBSF
ICMSR
PL
CAS
TP
TO
S1HO
IZO
GZO
Aud
S2
PV
IN
M
C
PR
PRh
1 mm
PirOl
D
RS
FRO
CAS
PM
GZO
V1
IZO
RFA
CFAR
CFAOv
PMBSF
ICMSR
PL
CAS
TP
TO
S1HO
IZO
GZO
Aud
S2
PV
IN
PR
PRh
PirOl

Fig. 5 Distribution of voxels and somata of the animal with the least number of voxels (R11-29) and most (R11-09) number of voxels. **A**. The section outline (black line) from animal R11-29, surrounds outlines of regions of interest (grey lines), along with the BDA10kDa core (large black shape) and CTB647 (small black dots). FRO, CFAR (light grey), ICMSR (dark grey), IZO, S2, PV, PR, and PRh receive many connections from RFA, as the areas are almost confluent with voxels containing >30 boutons (red), and voxels containing 2-30 boutons (blue). CFAOv (medium grey), GZO and PMBSF, S1HO, GZO, PM, PL, RSA, and IN regions have few, if any, voxels containing >30 boutons and minimal voxels containing 2-30 boutons. VIS, TP, CAS, TO, Aud, and PirOl receive the fewest connections from RFA, containing only a few, if any, blue voxels (containing 2-30 boutons). Regions of confluent axons (green lines) in Fr and IN were also noted. Arrows point in medial (M) and caudal (C) directions, and scale bar is 1 mm (same for **A**-**D**). **B**. Neuronal somata (green dots) distribution of same animal as in **A**. **C**. Outline of section (black line) from animal R11-09, surrounds outlines of regions of interest (grey lines), along with the BDA10kDa core (large black shape) and CTB647 (small black dots). Colors and labels are same as **A**-**D**. **D**. Neuronal somata (green dots) distribution of same animal as in **C**. This figure shows the stability of relative pattern in a qualitative assessment of corticocortical connectivity from RFA regardless of variability in total number of voxels.

Qualitative Description of Retrograde Corticocortical Connectivity

The pattern of retrogradely labeled somata follows the pattern of the voxel connectivity (Fig 1, 5, 7 and Table 1). Qualitatively, there are sparsely distributed, labeled neuronal somata dispersed throughout the section with minimal clustering. Within RFA, there are numerous labeled somata. FRO has multiple labeled somata in close proximity to the RFA. CFAR, CFAOv, ICMSR and IZO have multiple labeled somata scattered throughout. PMBSF, GZO, and S1HO have somata scattered throughout the regions, but most somata are in close proximity of IZO. S2, PV, PR, and PM have somata clustered in areas of high voxel connectivity within the regions. RS, CAS, VIS, TP, TO, Aud, PM, and PirOl rarely have any labeled somata within themselves.

Regions of interest with numerous voxels with labeled boutons, i.e. IZO, S2, FRO and CFAR (Fig 5A-B), also contained more labeled somata within them. Regions of interest with no or few voxels with labeled boutons, contained no labeled somata, i.e., PirOl and Aud.

Quantitative Description of Anterograde Corticocortical Connectivity

Total voxels were normalized for the area of each region of interest in each rat. These numbers were used for mean and standard error of the mean calculations (Fig. 6).

In order to delineate among dense, moderate, sparse and negligible connectivity, voxel counts/mm^2 were analyzed using a nonparametric procedure, the Wilcoxon Rank Sums Tests. Significant differences in voxel counts/mm^2 were found among the regions of interest (Chi-square = 95.22, $p < 0.0001$). Z-scores based on the Wilcoxon test were then used to derive arbitrary cut-off levels for densities. Regions with dense connections were defined as those with z-scores (>2.5); regions with moderate connections had Z-scores between 1 and 2.5, and regions with sparse connections had Z-scores between -0.5 and 1. Regions with z-scores < -0.5 were considered to have negligible connections (Table 2).

Based on z-scores for bouton densities, FRO, PR and CFAR had dense connectivity; IZO, CFAOv, S2, and PV had moderate connectivity, while ICMSR, S1HO, PRh, IN, PMBSF, and PM had sparse connectivity. PL, GZO, RS, Aud, Vis, TO, PirOl, CAS and TP had negligible connectivity (Figure 7A).

Quantitative Description of Retrograde Corticocortical Connectivity

Total soma counts were treated in the same manner as voxel counts. They were normalized for the area of each region of interest in each rat. These numbers were used for mean and standard error of the mean calculations (Fig. 6).

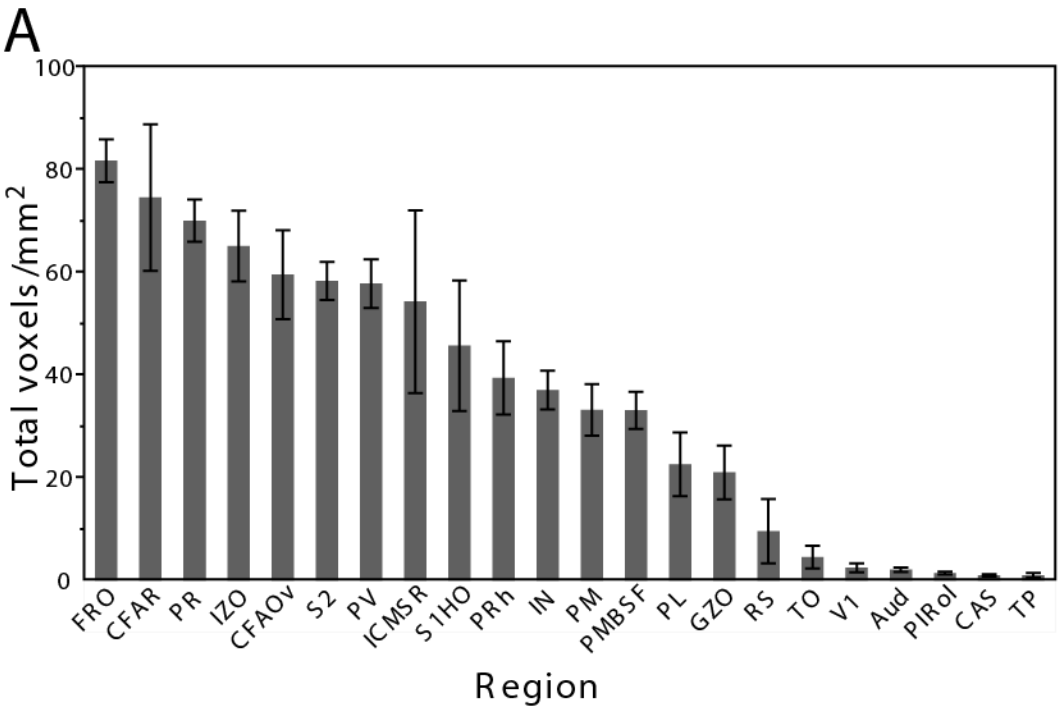
A
Total voxels/mm2
100
80
60
40
20
0
FRO
CFAR
PR
IZO
CFAOv
S2
PV
ICMSR
S1HO
PRh
IN
PM
PMBSF
PL
GZO
RS
TO
V1
Aud
PIRol
CAS
TP
Region

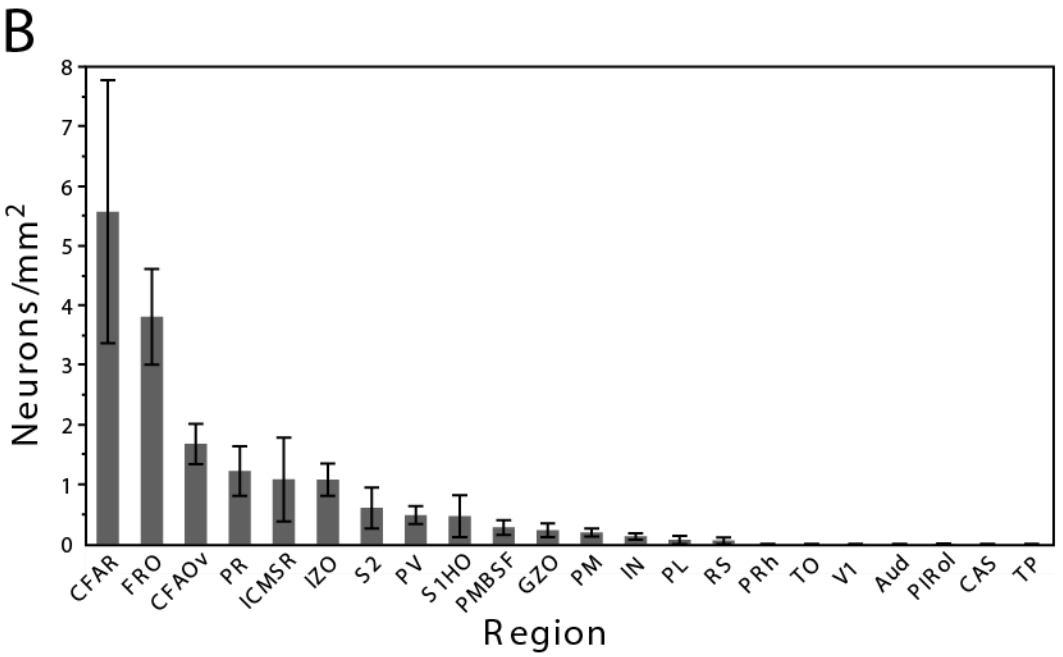
B
Neurons/mm2
8
7
6
5
4
3
2
1
0
CFAR
FRO
CFAOv
PR
ICMSR
IZO
S2
PV
S1HO
PMBSF
GZO
PM
IN
PL
RS
PRh
TO
V1
Aud
PIRol
CAS
TP
Region

Fig. 6 A-C. Histogram of the distribution of RFA connectivity. Percentage of voxels per region of interest was figured with the formula (X in region of interest)/(X in total section)/(area of region of interest), where "X" is either voxels containing >30 boutons (**A**) or voxels containing 2-30 boutons (**B**). Percentage of somata per region of interest (**C**) was figured with the formula (somata in region of interest)/(total somata in section)/(area of region of interest). Percentages (y axis) are displayed versus the region of interest (x axis), and height is equal to mean (n=6) with error bars equal to standard deviation (same for **A**-**C**). **A**. When considering total voxels, neurons within the RFA send dense projections to other parts of the RFA, FRO, PR and CFAR send moderate projections IZO, CFAOv, S2 and PV, send marginal projections to ICMSR, S1HO, PRh, IN, PMBSF and PM, and send negligible projections to PL, GZO, RS, Aud, VIS, TO, PirOl, CAS, and TP. Please notice the break in the bar for RFA. **B**. When considering the location of the retrogradely labeled cells, the region of interests are connected to the same level in a retrograde direction as they are in the anterograde, as in **A**, with the exception of CFAOv, PR, IZO, S2, PRh, and GZO. Please notice the break in the bar for RFA.

Table 1. Means and Standard Deviations

	Area (mm^2)		Total Voxels with Boutons		Voxels with ≥30 Boutons (Red)		Voxels with <30 Boutons (Blue)		Total Neurons	
Region	**Mean**	**Std Dev**	**Mean**	**Std Dev**	**Mean**	**Std Dev**	**Mean**	**Std Dev**	**Mean**	**Std Dev**
Aud	18.17	5.74	0.00	0.00	0.00	0.00	18.17	5.74	0.00	0.00
CAS	55.00	28.96	0.17	0.41	0.17	0.41	54.83	28.81	0.00	0.00
CFAOv	111.00	55.81	17.17	22.61	17.17	22.61	93.83	50.59	3.17	2.32
CFAR	229.33	111.86	131.00	107.57	131.00	107.57	98.33	73.75	19.17	20.55
FRO	1544.67	212.63	937.17	306.11	937.17	306.11	607.50	355.62	74.17	43.20
GZO	278.17	156.17	13.50	20.60	13.50	20.60	265.50	139.57	3.00	3.52
ICMSR	20.50	25.21	3.17	4.92	3.17	4.92	17.33	20.57	0.50	0.84
IN	530.83	111.06	107.00	60.27	107.00	60.27	423.83	93.60	2.00	2.00
IZO	391.33	84.92	98.50	60.07	98.50	60.07	292.83	60.97	6.17	3.49
TO	3.67	4.32	0.00	0.00	0.00	0.00	3.67	4.32	0.00	0.00
PIRol	58.33	37.72	0.83	1.33	0.83	1.33	57.50	37.29	0.17	0.41
PL	66.67	47.56	1.83	2.48	1.83	2.48	64.83	45.54	0.17	0.41
PM	138.33	40.66	15.17	20.18	15.17	20.18	123.17	29.59	0.83	0.75
PMBSF	206.50	65.80	12.83	11.57	12.83	11.57	193.67	56.00	1.83	1.83
PR	154.67	76.78	49.67	30.53	49.67	30.53	105.00	55.75	2.33	1.75
PRh	120.67	93.32	7.67	8.38	7.67	8.38	113.00	87.00	0.00	0.00
PV	272.50	47.86	94.83	38.88	94.83	38.88	177.67	22.50	2.33	1.75
RS	21.33	31.41	1.33	3.27	1.33	3.27	20.00	28.50	0.17	0.41
S1HO	49.50	42.56	3.00	6.00	3.00	6.00	46.50	37.04	0.33	0.52
S2	337.50	58.82	69.17	39.81	69.17	39.81	268.33	26.75	3.50	4.93
TP	1.83	2.04	0.00	0.00	0.00	0.00	1.83	2.04	0.00	0.00
V1	18.17	13.05	0.00	0.00	0.00	0.00	18.17	13.05	0.00	0.00

Table 2: Ranking of Bouton Densities

Region	Score Mean	Z-scores
FRO	119.000	3.437
PR	108.833	2.770
CFAR	107.000	2.650
IZO	104.000	2.453
CFAOv	97.667	2.038
S2	97.333	2.016
PV	96.667	1.973
ICMSR	81.500	0.978
S1HO	78.250	0.765
PRh	75.000	0.552
IN	72.167	0.366
PMBSF	69.167	0.169
PM	66.833	0.016
PL	57.000	-0.617
GZO	56.167	-0.672
RS	32.833	-2.202
Aud	28.333	-2.497
V1	28.250	-2.503
TO	25.250	-2.699
PirOl	24.333	-2.759
CAS	19.500	-3.076
TP	17.917	-3.180

Note: Total Voxels (with labeling) Per Region of Interest was subjected to a nonparametric test (Wilcoxon Rank Sum Test). Z-scores were used to determine cutoff values for defining regions of interest with dense, moderate and sparse connectivity. Cutoff values for z-scores were set at ≥ 2.5 (dense), ≥ 1.0 and < 2.5 (moderate), ≥ 0 and < 1.0 (sparse). Connectivity for regions of interest with z-scores < 0 were designated as negligible.

Table 3: Ranking of neuronal somata densities

Region	Score Mean	Z-scores
FRO	123.833	4.025
CFAR	118.500	3.650
CFAOv	112.167	3.205
IZO	103.333	2.584
PR	96.333	2.092
PV	84.167	1.236
GZO	78.833	0.861
S2	76.500	0.697
PMBSF	70.833	0.299
PM	68.667	0.146
ICMSR	64.167	-0.158
IN	63.667	-0.193
S1HO	59.333	-0.498
PL	43.500	-1.611
RS	43.000	-1.646
CAS	40.667	-1.810
PIRol	39.833	-1.869
Vis	39.667	-1.881
PRh	34.000	-2.279
TO	34.000	-2.279
Aud	34.000	-2.279
TP	34.000	-2.279

Note: Total Somata Per Region of Interest was subjected to a nonparametric test (Wilcoxon Rank Sum Test). Z-scores were used to determine cutoff values for defining regions of interest with dense, moderate and sparse connectivity. Cutoff values for z-scores were set at ≥ 2.5 (dense), ≥ 1.0 and < 2.5 (moderate), ≥ -0.5 and < 1.0 (sparse). Connectivity for regions of interest with z-scores < -0.5 were designated as negligible.

Dense, moderate, sparse and negligible connectivity were delineated in the same manner as voxel counts. Somata/mm^2 were analyzed using a nonparametric procedure, the Wilcoxon Rank Sums Tests. Significant differences in somata/mm^2 were found among the regions of interest (Chi-square = 95.22, $p < 0.0001$). Z-scores based on the Wilcoxon test were then used to derive arbitrary cut-off levels for densities. Regions with dense connections were defined as those with z-scores (>2.5); regions with moderate connections had Z-scores > 1 and $\leq$ 2.5; regions with sparse connections had Z-scores > -0.5 and $\leq$ 1. Regions with z-scores < -0.5 were considered to have negligible connections (Table 3).

Based on z-scores for neuronal somata densities, FRO, CFAR, CFAOv, and IZO had dense connectivity, PR and PV had moderate connectivity, and GZO, S2, PMBSF, and PM had sparse connectivity. ICMSR, IN, S1HO, PL, RS, PL, PirOl, VIS, Aud, CAS and TO had negligible connectivity (Figure 7B).

Discussion

Based on quantitative methods describing the density of cortico-cortical termination patterns, this study provides several findings. 1) The connectivity pattern of RFA was determined throughout the cerebral cortex. The RFA sends dense projections to FRO, PR and CFAR, moderate projections to IZO, CFAOv,

S2, and PV, and sparse projections to ICMSR, S1HO, PRh, IN, PMBSF, and PM. Retrograde labeling revealed that somata projecting to RFA were dense in FRO, CFAR, CFAOv, and IZO, were moderate in PR and PV, and were sparse in GZO, S2, PMBSF, and PM. Figure 7 is a summary of the findings of both anterograde and retrograde connectivity. 2) More specifically, this study provides convincing evidence that RFA projects heavily to the intercalated zone of the somatosensory cortex, but sparsely to the granular portions of the somatosensory cortex, including the S1 hand area caudal to the FIA/S1 hand area overlap zone. 3) The FIA tail was found to be further caudal than previously described, overlapping the intercalated zone, and densely connected to RFA.

This study also provides further evidence for the location of S2 and PV directly lateral to S1, in which PV does not share a border with S1. In the following sections, we will also discuss the status of RFA as a premotor area, the unique connectivity of RFA, the importance of our quantitative approach to understanding RFA's hierarchy of connectivity, and caveats of the study.

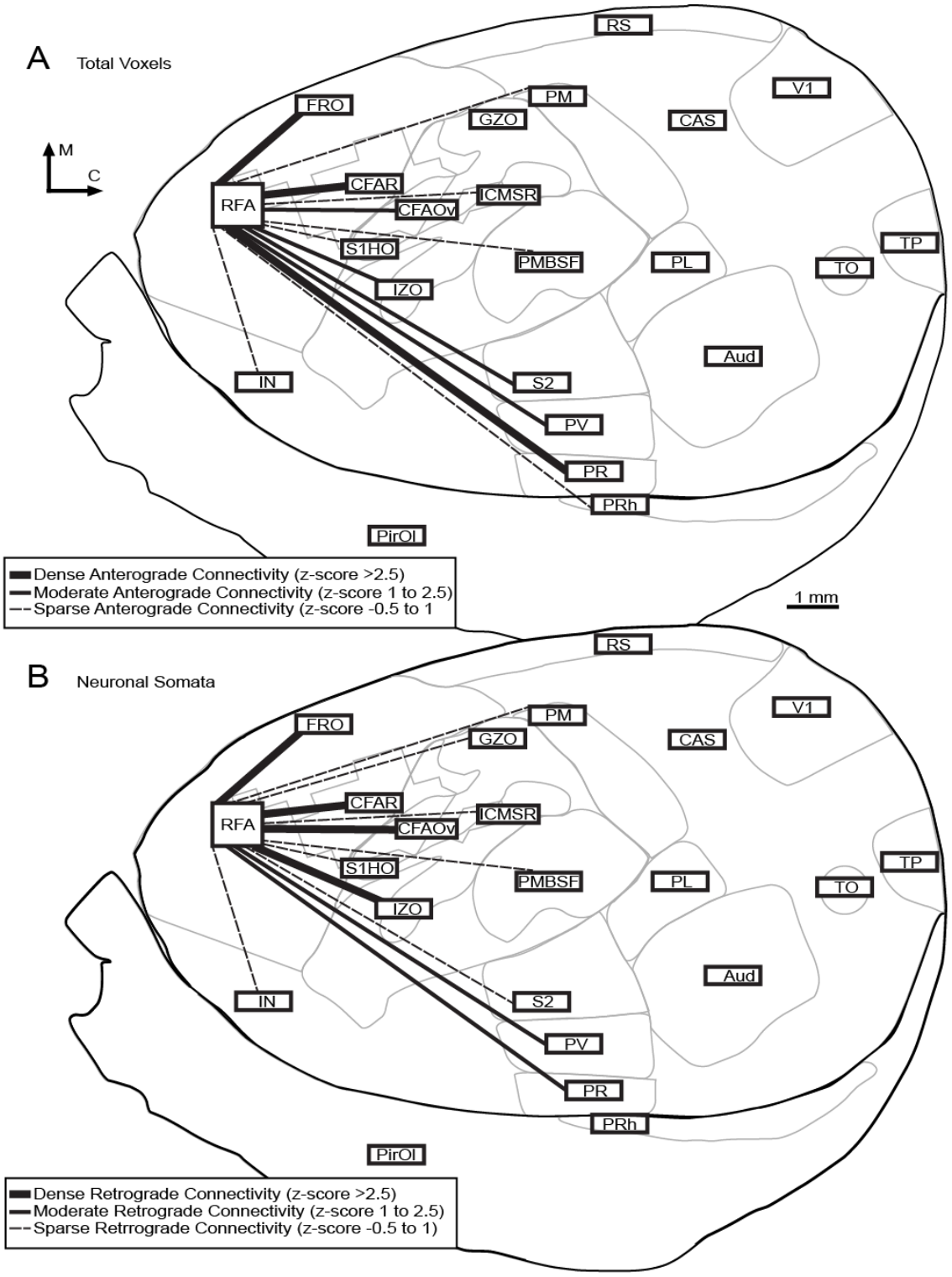
A
Total Voxels
M
C
RS
V1
FRO
PM
GZO
CAS
RFA
CFAR
ICMSR
CFAOv
S1HO
PMBSF
PL
TP
TO
IZO
Aud
IN
S2
PV
PR
PRh
PirOl
Dense Anterograde Connectivity (z-score >2.5)
Moderate Anterograde Connectivity (z-score 1 to 2.5)
Sparse Anterograde Connectivity (z-score -0.5 to 1
1 mm
B
Neuronal Somata
RS
V1
FRO
PM
GZO
CAS
RFA
CFAR
ICMSR
CFAOv
S1HO
PMBSF
PL
TP
TO
IZO
Aud
IN
S2
PV
PR
PRh
PirOl
Dense Retrograde Connectivity (z-score >2.5)
Moderate Retrograde Connectivity (z-score 1 to 2.5)
Sparse Retrrograde Connectivity (z-score -0.5 to 1)

Fig. 7 A-B. Diagram of the distribution of RFA connectivity. Labels (boxes) for the regions of interest (grey lines) are placed within the section outline (black line) and have high (thick black line), moderate (medium black line), low (dotted line), or no (no line) representing connectivity to RFA. **A**. Anterograde connectivity considering total voxels in each region of interest. Arrows point in medial (M) and caudal (C) directions, and scale bar is 1 mm (same for **A**-**B**). **B**. Retrograde connectivity from the regions of interest to the RFA, considering location of retrogradely labeled somata. This shows that areas are largely interconnected anterogradely (total voxels) and retrogradely (somata) to the same degree. Only CFAOv, PR, IZO, S2, PRh, and GZO change designations.

Description of Functional Connectivity with RFA.

Dense and Moderate Connectivity

Greater connectivity to a functionally characterized cortical region suggests the region is more essential to proper function than an area of less connectivity. As such, those regions with dense and moderate connectivity will be discussed further, while regions with sparse or negligible connectivity will not.

Qualitatively, FIA, FRO, PR, CFAR, IZO, CFAOv, S2 and PV are almost confluent with voxels. Quantitatively, regions FRO, PR, CFAR, IZO, CFAOv, S2 and PV had dense and moderate connectivity, which suggests important roles for each of these areas in movement coordination of the forelimb. To facilitate description, these regions can be divided into frontal, somatosensory, and lateral somatosensory cortex.

Connectivity to Frontal Cortex (FRO and CFAR)

Fr is the location of the primary motor, secondary motor, and medial frontal cortex, and nearly half of all voxels are located within FRO. Connections to other parts of the Fr cortex would allow communication of multiple muscle systems working together for postural support and hand/face coordination, necessary for feeding. Connections to the primary motor hand area allow access to corticospinal projections for movement activation. Higher order functions are

encompassed within the other areas of frontal cortex as well. The medial frontal cortex has a role in the aiming component of reaching tasks (Whishaw IQ et al. 1992). Maintaining concentration on a task is also related to this area. Bilateral frontoparietal ischemia led rats to increase premature lever release errors on a lever task to receive food reward thereby increasing reaction time errors to visual cues, while rats affected with rostral pole lesion had major effects leading to a premature release signifying attentional deficits (Baunez C et al. 1998). These functional deficits are seen in similar regions in the primate. Connections to the Fr are not only instrumental in firing of corticospinal neurons but also important in aiming of the forelimb and attention to tasks related to forelimb movement.

Connectivity to Somatoensory Cortex (IZO and CFAOv): Granular vs Dysgranular

One of the most striking results is the different strength of connectivity to the different subareas of S1. As S1 of the rat can be separated into granular and dysgranular areas, one might expect differences in connectivity, but the differences are quite stark. IZO received dense connectivity while most the granular region was devoid of connectivity. In fact, the space of absent voxels in S1 was the negative image of the somatosensory area, making it easy to estimate the final overlap position of the CO stained sections during section registration. The granular cortex (S1H, PMBSF, and GZO) and dysgranular cortex (IZ) of S1 are different in several aspects besides connectivity to RFA.

The most obvious difference is a reduced Layer IV in the dysgranular cortex and how this affects function. The caudal half of the IZ receives deep sensory information from joints, while the granular zone containing S1H, PMBSF, and GZO receives cutaneous information (Chapin JK et al. 1987). There is also a distinction between subcortical projections that may be involved in sensorimotor integration. Dysgranular IZ has been shown to send projections that overlap with projections from granular S1 within the striatum, while projections from dysgranular S1 to the thalamus and spinal cord overlap with projections from other sensory and motor areas suggesting that both areas play distinct roles of modulating motor and sensory signals (Lee T and U Kim 2012).

There is one exception to the granular dysgranular distinction regarding connectivity with RFA. CFAOv does have moderate connectivity with RFA. This is a special case in that the CFAOv zone is defined as an electrically excitable area of granular cortex capable of eliciting forelimb movements. RFA connects densely to the other parts of M1, and thus one would expect dense projections to the primary motor cortex of the rat that extends through CFA including the granular sensorimotor overlap area CFAOv. This suggests RFA modulation of motor function within the overlap zone is necessary, but to a lesser degree than to the modulation of motor cortex within Fr (CFAR).

Connectivity to Lateral Somatosensory Cortex (S2, PV and PR)

S2 and PV are multimodal somatosensory regions. They both have somatotopically organized full-body representation in the rat (Remple 2003). Both S2 and PV have corticospinal and medullary projections (Li 1990). These connections suggest that RFA is both receiving and modulating the signal from these multimodal areas. Given the specificity in topography of S2 and PV, an unexpected finding is the seemingly non-homotopic nature of connectivity these areas have with RFA. This is an atypical connectivity pattern for somatotopically organized sensory areas of cortex. Other studies show the connectivity of somatosensory areas is somatotopic in nature, i.e. injection into the forelimb area labels other areas associated with forelimb sensation. However, after RFA injection, S2 and PV do not have clusters of connectivity within forelimb regions. S2 and PV are joined at the forelimb and hind limb representations, so a homotopic pattern would be expected to include one cluster of connectivity located at the joined forelimb representation of both S2 and PV that forms a border between the two regions surrounded by the empty space of negligible connectivity to the rest of the body representations. Instead, there are two clusters of connectivity with one cluster of voxels in the middle of each region separated by a blank area of no voxels. The densely connected zone is located in the proximal body representation of both S2 and PV, while the empty space corresponds to the forelimb and hindlimb area of others (Koralek K-A et al. 1990; Remple MS *et al.* 2003). It is interesting to note that even though the dense connectivity is to unexpected representations within the S2 and PV, the pattern is

consistent within the group. Areas of red voxels (>30 boutons/voxel) are located in the middle to medial area of each S2 and the middle to lateral area of each PV. This pattern is also consistent with the orientation of S2 and PV being mirror images of each other (Koralek, et al. 1990, Remple, et al. 2003). Figures of the current study reveal the consistency (Fig 1a, 5a, 5c). This pattern could be explained by incorrectly drawn regions, or be an artifact of the superficial layer. This is unlikely however due to the consistency of the pattern within the group and suggests the importance of modulation of the proximal body during forelimb function.

PR, located laterally to S2 and PV, may relay visceral information based on its thalamic connectivity (Cechetto DF and CB Saper 1987). It is described as a thin strip of cortex on the medial rhinal sulcus, though Remple found it more medial than previously reported (Remple MS *et al.* 2003). Li (Li X-G *et al.* 1990) found labeled neurons after tract tracer injection into the lumbar and cervical enlargement, which he labeled PR. The location of PR in those studies is much more rostral than the current study. A similar cluster of connectivity was found in the current experiment in the rostral region of IN. The location of PR identified in this study is more in line with Remple (Remple et al. 2003) in an area of the cortex, which did not have corticospinal or medullary connections (Li, Florence et al. 1990), but that was heavily interconnected to the S1 granular zones (Fabri and Burton 1991). It has been suggested that this area could be a fusion between internal and external body maps (Fabri and Burton 1991).

PV and S2 Location

The rat has several secondary sensory regions lateral to S1 that are thought to be higher order and multisensory integration areas, S2 and PV. However, the precise position of these regions and the number of sensory areas in the rat has been subject to debate. This issue is important in that the functional significance of PV can be very different depending on which cortical space it occupies.

In the rat, Zilles describes S2 (labeled Par 2) lateral to S1 (labeled Par1) in the rat, sharing a medial border with the lateral aspect of S1 (Zilles K 1990). He then describes a visceral area (Vi) lateral to S2, which includes part of the gustatory area (Gu) and agranular insular posterior (AIP), the PV had not been identified yet. PV was first described in rodents in the squirrel (Krubitzer LA et al. 1986). In the squirrel, PV is rotated more rostrally to S2. Campi and Krubitzer put the S2 and PV of the rat in a similar relationship to that of the squirrel cortex, placing them rostrolateral to S1 (Campi KL and L Krubitzer 2010). This gives the impression that both S2 and PV share a border with S1, that S2 shares a border with PMBSF, and that PV shares a border with ALBSF.

Our results are in general consistent with the interpretation of Remple (Remple MS *et al.* 2003). The authors overlaid microelectrode recording maps with CO stained tangential sections. CO-rich zones corresponding with the rat's

foot and mouth sensory representation aided in defining the border between S2 and PV. Similar CO-rich zones were used in the current study. Remple defined two areas directly lateral to S1--each with a full somatotopic representation (Remple, Henry et al. 2003). The areas mirrored each other in orientation, as they were joined at the forepaw and hindpaw representation. In the current study, we found two distinct clusters of connectivity directly lateral to S1, which we divided into S2 and PV. The clusters corresponding to S2 and PV are consistent in length and shape, and separated by blank areas (devoid of voxels), which aided in the recognition of the different regions. However, there are discrepancies with Remple et al. (Remple MS *et al.* 2003) in that they describe a more lateral orientation of S2 and PV. Krubitzer places PV in an area of cortex, which is devoid of connectivity in the current study (Krubitzer L *et al.* 2011). The same area corresponds to the mouth representation of Remple (Remple, Henry et al. 2003). It is easy to surmise the existence of similar connectivity to the S2 and PV, and that these two areas correspond to the clusters of connectivity seen lateral to S1. It stands to reason that the RFA would exhibit similar connectivity to two areas concerned with body and limb movement, while sending negligible connectivity to a mouth representation.

In the current study, S2 and PV display a clear somatotopic organization. The caudal part of their shared border is the hindpaw representation of both S2 and PV, as they are reflections of each other (Fabri M and H Burton 1991; Remple MS *et al.* 2003). The hindpaw representations of S2 and PV were

devoid of voxels, while the proximal forelimb and trunk representations contained many voxels. It stands to reason that the RFA would exhibit similar connectivity to two areas concerned with body and forelimb movement, while sending negligible connectivity to the mouth representation. As S2 and PV are both integrative sensory in nature, it is easy to suggest that sensory-modulation is necessary for accurate forelimb movement. S2 and PV also have labeled somata, suggesting the necessity of feedback from the regions.

Other Parietal and Perirhinal Connectivity (PM, PL and PRh)

Although the other parietal areas, PM and PL, and perirhinal cortex, did not reach significant dense or moderate connectivity, the consistent clusters of connectivity within the regions warrant more discussion.

The failure of these areas to reach the quantitative threshold may be a byproduct of region shape. Both PM and PL were drawn larger than the cluster of voxels would dictate. PM was extended to span the entire caudal border of S1 in its mediolateral aspect beyond the cluster edge, while the widest part of the cluster was taken as the width of the entire region along its anterioposterior aspect, in a manner similar to Reep (Reep RL and JV Corwin 2009). PL was extended both anterioposteriorly and mediolaterally so that it shared a border with PM and S1 medially, S2 rostrally, Aud laterally and ended in a line even with the PM caudally. This is in a manner similar to an unnamed region of Reep,

which is smaller than our representation but which occupies the same space (Reep RL and JV Corwin 2009), and is in agreement with the general placement of Fabri and Burton (Fabri M and H Burton 1991). Reep (Reep and Corwin 2009) visualizes PM as thinner and with a lateral aspect that extends further medially than ours; the medial aspect of our PM ends in a line even with the medial aspect of S1, as with Fabri and Burton (Fabri M and H Burton 1991).

PL is a multisensory region found on the caudal lateral edge of S1 barrel cortex, and the caudal border ends at the caudal border of PM (Brett-Green B et al. 2003). PL shares a border with PM on the caudal medial side, S1 on the rostral medial side, S2 on the rostral side, and Aud on the lateral side. Although Brett-Green identify the region between Aud and S1 as having a multisensory component on its caudal end (Brett-Green B *et al.* 2003), the authors included it with S2. The connectivity found in the current study revealed a distinct cluster of voxels in PL, and which deserves designation. We have identified the area as PL in accordance with Remple (Remple MS *et al.* 2003) because it has multisensory responsiveness and connectivity that differentiates it from the rest of S2. Integration of multisensory information for correct stimulus-driven guidance of the forelimb is again intuitively important.

The role of the posterior parietal cortex as a sensory integration area has been previously studied. Like humans and non-human primates, the rat suffers from attentional and visual-spacial deficits when the parietal cortex is lesioned

(DiMattia BV and RP Kesner 1988). Connections to PM would aid in the correct movement selection moving through 3-dimensional space.

Although other studies have not specifically labeled the RFA, the current results are consistent with other studies on PRh connectivity to the motor cortex and extend the findings somewhat. Fr2 (Prcm), which may or may not include the RFA, projects to the perirhinal cortex, with a large part extending into the ventral bank of the rhinal sulcus (Deacon TW et al. 1983). The current results are at least consistent with studies involving retrograde tracer injections into the entorhinal and perirhinal cortex, which labeled cell bodies in primary and secondary motor cortex (Burwell RD and DG Amaral 1998). This current study extends these findings to identify physiological areas that were not defined in previous research. Previous research revealed how RFA and CFA are connected to the perirhinal cortex in the upper layers I, II and VI by anterograde injection of the perirhinal cortex (Kyuhou S-i and H Gemba 2002). The sensory cortex has also been shown to connect to PRh. Although Fabri and Burton do not specifically name it as such, after close examination of their figures, our PRh is also present in their diagrams as a thin strip of connectivity coursing lateral along the entire caudal length of the rhinal fissure (Fabri and Burton 1991).

Previous findings not only show that connections exist between the frontal and perirhinal cortex, but connections have some functional relevance. The transfer of auditory information is carried by such connections, as lesioning perirhinal cortex abolishes auditory signal potential in the frontal cortex (Kyuhou

S-i et al. 2003). The perirhinal cortex is also related to object recognition. Lesioning perirhinal cortex creates deficits in object recognition that are not evident with amygdala lesion (Mumby DG and JP Pinel 1994). Also, the perirhinal sulcus layer V projects to frontal cortex while the perirhinal cortex projects to agranular insular, infralimbic, orbital, parietal and entorhinal cortices (McIntyre DC et al. 1996). The involvement of PRh in multiple areas, i.e., object recognition and auditory information, supports the idea that PRh participates in stimulus-driven guidance of the forelimb.

Primate and Rat Premotor Connectivity Similarities

Since the early days of rat research, brain region homology between primate and rat is a constant question. The rat is used frequently in neurological studies, but in order to appreciate the generalizability of results, the relationship to other species, especially primates needs to be addressed. One area of concern, which this study elucidates, is the relationship of RFA to the premotor areas of primates.

In primates, the premotor areas are classically defined as 1) regions within the frontal cortex that 2) directly projected to M1 (Dum RP and PL Strick 2002). RFA fulfills both of these, and also has corticospinal projections, as all primate premotor regions do (Rouiller EM *et al.* 1993; Dum RP and PL Strick 2002). A major roadblock is the number of premotor areas in primates, which is far greater

than the one premotor area of the rat. The RFA could be homologous to SMA, CMA, PMd or PMv areas; it could also be a combination of all or some of the areas or it could be an independently evolved region.

The simplest approach to ascertaining brain region homology is by comparing connectivity patterns of areas. In general, the premotor cortex of a rat projects in a similar fashion to that of primate. The fundamental concept a researcher learns when first approaching this field of research is that the cortex involved in special senses (taste, sight and hearing) are devoid of connectivity while sensory and motor areas have various levels of connectivity.

Similar connectivity studies regarding PMv have been done in squirrel monkey (Dancause N *et al.* 2006b). PMv of primates has corticocortical connectivity very similar to RFA concerning projection target regions and relative strength of connectivity to those regions. As one can see from the current study (Fig. 7), RFA sends dense projections to the rostral portion of the ICMS defined borders of M1, while only moderate connections are sent to the caudal portion. PMv shows increased connectivity to the rostro-lateral portion of M1 as well. While the difference between rostral and caudal M1 is greater in primates, both rats and primates show a clear preference for the rostral half of the motor cortex. In rats, the caudal portion of FIA is coincident with the sensorimotor overlap, and lower connectivity may be explained by the overlap itself. Both PMv and RFA send dense connections to parts of the Frontal cortex rostral to itself, and moderate projections to S2 and PV. Both PMv and RFA largely avoid sending

projections to S1, while sending projections to posterior parietal cortex. RFA and PMv both display reciprocal connections; in addition, areas of increased anterograde connectivity have increased retrograde connectivity as well. As shown in Table 1, regions of interest with high anterograde connectivity also have high retrograde connectivity. The rostral part of IN has both confluent voxels and sparse neuronal somata, while the caudal part of IN has neither. The interconnectivity of RFA to other areas is important in the function of RFA.

The main differences between PMv and RFA exist because of the decreased number of brain regions in the rat. PMv sends moderate and minor projections to the other premotor areas (PMd, SMA and CMA), while RFA has no other premotor area to project to. There is also a moderate connection to anterior operculum, which is a brain region the rat does not have.

Compounding the issue, RFA has connectivity patterns similar to other primate premotor regions. Both the SMA and premotor cortex of primates project to the insular cortex (Jurgens U 1984; Matelli M *et al.* 1986) as well as to RFA. In the current study, RFA displays extensive connectivity to the rostral part of the insular cortex. The connectivity was not significant during statistical analysis, but the heterogeneous nature of IN make it difficult to capture the connectivity in only the rostral part of the region. While this connectivity pattern helps validate RFA as a premotor area, it does not help distinguish which region it is. Although, the similarities between PMv and RFA are striking, and it is tempting to say PMv and RFA are homologous, more study is necessary.

Connectivity to Overlap Zones

The different anatomical aspects of the cortex have long been studied. In the earliest analysis, the motor cortex was defined by large pyramidal neurons in Layer V projecting to the spinal cord, and the sensory cortex was defined by a dense granular Layer IV, which received thalamic inputs. In primates, the sensory and motor cortex are separate. Stimulation of the motor cortex drives muscle movements detectable by unaided eye or EMS, and electrical activity from peripheral stimulation can be recorded within the sensory cortex. Recording within the motor cortex or stimulating neurons within the sensory cortex in order to drive movement is less effective. However, the rat contains a cortical overlap zone with both properties, electrically excitable motor cortex and sensory cortex with peripheral stimulus-driven recording. The potential evolutionary pressures for such arrangement are numerous, including the smaller size of the rat brain dictating that the same region accomplish multiple activities, or response time may decrease between sensory stimulus and motor activation with close proximity.

This overlap zone was first described by Hall and Lindholm (Hall RD and EP Lindholm 1974) using electrical stimulation and recording, and verified by other authors (Chapin JK and DJ Woodward 1986). It was reported as a 1 mm wide strip of cortex, running obliquely across the rostral border of S1, which

encompasses the caudal half of the motor cortex hand representation and all of the motor cortex hindlimb representation. Donoghue did further anatomical studies and found the motor cortex within the overlap zone connected to both sensory and motor thalamic nuclei, while the motor cortex outside of the overlap zone connected to motor-only nuclei (Donoghue JP et al. 1979). After retrograde tract-tracer injection into the hindlimb cortex, both motor thalamus (ventrolateral nucleus, recipient of cerebellar connections) and the sensory thalamus (ventrobasal nucleus, recipient of the lemniscal pathway) were labeled. However, retrograde tract-tracer injection into the motor face representation (outside the overlap) led to motor thalamus neuronal staining, while retrograde tract-tracer injection into the sensory cortex (outside the overlap) led to sensory thalamus neuronal staining (Donoghue JP *et al.* 1979). In other experiments cytoarchitecture was compared with electrical stimulation maps (Donoghue JP and SP Wise 1982) to show stimulation sites covering most of the sensory forelimb region and all of the sensory hindlimb. Neurons within the forelimb sensori-motor overlap fire in correlation with active movements (Chapin JK and DJ Woodward 1986).

After aligning the sections in our study, the FIA was found to overlap S1H cortex in all six rats, and in two of the six rats--the overlap extends past the S1H to the GZ and IZ. This encroaches into territory not previously identified as sensorimotor overlap. The FIA (Fig. 2B) was subdivided into CFAR, CFAOv and ICMSR, based on its overlap with S1 and its subdivisions (GZ, S1H, and IZ).

CFAR includes the FIA in the frontal cortex, outside of S1 borders, and the intersection between the FIA and the rostral part of IZ. The rostral parts of IZ have a larger cortical layer, V, than the caudal parts, and was included with the motor region overlap to reflect its motor-cortex-like morphology. The CFAOv includes the overlap between FIA and S1H and some of GZ. ICMSR includes the overlap between FIA and the caudal parts of IZ, which are more dysgranular in nature, but without the motor-cortex-like layer, Vb, of the rostral half. PMBSF did not overlap with FIA in any of the rats, so a change was not necessary. The parts of S1H, GZ and IZ that were not otherwise delineated by FIA overlap were renamed S1HO, GZO, and IZO, respectively, to reflect this new stature. To our knowledge this is the first report of this naming system.

We believe the ICMS response within the caudal part of IZ (ICMSR) is not an artifact of section alignment because eliciting movements within the caudal part of IZ is not without precedent in rodents. Both Li, and Miller show location of corticospinal neurons consistent in position with our ICMSR after cervical cord injection, and as such, stimulation of forelimb movements is a reasonable finding (Miller MW 1987; Li X-G *et al.* 1990). Donoghue shows connectivity of RFA, but they used coronal sections, which are harder to aggregate for areal representations of regions of interest; furthermore, the sensory forelimb region of interest on their standard model (see their Fig 10) (Donoghue JP and SP Wise 1982) is of a different shape than the current study. Since, the general pattern of stimulation sites in the former experiment is consistent with the current

experiment, it is quite feasible that the authors would have shown stimulation sites in the caudal part of IZ if tangential sections and CO staining had been used. In squirrels, the area between granular somatosensory areas is called the unmyelinated zone (UZ). Recently, Cooke (Cooke DF et al. 2011) reported eliciting movements by stimulating within the UZ, while using similar parameters as the current study. Although differences do exist, UZ in squirrel and IZ in rat may be homologous to one another, and therefore, it is not surprising that low threshold movements were elicited in the current study.

One might ask why such things have not been reported previously. One answer points to the cortex motor region, which is inherently difficult to define because excitable cortex is sensitive to all manner of experimenter protocols, (i.e., anesthetic depth, current level). Even in the first experiments of Hall and Lindholm, forelimb stimulation sites were reported further lateral than our own ICMSR (see their Fig 4)(Hall RD and EP Lindholm 1974). Neafsey's (see their Figure 3) extent of CFA is consistent with our FIA (Neafsey EJ *et al.* 1986). In a similar ICMS study, the overlap of ICMS and CO sections were accomplished with lytic lesions of the cortex during the surgical procedure, and the extent and placement of CFA was consistent with our results (Xie N et al. 2010). In particular, their Fig 3c shows the caudal end of CFA extending past the forearm representation into the Intercalated Zone, as we have shown.

The caudal and rostral part of IZ were included in different overlap zones due to various properties of the IZ. FIA overlap with the rostral part of IZ was

included with Fr in CFAOv, while overlap with the caudal part was named ICMSR. The rostral part of IZ is a thin strip of cortex between the forelimb and hind limb representations of S1 and the Fr cortex. It has a mixture of the cytoarchitectural and physiological properties of the motor and sensory cortex that it resides between. This area has a layer of large pyramidal cells in layer Vb, but also a variable granular Layer IV that would be expected in the sensory cortex. Neurons in this area also respond exclusively to passive joint movement in anesthetized rats; however, ICMS in this area evoked muscle movement in Chapin and Lin's study (Chapin JK and C-S Lin 1984) and also in the current study. The mixture of both motor and sensory properties led Chapin and Lin to name it the transition zone (TZ) (Chapin and Lin 1984). The difficulty in pinning one or the other term on these properties has led us to include the rostral IZ within S1, as it is clearly sensory, but we are also including it in CFAR with the classical motor cortex of Fr. Future studies may elucidate its characteristics as worthy of its own designation.

Functional Aspect of the Connectivity

In general, the RFA connects heavily to non-primary somatosensory areas and other motor and sensory cortex involved in upper body motion while largely avoiding cortical areas involved in lower body movement or primary sensory cortex areas controlling taste, sight, and hearing.

Because of the sensorimotor overlap in the rat, the motor and sensory cortex areas responsible for hindlimb function completely overlap each other. It is interesting to note that while the hindlimb area of GZO was not given a specific designation, there is a paucity of connectivity from the RFA to this area, even though RFA projects to most of the remaining primary and secondary motor cortex area, Fr (Fr1-3 of Zilles (Zilles KJ 1985)). This suggests that while hand areas controlling hand, face, trunk and nose need to communicate for proper function, this control may be less important for hand and foot coordination. This pattern also supports a somatotopic organization of RFA projections.

It was not surprising that RFA connectivity to the motor trunk area and forelimb area followed the same somatotopic order in S2, PV, PM and Fr. The secondary motor and sensory cortex are connected in the same somatotopic order to each of these regions, i.e., in rats where RFA connected more heavily to the neck/trunk area of motor cortex, there were more voxels of the appropriate color in the appropriate somatotopic orientation in the S2, PM, PV, and Fr. This pattern was not just held by relative placement in each of the regions, but also the pattern of density voxels in most animals to the point where sparse and dense voxels (blue and red, respectively) from one region of interest were in the appropriate places to conform to the somatotopic pattern set forth in the other regions of interest. As a negative control, the caudal IZ and PR, had no reported somatotopic organization and did not show the same pattern involving dense or sparse voxels. As mentioned above, the RFA did not connect heavily to the foot

representation of S1, considered to be in the primary motor cortex of the hindlimb. There was also a paucity of voxels in the caudolateral corner of S2, the caudomedial corner of PV and the medial side of PM, which are all areas of the hindlimb representation in those regions (Remple MS *et al.* 2003).

Although, these anatomical projections found in the current experiment could be nonfunctional, there is good reason to assume them functional, since similar anatomical connections found in the somatosensory cortex have proven functional. Anatomical connections from S1 to PL were described first (Fabri M and H Burton 1991), but in later experiments, stimulation of the A2 barrel in S1 led to an activity spread encroaching into PL (Brett-Green BA et al. 2001). This is evidence for the functional relevance of anatomical connectivity. Although, this is not evidence for functional relevance for the connectivity in the current experiment, the methods used to describe these connections are similar, and it is reasonable to hypothesize that similar methodology will label similar kinds of connections.

Caveats

Differences in Parcellation of Sensory Cortex from Previous Studies

S1 has been defined differently from previous reports. Although our S1 is largely consistent with the Zilles regions (FL, HL and Par1) pooled together (Zilles KJ 1985) and the S1 of Chapin and Lin (1984) (Chapin JK and C-S Lin

1984; Zilles KJ 1985; Chapin JK *et al.* 1987) our S1 contains two CO-rich zones rostral to the S1, which are not usually reported as S1. They are two CO-rich areas separated from the rostral borders of the lower and upper lip representations by a small strip of CO-sparse cortex, which are the somatosensory representation of the bottom teeth and tongue, identified by Remple (Remple MS *et al.* 2003). S1 is further divided into the CO-dense region of granular sensory neurons and an intermingled CO-sparse region of the IZ of Krubitzer (Krubitzer L *et al.* 2011), which combines the DZ and TZ of Chapin and Lin (Chapin JK and C-S Lin 1984). The granular portion of S1 is divided into the S1H, GZ and PMBSF. All of these are readily identifiable as CO-dense regions consistent with Chapin and Lin (Chapin JK and C-S Lin 1984). S1H is the forelimb sensory cortex with forepaw sensory inputs; PMBSF is the caudal half of the barrel cortex, while GZ contains the rest of the CO-dense sensory cortex not contained in S1H or PMBSF.

Voxel Analysis

Although voxels were counted as either red (>30 boutons) or blue (2-30 boutons), the importance of either was indeterminate; so, both red and blue voxels were pooled into one number called total voxels for each region of interest. This step removed some detail as voxels with higher bouton count and voxels with lower bouton count were analyzed with the same weight. Although red and blue were condensed for the purposes of statistical analysis, Figures 1

and 5 display the red and blue voxel symbols in the interest of a more complete qualitative understanding of the distribution.

Bouton Selection

The strength of retrograde label was variable and created dark staining dendritic trees in some cases. These dendritic trees were thicker and their attached boutons had different morphology than the axonal boutons. Some will surmise that areas containing somata will have inflated anterograde connectivity from incorrectly counting the dendritic tree boutons. Although this affect cannot be dismissed, it was minimized by counting only boutons on thin fibers and not counting boutons on obvious dendrites. The effect of this can be found on Fig 8 where both the rostromedial corner of S2 and the rostrolateral tip of S1 have a neuronal body present, but no voxels.

Feedforward vs Feedback Connections

The nature of flattening a cortex is not exact and thickness may vary from animal to animal, even though the same procedures, methods and personnel were used. Although no attempt was made to ascertain the exact cortical layer of the section used for bouton quantification for each rat, an attempt at normalizing the section between rats was made. Brains were sectioned from superficial to deep layers. The first complete section and the section displaying the most

complete S1 representation based CO staining were noted for each rat separately. Voxels were quantified on one superficial section halfway between the first complete section and the section displaying the most complete somatosensory representation, cortical Layer II/III. Assuming the most complete S1 representation occurs at the same level in each rat, our method of choosing the section for bouton quantification would allow for comparison of a cortex between animals with some variation in thickness resulting from histological processing. Although the absolute distance from pia to cortical Layer II/III changes, the relative distance between pia and cortical Layer IV should remain more stable.

Feedforward connections are defined as brain areas involved in higher order processing connecting to brain areas involved in lower order or associative processing, and have traditionally been deemed instructive. The typical feedforward pattern is connections from the upper cortical layers of areas involved in higher order or associative processing to deeper cortical layers of areas involved in primary processing. These connections are considered to be instructive, modifying activity in the primary sensorimotor activity for adaptive changes to the internal and external environments. In the case of connectivity from the RFA to CFAR, CFAOv or ICMSR, Layers II/III of RFA would be expected to project to Layer V of the FIA. Feedback connections are seen as the reverse of this, and parallel communication would show connectivity to and from similar

layers and areas where similar processing took place. Both feedback and parallel connections are suggested to be informative.

BDA injection cores were present on all tangential sections and were consistent throughout the cortical layers; therefore, the quantified boutons necessarily emanated from any level of the tissue column encompassed by RFA. The cortical layer of somata giving rise to any specific bouton clusters was not determined; neither was the cortical layer of the target of retrogradely labeled somata. Since feedforward and feedback connection definitions rely somewhat on the cortical layer occupied by both the efferent boutons and somata, questions answered by the current study regarding feedforward and feedback projections are minimal. What can be ascertained is that RFA projects to cortical Layer 2/3 of other areas, and neurons located in cortical Layer 2/3 of other areas project to RFA. These connections are parallel creating feedback in the strict sense of cortical layer location.

If only the higher and lower order processing aspects of regions are taken into account, it is reasonable to suggest that most of the connectivity to regions outside the motor cortex is parallel in nature. RFA has heavy or moderate connectivity to regions of multimodal or higher order processing: PM, PL, S2, PV, PR and the caudal half of IZ. RFA seems to be absent from other primary sensory areas.

Summary

The tangential sectioning and specific injection of anterograde tracer make clear that ipsilateral corticocortical connectivity of RFA has clusters of connectivity with a preference for motor regions and higher order processing areas. The RFA does not send many projections to the primary somatosensory area or areas associated with the special senses of taste, vision or hearing. RFA was densely connected to FRO, PR, and CFAR, while lZO, CFAOv, S2, and PV received moderate connectivity. ICMSR, S1HO, PRh, IN, PMBSF and PM received sparse connectivity, and PL, GZO, RSA, A1, VIS, OT, PiRol, CAS, and TP received negligible connectivity. The retrograde labeling of neurons that connect to RFA from other regions shared a similar pattern. FRO, CFAR, CFAOv, and lZO have dense labeled neurons, while PR and PV have moderate density. GZO, S2, PMBSF, PM, ICMSR, IN, and S1HO have sparse density, and PL, RS, PirOl, VIS, A1 CAS, OT, PRh, and TP have negligible density. FRO, PR and CFAR are almost confluent with voxels, which suggests important roles for each of these areas in the proper function of movement coordination of the forelimb.

Also, this study provides further evidence for the premotor nature of RFA, the position of S2 and PV being directly lateral to the PMBSF and ALBSF of S1, and further defines the overlap of physiologically defined (by ICMS) excitable motor cortex with the anatomically defined motor (Fr) and primary somatosensory (S1) cortex.

Acknowledgements

This work was supported by the National Institutes of Health (R37 2012-2036).

Chapter 3

Premotor Connectivity Changes After Ischemic Infarct

Abstract

The mechanism for recovery after ischemic injury is not well understood. Adult neuronal reorganization has been reported after cortical lesion, which may provide the basis for recovery of function. The premotor area of the cortex is becoming more interesting to study for its possible role of reorganization from motor cortex ischemic lesion. Changes in connectivity of the premotor area controlling the forelimb (RFA) after primary motor cortex ischemic infarct have not been document in the rat. In the current study, the RFA of adult male Long-Evans rat was located *in vivo* with intracortical microstimulation (ICMS), then anterograde label, biotinylated dextran amine 10,000 MW (BDA10kDa), was specifically injected into the RFA. By visualizing primary sensory regions with cytochrome oxidase (CO) stained sections, and utilizing tangential sectioning, connectivity to other cortical regions of interest were mapped in clear areal representations. Connectivity was semi-quantitatively assessed by bouton counts within a 100 μm square grid (voxel). We divided voxels into 2-30 boutons (blue) and >30 boutons (red). Retrogradely-labeled neuronal somata were also recorded. We provide evidence for anatomical reorganization of RFA in both anterograde and retrograde connectivity after motor cortex lesion. There was a significant ($p=0.05$) reduction in total voxels within PirOl, red voxels within PR, and increase in red voxels within both CAS and IN, a trend towards decrease ($p=0.071$) within PR, and a trend towards increase ($p=0.071$) for total voxels within IN in animals with ischemic infarct compared to control animals. There is also significant decrease ($p=0.05$) in neuronal somata within FRO, IZO and PM,

and a trend toward increase (p=0.071) within IN in animals with ischemic infarct compared to control animals. These changes in anatomical connectivity may represent the substrate for recovery of function after cortical lesion.

Introduction

Reorganization in the adult central nervous system (CNS) once merely a suggestion has become a basic tenet of modern neurophysiology. The injured brain is no longer seen as naïve brain with a missing puzzle piece (Nudo RJ 2006). The adult brain is actively changing in response to injury. This reorganization is a possible substrate for behavioral deficit recovery (Xerri C *et al.* 1998).

Ischemia of cortical tissue, as often occurs in stroke, is a major cause of long-term disability in humans (Muntner P et al. 2002). The motor and premotor cortex are advantageous cortical areas for study, because of their obvious role in motor control and concomitant effect on function that result if they are lesioned. Premotor cortex physiological reorganization was found by Nudo et al. (Nudo RJ et al. 1996c) after motor cortex lesion in the primate, and later studies in the same model showed anatomical reorganization in primate premotor area (Dancause N et al. 2005).

A similar premotor area exists in rat, though the exact homology is still debated (Rouiller EM *et al.* 1993). The premotor area controlling the forelimb of

the rat (RFA) has remarkably similar cortical connectivity pattern to the premotor ventral (PMv) in primates (Urban et al. in process), and fulfills both criteria for premotor cortex in primates (Dum RP and PL Strick 2002). Although there are several models of reorganization involving the somatosensory cortex (Carmichael ST et al. 2001), none has yet determined the affects of motor cortex lesion on the premotor area in the rat. In a previous study using the same lesion model as the current study, genetic expression changes were found in neurons of the rat premotor area 7 days post-infarct of the primary motor area ischemic infarct when compared to control animals (Urban ET, 3rd *et al.* 2012). These changes were consistent with axonal reorganization, and it is reasonable to expect anatomical changes to be present.

In the current study, we created ischemic lesions in the primary motor cortex controlling the forelimb and examine the corticocortical connectivity of the premotor area controlling the forelimb (RFA). Using a semi-quantitative method for counting axonal boutons within a superficial layer of tangentially sectioned cortex, we show the RFA of lesion animals connects in significantly different ways 1 month post-lesion, when compared to control animals. Retrograde connectivity, assessed by counting neuronal somata, also shows significant changes in animals with ischemic lesions.

Materials and Methods

Ad libitum food and water were provided to 12 adult male Long-Evans

Hooded rats (370-450 g, 3.5 months old, Harlan, Indianapolis, IN). Rats were singly-housed with a 12hr:12hr light:dark cycle. Animal use was approved by the Institutional Animal Care and Use Committee of the University of Kansas Medical Center.

Surgical Procedure I

The surgical procedure was described in detail in previous studies (Urban ET, 3rd *et al.* 2012). Sedation by inhaled isoflurane was followed by anesthesia with ketamine [100-80 mg/kg, intramuscularly (IM)] and xylazine [30 mg/kg, intraperitoneal (IP)]. Doses of ketamine (20 mg/kg IM) were provided throughout the procedure as needed to maintain stable anesthetic depth. The rat was secured in a stereotaxic frame, then Bupivacaine (2.5 mg, local anesthetic) was applied to the scalp. Physiological body temperature was maintained with a homeothermic blanket system. Scalp incision and reflection, was followed by release of muscles attached to temporal and occipital ridges. The cisterna magna was opened to relieve cerebrospinal fluid pressure, and craniotomy performed anterior posterior to Bregma, +5 and -4 mm respectively, and laterally from 1 mm lateral of the sagittal suture to the temporal ridge. After dura reflection, warm sterile silicone oil was applied to the cortical surface.

Motor and premotor areas were identified by intracortical microstimulation (ICMS) (Urban ET, 3rd *et al.* 2012). A digital photomicrograph of the cortical surface vasculature was taken through the surgical microscope. The image was overlaid with a grid pattern (250 μm) in image software (Canvas, Deneba

Software, Miami, FL). A glass electrode, which was tapered to 20 μm outside diameter, beveled and filled with concentrated saline solution (3.5 M), was inserted 1725 μm below the cortical surface at every other grid intersection to give a resolution of 500 μm. A pulse train of 40 msec duration, made of 13 monophasic cathodal pulses (200 μsec duration, 350 Hz) was delivered at 1 Hz from an electrically isolated, charge-balanced, constant-current stimulation circuit (BSI-2, Bak Electronics Inc, Mount Airy, MD). Current was increased from 0 μA until a visible movement was recorded, then decreased until the movement was no longer visible. “Nonresponsive” sites had no elicited movements at the maximum current level of 80μA.

The RFA and FIA (CFA of others) size and location were consistent with previous reports from this lab and others (Neafsey EJ and C Sievert 1982; Nishibe M *et al.* 2010). RFA was found between +3.7 and +2.7 mm anterior to Bregma and 2 to 4 mm lateral of the sagittal suture. FIA was located anterior posterior to Bregma +2.7 and -1 mm respectively and laterally from 2 to 4.5 mm from the sagittal suture. CFA’s name was changed to FIA (Forelimb ICMS Area), because this ICMS responsive region overlapped the IZ, which is outside the classically defined sensorimotor overlap zone. The new name is reflective of the extended border.

Borders of RFA were defined, then a micropipette containing the neuronal tract tracer, biotinylated dextran amine, 10,000 MW (BDA10kDa, 10% w/v in 0.9% sterile saline) was placed in the approximate center of RFA. A glass micropipette tapered to 60μm outside diameter was attached with beeswax to a

1µL Hamilton syringe (30100, Hamilton Company, Reno, NV), and actuated by a microinjector (Micro4, World Precision Instruments, Sarasota, FL). A hydraulic Microdrive (650 Micropositioner, David Kopf Instruments, Tujunga, CA) on a stereotaxic arm was used to control injection depth. For control animals, pressure injection of BDA10kDa was accomplished in 3 boluses of 33.3 nL (100 nL total) at 1500, 1250 and 1000 µm below the cortical surface, and CTB-647 injections were delivered in 2 boluses of 75 nL (150 nL total) at 1500 and 1000µm below the pia. Fiducial marker, cholera toxin beta subunit conjugated to AlexaFluor 647 (CTB647, 5 µg/µL in 0.9% sterile saline, C34778, Invitrogen, Grand Island, NY), was injected (same configuration as used with BDA10kDa) at 2 sites roughly 1mm caudal to the caudal border of FIA, and separated by 1mm from each other. For lesion animals, the fiducial marker injection was the same, but no BDA10kDa was injected at this point. Instead of BDA10kDa, the vasoconstrictor, endothelin-1 (ET-1) was injected for lesion animals, while BDA10kDa was injected during Surgical Procedure II, described below. A glass micropipette tapered to160 µm outside diameter was secured with wax to a 2 µL Hamilton syringe filled with ET-1 (0.33 mg/mL 0.9% sterile saline, H-6995, Bachem Americas, Inc, Torrance, CA), and attached to a microinjector clamped to a microdrive on a stereotaxic arm. Four to five ET-1 injections sites, determined by the size of the CFA, exposed most of the FIA to ischemic damage. The micropipette tip was lowered perpendicularly to 1500 µm below the cortical surface. ET-1 was injected at 5 nL/sec in three 110 nL boluses. There was a 1 min delay between boluses, and a 5 min delay before tip extraction. The craniotomy was flushed constantly with

sterile saline during the injection and delays to prevent non-specific spread of ET-1.

At the end of the procedure, the cortical surface was rinsed with warm sterile saline (0.9%) and a protective cap formed by placing a silicone sheet (Invotec International Inc, Jacksonville, FL), gel foam, (Surgifoam, Ethicon, Sommerville NJ) and dental acrylic and resin (Lang Dental Mfg Co Inc, Wheeling, IL) over the craniotomy. To close the incision, the skin was sutured, penicillin injected (45,000 U, SQ) into the nape of the neck and local anesthetic (Bupivicaine, 2.5mg, APP Pharmaceuticals, Schaumburg, IL) and topical antibiotic (Vetropolylycine gel, Dechra Veterinary Products, OP, KS) applied. Post procedural pain management was accomplished with Buprenorphine (0.05 mg/kg SQ, Reckitt Benckiser Farmaceuticals Inc, Richmond, VA) and acetaminophen (40 mg/kg oral). After allowing the rat to recover on the heating pad until alert and moving spontaneously, it was returned to its home cage. Buprenorphine and Acetaminophen were given an additional 3 times during the subsequent 48 hours.

Surgical Procedure II (Lesion Animal BDA10kDa Injection)

Lesion group animals (n=6) underwent a second surgical procedure 21 days after Surgical Procedure I. The 21-day interval allowed sufficient time for the lesion to mature and any axonal sprouting to occur (Fig. 1). A second procedure was not done to animals in the control group. The same protocol was followed as for Surgical Procedure I above, with some minor changes. As the craniotomy

was performed during the Surgical Procedure I, removing the protective cap from the cranium re-exposed the cortex. As ICMS, ET-1 injection and fiducial marker injection were done during the Surgical Procedure I, these were not repeated. BDA10kDa was injected the same as stated in Surgical Procedure I, and the blood vessel pattern in the photomicrograph taken during that procedure was used as guidance of injection placement. The craniotomy cap formation, incision closure and post-procedure recovery were the same as stated for Surgical Procedure I above.

A Lesion Animals

B Control Animals

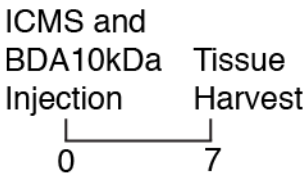

Fig. 1 The experimental time line. Lesion animals (**A**) underwent the 1st surgical procedure involving ICMS mapping and lesioning on day 0. On day 21 the cortex was re-exposed and BDA10kDa injected into RFA. The tissue was harvested on day 28. Control animals (**B**) underwent the 1st surgical procedures involving ICMS mapping and BDA10kDa injection into RFA. This ensured enough time for any reorganization to take place in lesion animals, allowed adequate time for tract tracer transport, and equalized tract tracer transport time for both groups.

Histology

Tissue Harvest

Seven days after Surgical Procedure I (control animals) or Surgical Procedure II (lesion animals), rats were sedated with isoflurane, and euthanized with Beuthenasia-D (390mg pentobarbital, 50mg phenytoin sodium IP, Shering Plough Animal Health, Union, NJ). The rib cage was reflected, the heart was exposed, heparin sodium (500 USP Units, Hospira Inc, IL) was injected into the left ventricle, and animal exsanguinated by transcardial perfusion of saline solution [0.9% saline in distilled water, heparin sodium (1,000 USP Units, APP Pharmaceuticals, Schaumburg, IL) and lidocaine HCl (20 mg, APP Pharmaceuticals, Lake Forest, IL)] followed by 3% paraformaldehyde in 0.9% saline. After brain extraction, underlying structures of both hemispheres were separated from the cortex. The cortices were flattened between glass slides and exposed to 4% paraformaldehyde-20% glycerol in 0.9% saline (2 hr), 20% glycerol-2% dimethylsulfoxide in 0.9% saline (overnight), and 20% glycerol in 0.9% saline (24 hr). Cortices were sectioned at 50 μm thickness on a freezing microtome chilled with dry ice, and sections were placed in 0.1 M PBS solution and refrigerated (4°C) until processed further.

Cytochrome Oxidase Staining

Sections were floated in 0.1 M PBS solution, and inspected with the unaided eye for the S1 representation (visible as slightly opaque white areas

within the translucent section). Three to four sections per cortex with the most complete representations were chosen for cytochrome oxidase (CO) staining. Sections were rinsed (2 x 10 min in 0.1 M PBS), and reacted with CO solution at 37°C [cytochrome c oxidase (20 mg, Sigma, #C2506-500MG), sucrose (4 g, Fisher Scientific), and DAB (50 mg) per 100 mL of 0.1 M phosphate buffered distilled water (pH 7.4)] until dark CO-rich areas were easily detectable against the lighter background (2-3 hours). Then, sections were rinsed (2 x 10 min) in 0.1 M PBS.

BDA10kDa Visualization

Every section underwent an Avidin-Biotin Complex (ABC) linked staining procedure with 3,3' Diaminobenzidine (DAB, MP Biomedicals, Solon, OH, #980681) reaction product as the chromogen. After rinsing sections in 0.1 M PBS (2 x 10 min with agitation), they were exposed to 0.4% Triton X-100 (Sigma, #X100-500ML) in 0.05 M PBS for 1 hr with agitation. After rinsing sections in 0.1 M PBS (3 x 10 min, with agitation), they were incubated overnight in 0.1 M PBS with reagents "A" and "B" added according to Vectastain Elite Kit (Vector Laboratories, Burlingame, CA, #PK6100). After rinsing sections (4 x 10 min, 0.1 M PBS), they were exposed to DAB solution (0.05% w/v DAB and 0.01% v/v H_2O_2 in 0.1 M PBS), and wet mounted in 0.05 M PBS onto subbed slides, then allowed to dry overnight.

BDA10kDa Signal Intensification

After slide-mounted sections were dehydrated in ascending alcohol concentrations (50%, 70%, 95% and 100% for 5 min each), they were cleared with xylene (5 min), and rehydrated in descending alcohol concentrations. Sections were exposed for 1hr in 1.42% silver nitrate in distilled water (55°C), rinsed in distilled water (15 min), exposed to 0.2% gold chloride (10 min), rinsed in distilled water (15 min), exposed to sodium thiosulfate (5 min), and rinsed in distilled water (15 min). Sections were dehydrated again, as before, cleared in xylene, and coverslipped with DPX mounting medium (Sigma, #44581-500ML).

Quantification

Alignment Procedure

BDA10kDa and CTB647 injection cores were used as fiducial markers to align the ICMS maps and section outlines containing voxel counts, somata counts, and CO-rich zones. The CTB647 and BDA10kDa injection cores were marked on all ICMS maps and section outlines. The overlap procedure was accomplished in Photoshop (Adobe). The ICMS map was scaled and rotated until the 3 injection cores were in register with other outlines. Symbols present in and around RFA and FIA aided in transferring the position of RFA and FIA back to StereoInvestigator.

Bouton and Soma Quantification

A computerized microscope (Axiophot 2, Zeiss) and stereology program (Stereoinvestigator, Microbrightfield) was used to trace flattened section outlines, then a 100 μm square grid was overlaid on the outlines. Each voxel with dimensions 100 x 100 x 50 μm was examined throughout the section.

BDA10kDa labeled axons appear as thin dark lines (Fig 2). A bouton (or varicosity) was defined as a dark (chromogen dense), round object, about twice as wide as the axon on either side of it (i.e. en passant bouton), or at the end of a thin projection attached to the main axon (i.e. terminal bouton). Boutons were counted semi-quantitatively within each 100 μm x 100 μm x 50 μm voxel (section thickness is 50 μm). Blue dots were used to mark voxels containing 2-30 boutons, while red dots were used to mark voxel containing greater than 30 boutons.

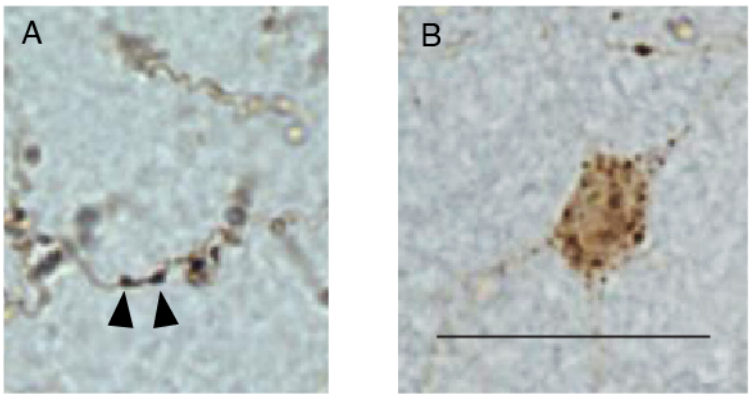
A
B

Fig. 2 Bouton and neuronal somata identification with BDA10kDa tract tracer. **A**. The photomicrograph displays boutons in tangential section seen at 40x magnification. Boutons are identified as dark, circular varicosities (arrowheads) attached at either side to an axon (dark thin line, en passant bouton) or at the end of thin projection off the main axon (not shown, terminal bouton). **B**. The photomicrograph displays a back-filled neuronal soma in tangential section seen at 40x magnification. Somata (brown density in center) are identified as granular, circular densities with evidence of at least one cellular projection. Bar is 25 μm, same for A and B.

BDA10kDa is an effective anterograde tract tracer, though retrograde labeling does occurs. Therefore, BDA-labeled somata were plotted on the same section as boutons. Somata were counted if they had a confluently dark, smooth-edged shape, and evidence of at least one thin projection (Dancause N *et al.* 2006b). BDA-labeled somata were marked with a green dot.

The distribution of BDA-labeled boutons and somata forms a column of connectivity throughout the cortical laminae, similar to descriptions in previous connectivity studies in rat (Reep RL *et al.* 1987; Rouiller EM *et al.* 1993). Therefore, the current study uses one superficial layer section. It was deemed that a single section was representative of a particular animal's connectivity patterns. This approach was the most feasible, because of the extensive amount of time required to plot BDA-labeling in each section.

Region Nomenclature and Identification

Regions of interest nomenclature, location and description were procured from various sources in order to achieve the most accurate and reliable description. In order to identify all regions several criteria were used, including, ICMS response, CO staining, voxels clusters, region overlap and the spatial relationship to other identified regions. These regions are consistent with previously reported nomenclature.

Regions Identified as Cytochrome Oxidase Dense Zones

CO staining reveals dark zones in several regions of the cortex, including S1, VIS, RS, TP and Aud cortex. CO-dense zones are the histological representation of the sensory cortex (Li H and MC Crair 2011). In the middle of the flattened cortex, S1 is positioned as an inverted ratunculus (body representation of the rat) facing rostral. Hind limb and tail representations are medial, while head and face representations are lateral. Wider at its caudal edge, S1 tapers to the rostral aspect. Our S1 is consistent with previous work (Chapin JK and C-S Lin 1984; Remple MS *et al.* 2003; Krubitzer L *et al.* 2011). VIS is consistent with the Oc1M and Oc1B of Zilles (1985) pooled together (Zilles KJ 1985). TP is consistent with Krubitzer (Krubitzer L *et al.* 2011). Aud is consistent with Aud of Remple et al. (Remple MS *et al.* 2003), and Polley et al. (Polley DB *et al.* 2007). RS contains both a CO-dense and sparse region (Harley CA and CH Bielajew 1992).

Regions Identified by Topographic Relationships to Other Identified Regions

Some regions were identified by their spatial relationship to other regions. S1 was useful in identifying Fr and IN, because its extensive border, and consistent presence. Fr, and IN are consistent with Zilles 1985 (Zilles KJ 1985) with some modification. Zilles' Fr1, Fr2, and Fr3, and Cingulate cortex were pooled into our Fr. Zilles' Insular cortex AID and AIV were pooled with the rostral half of Vi to form our IN. To determine the border between IN and FR, a line was drawn from the mediorostral edge of S1 to a small consistent area of dense axons and boutons in the rostral pole.

A large portion of the caudal cortex is named CAS, which borders FRO, PM, PL, Aud, PV, PR, the rhinal fissure, TP, VIS, and RS. This cortex has neither dense CO staining or readily identifiable clusters of voxels. The region is made up of association areas with indeterminate borders with the current borders and the name is reflective of that: Oc2MM, Oc2ML, Oc2L, Te2, and Te3(Zilles KJ 1985).

Neither the piriform nor olefactory bulb were removed during sectioning and thus included in the analysis for completeness sake. There is negligible connectivity to either area, so the areas lateral to the rhinal fissure are pooled together as PirOl, excluding the PRh.

Analysis

Calculation of Cortical Surface Area for each Region of Interest

Areal representations of the regions of interest was determined using the image processing programs Adobe Illustrator and NIH Image J. The region borders were first outlined in StereoInvestigator, and imported into Adobe Illustrator, and then the area (in mm^2) of each region was measured with Image J.

Stereological Estimates of Bouton Counts in Selected Regions

The connectivity of certain regions of interest were further investigated with unbiased stereological techniques for estimates of bouton counts. Although

the cut thickness of sections was 50 μm, actual thickness was measured on every-other counting field. The same computerized microscope and stereology program described above was used. After alignment procedures and region of interest borders were determined, the regions of interest outlines were applied to each section. Sections 8-24 of each animal were found to be consistent and complete in each animal and every other section was used for the analysis. Boutons were counted with the Optical Fractionator probe at 100 x magnification. The counting frame was 14 x 14 μm square, and both top and bottom guard zones were set at 3μm. The SRS grid layout was set to distances that would give 15-30 counting frames per region of interest. After Optical Fractionator parameters were established for a particular region of interest for a particular animal, they were constant through all sections of that animal. The parameters were adjusted for different animals' regions of interest to maintain a similar number of counting frames per region of interest throughout the study.

Lesion Volume and Dye Core Volume Estimate

The volumes of the lesion and dye core were both estimated in the same way. The same computerized microscope and stereology program was used as described above. Lesion outlines were traced on every other section from 8-24 as before. BDA10kDa staining led to darkening of all cortical tissue. This darkening was used to discriminate normal tissue from lesion tissue. The lesion was identified by the absence of tissue in the appropriate location. It also included lighter stained tissue around the edges of the infarct hole, which may or

may not have contained darkly staining lesional debris or multiple cells consistent in morphology with lymphocytes (darkly staining, small, round objects). Recognition of lesion extent by such color difference on CO-stained sections has previously been reported (Katsman D et al. 2003). Again, sections 8-24 were consistent through animals. The area of each lesion outline was estimated using the Cavalieri Probe with Stereo Investigator.

The dye core estimate was done in the same manner as described for lesion volume. The dye core was identified as the densely colored area where neuronal morphology was not discernable (Dancause N et al. 2006).

Statistical Analysis of Voxel and Soma Counts

Voxel and soma counts were normalized to the surface area of the region of interest. The statistical program, JMP (v10, SAS Institute), was used to examine the values (voxels/mm^2, somata/mm^2). The variance in the different regions was determined to be unequal (O'Brien test, $F = 4.34$; $p < 0.0001$), so the Wilcoxon Rank-sum test, a nonparametric analysis, was used to compare values in the different regions. Z-scores generated were used to define cutoff levels for connectivity (dense, moderate, sparse and negligible).

Results

Lesion Volume

During Surgical Procedure I, the FIA (CFA of others) was found in a similar location to other reports (Urban ET, 3rd *et al.* 2012). ET-1 injection resulted in

consistently produced cell death, and cavitation in cortical tissue, through all layers of the cortex (Fang PC et al. 2010). The lesion volume was 1.86 mm^3 ± 0.74 mm^3 (mean ± standard deviation; n=6).

Based on CO staining of S1 cortex and ICMS map registration, the ischemic territory encompassed the entire rostral extent of FIA, but only partly encroach upon the CFA/S1 overlap zone (CFAOv). Rostrally, the lesion extended to the caudal border of RFA in four animals and encroached into the lateral portion of RFA in two animals. Medially, the lesion extended to or just before the upper medial border of the FIA. Laterally, the lesion ended just before the lateral border of FIA. Caudally, the lesion extended past the caudal border in three animals and ended just before the caudal border in three animals.

Dye Core Volume

Dye core volume was also assessed. For the lesion group, the dye core volume was 1.11 x 10^8 mm^3 + 1.16 x 10^7 mm^3 (mean + SEM; n=6), and the control group, the dye core volume was 7.66 x 10^7 mm^3 + 7.54 x 10^6 mm^3 (mean + SEM; n=6). The difference between groups was not significant (ANOVA, F = 3.3025, P = 0992).

Lesion Induced Changes to Regions of Interest

Anterograde and retrograde connectivity of RFA in both control and lesion animals was counted and projected onto the cortical surface. The anterograde connectivity in both groups was qualitatively similar (Fig 3). Projections of RFA to other brain regions were most prominent to the primary motor region, and higher order somatosensory areas. RFA projections were least to the special sensory cortex, and PirOl. The retrograde connectivity in both groups was also qualitatively similar (Fig 4). Regions projecting to RFA followed the anterograde connectivity closely. Those regions projecting to RFA were the same regions, which received anterograde connectivity from RFA.

Lesion Induced Change in Area of Region of Interest

To determine if the lesion itself significantly changed the area of regions of interest in the rat cortex, the area of regions was compared in lesion and control animals. There was a significant ($p<0.05$) decrease in area for both S1HO and IZO in lesion animals when compared to control animals (Fig. 5). The area of PV was not significantly changed in lesion animals when compared to control animals (Fig. 5). Other regions of interest were not significantly changed.

Lesion Induced Change in Voxel and Soma Count

Connectivity from RFA to several regions of interest was significantly different in lesion animals when compared to control animals. When comparing the least squared means of voxel and soma counts per region of interest, it was

found that the size of the region of interest itself was a covariate. This covariate was accounted for by using ANCOVA.

Voxel counts were compared between control and lesion groups using ANCOVA with area of the region as the covariate. There was a significant increase for IN in red voxels, and an increase in red voxels for CAS after lesion compared to control animals (Fig. 6). Total voxels for PirOl and red voxels for PR were significantly ($p<0.05$) reduced after lesion compared to control regions (Fig. 6). Although total voxels for IN was not significantly different after lesion compared to control animals, there was a trend for significance with $p=0.085$.

Neuronal soma counts were compared between control and lesion groups using ANCOVA with area of the region as the covariate. Soma number was significantly reduced in FRO, IZO, and PM in lesion animals when compared to control animals (Fig. 7). IN showed a trend toward a significant increase in soma number in lesion animals compared to control animals with a $p=0.071$ (Fig. 7).

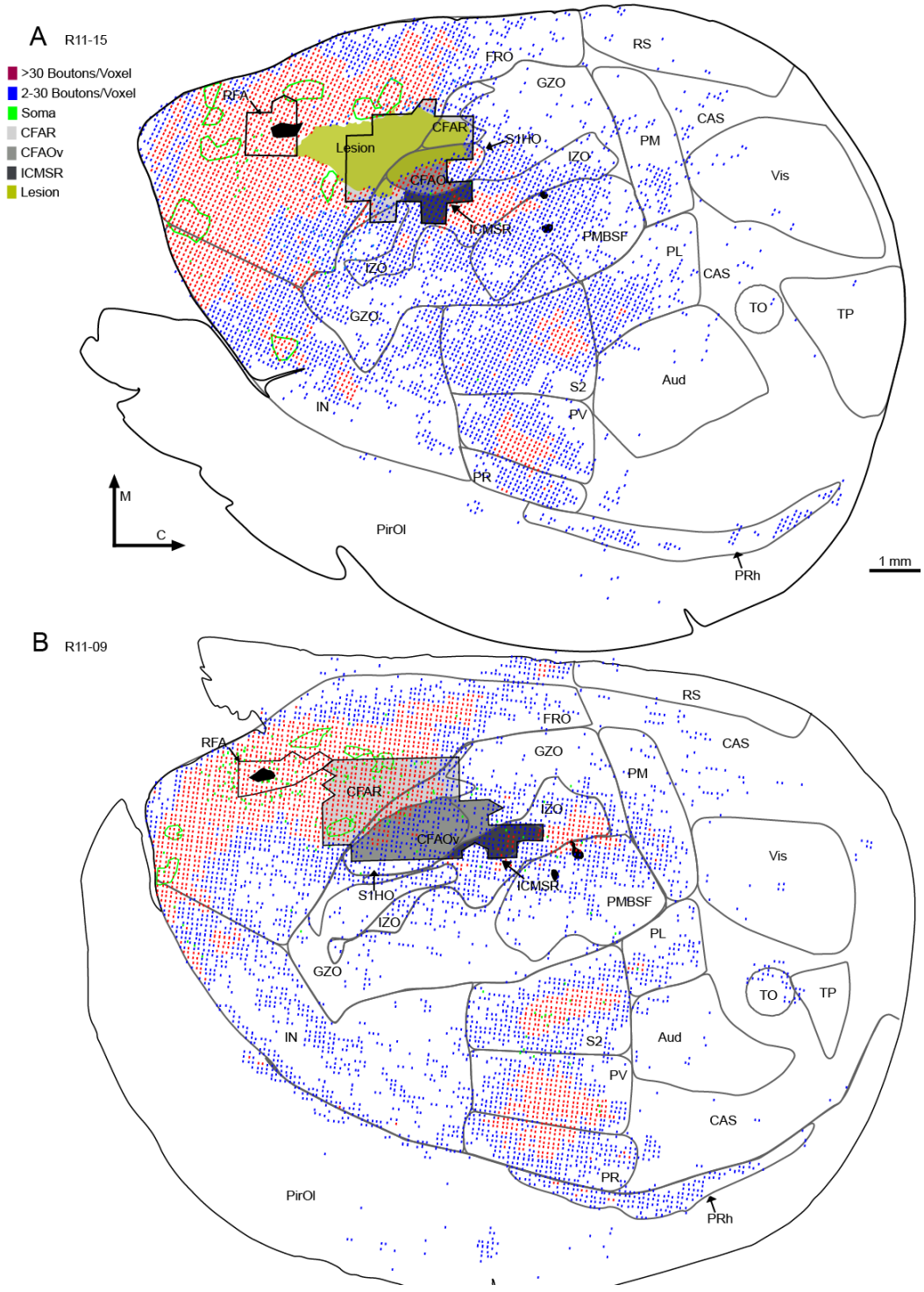
A
R11-15
>30 Boutons/Voxel
2-30 Boutons/Voxel
Soma
CFAR
CFAOv
ICMSR
Lesion
RFA
Lesion
CFAR
S1HO
FRO
GZO
IZO
CFAOv
ICMSR
RS
CAS
PM
Vis
PMBSF
PL
CAS
TO
TP
Aud
S2
PV
PR
IN
PirOl
PRh
M
C
1 mm
B
R11-09
RS
FRO
RFA
CAS
GZO
PM
CFAR
IZO
CFAOv
Vis
S1HO
ICMSR
PMBSF
IZO
PL
GZO
TO
TP
IN
S2
Aud
PV
CAS
PR
PirOl
PRh

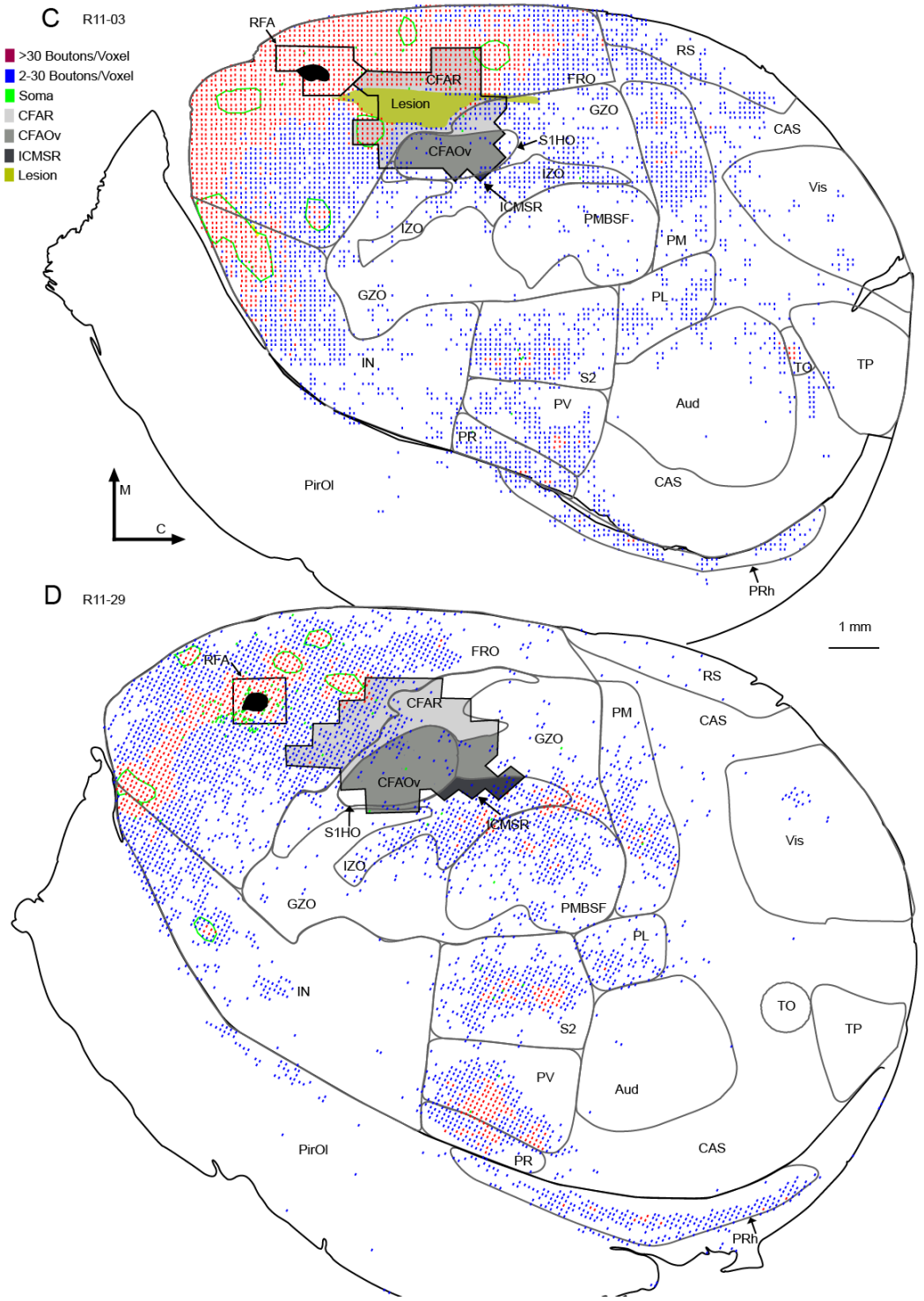
C
R11-03
>30 Boutons/Voxel
2-30 Boutons/Voxel
Soma
CFAR
CFAOv
ICMSR
Lesion
RFA
CFAR
Lesion
FRO
GZO
RS
CAS
S1HO
CFAOv
IZO
Vis
ICMSR
PMBSF
IZO
PM
GZO
PL
IN
S2
TO
TP
PV
Aud
PR
CAS
PirOl
M
C
PRh
D
R11-29
1 mm
RFA
FRO
RS
CFAR
PM
CAS
GZO
CFAOv
S1HO
ICMSR
Vis
IZO
GZO
PMBSF
PL
IN
TO
TP
S2
PV
Aud
PirOl
PR
CAS
PRh

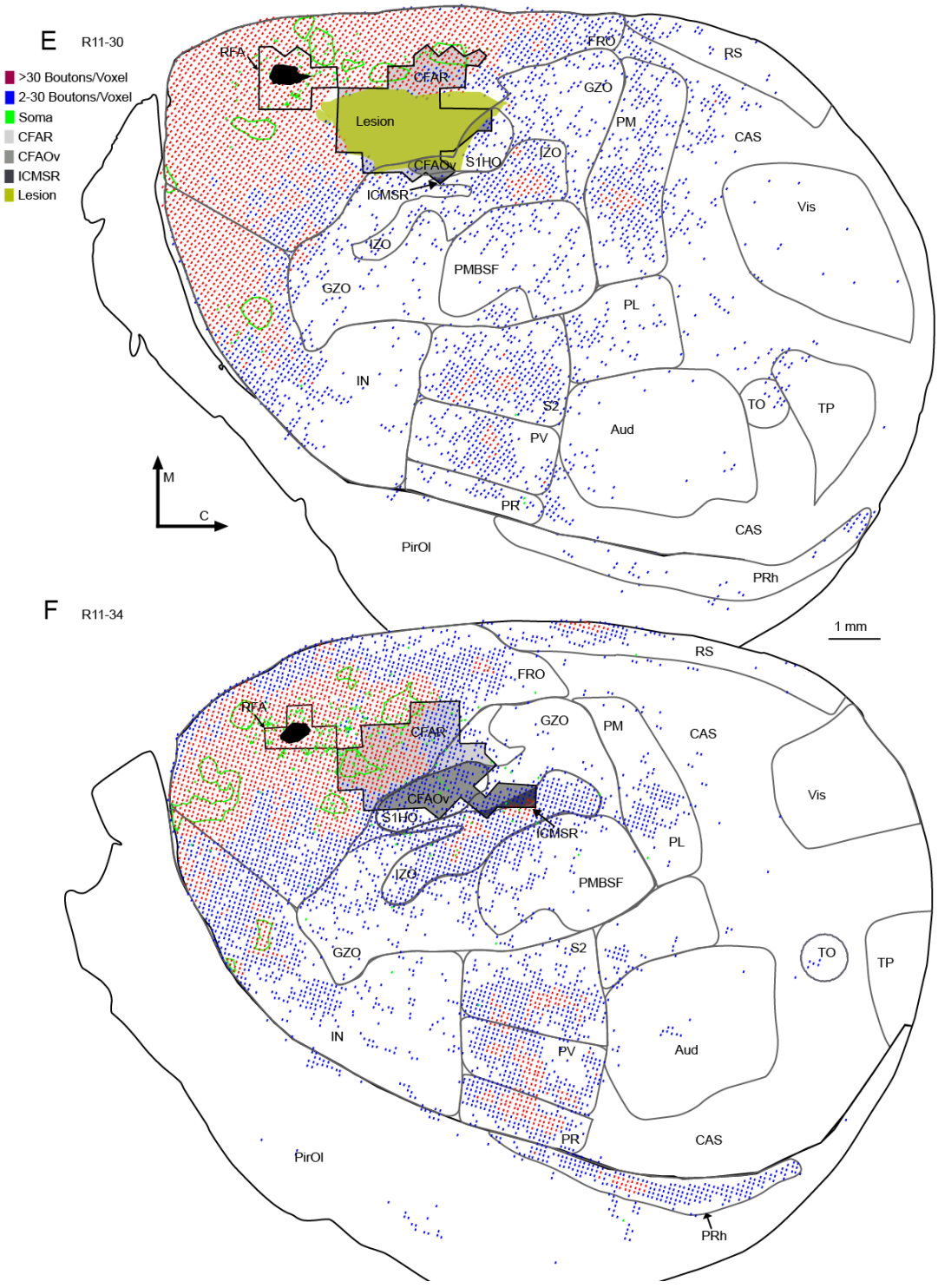
E
R11-30
>30 Boutons/Voxel
2-30 Boutons/Voxel
Soma
CFAR
CFAOv
ICMSR
Lesion
RFA
CFAR
Lesion
CFAOv
S1HO
ICMSR
FRO
RS
GZO
PM
CAS
IZO
Vis
PMBSF
GZO
PL
IN
S2
TO
TP
PV
Aud
M
C
PR
CAS
PirOl
PRh
F
R11-34
1 mm
RS
FRO
RFA
GZO
PM
CAS
CFAR
Vis
CFAOv
S1HO
ICMSR
PL
IZO
PMBSF
GZO
S2
TO
TP
IN
PV
Aud
PR
CAS
PirOl
PRh

Fig. 3 Anterograde RFA connectivity patterns with cortical regions on tangential section in control and lesion animals. **A-F**. Each lesion animal outline (R11-15, **A**; R11-03, **C**; R11-30, **E**) is displayed on the same page as a control animal outline (R11-09, **B**; R11-29, **D**; R11-34, **F**). The flattened section outline (black outline) surrounds the labeled regions (grey lines). The borders of RFA (black outline), and divisions of FIA (black outline) are labeled (CFAR, light grey; CFAOv medium grey; ICMSR, dark grey). Voxels containing 2-30 boutons (blue dots) and voxels containing >30 boutons (red dots) are labeled throughout the section, while the core of BDA10kDa (black dot) is within RFA. The lesion (yellow-green), when present, is centered in the CFAR. Medial (M, up) and caudal (C, right) are labeled on directional arrows. The Bar is 1mm.

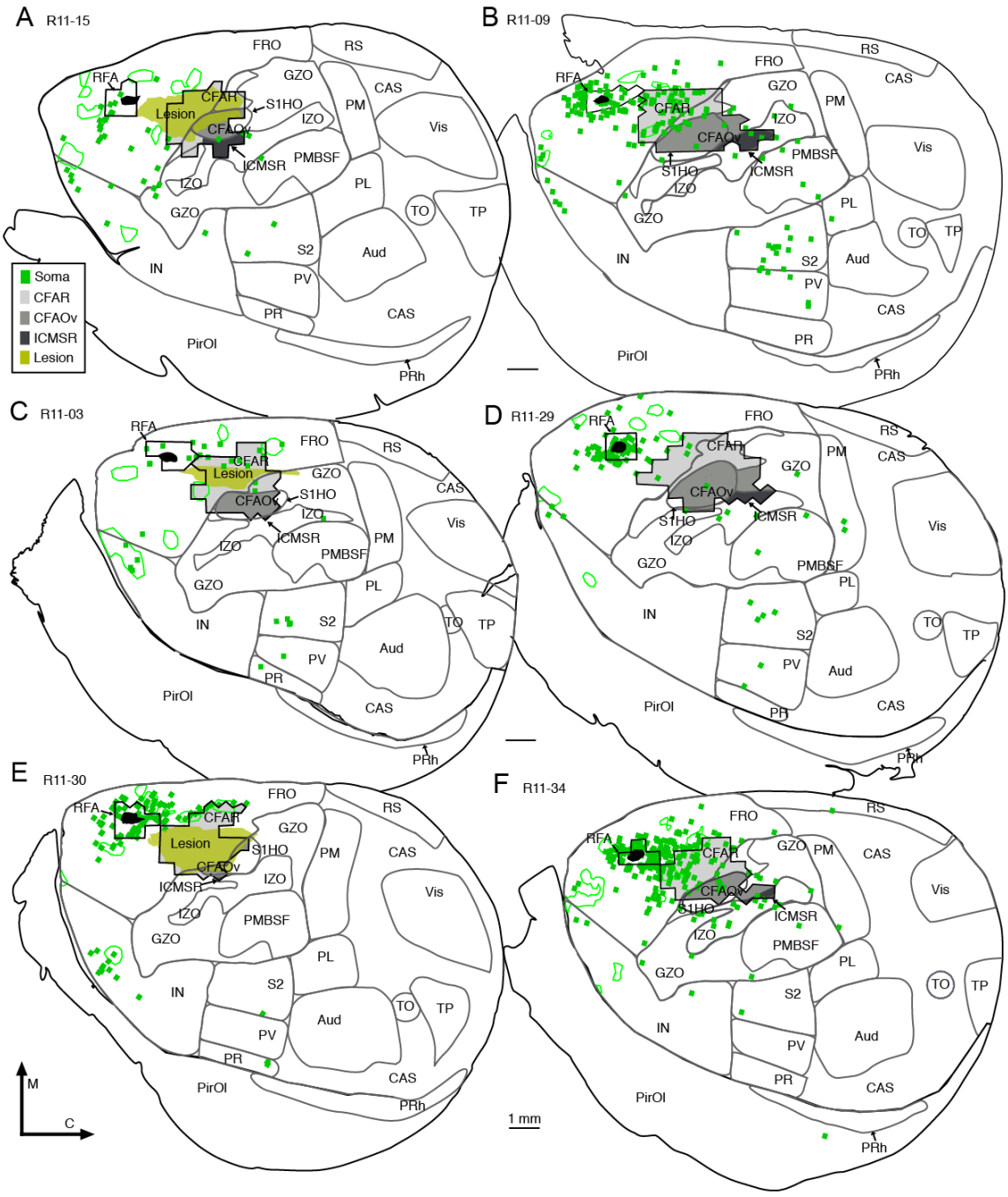
A R11-15
B R11-09
C R11-03
D R11-29
E R11-30
F R11-34
Soma
CFAR
CFAOv
ICMSR
Lesion
RFA
FRO
RS
GZO
CAS
CFAR
Lesion
S1HO
IZO
PM
Vis
CFAOv
ICMSR
PMBSF
IZO
PL
GZO
TO
TP
S2
Aud
IN
PV
PR
CAS
PirOl
PRh
M
C
1 mm

Fig. 4 Retrograde RFA connectivity patterns with cortical regions on tangential section in control and lesion animals. **A-F**. Lesion animal outlines are displayed to the left (R11-15, **A**; R11-03, **C**; R11-30, **E**) of control animal outlines (R11-09, **B**; R11-29, **D**; R11-34, **F**). Each flattened section outline (black outline) surrounds the labeled regions (grey lines). The borders of RFA (black outline), and divisions of FIA (black outline) are labeled (CFAR, light grey; CFAOv medium grey; ICMSR, dark grey). Somata (green dots) are labeled throughout the section, while the core of BDA10kDa (black dot) is within RFA. The lesion (yellow-green), when present, is centered in the CFAR. Medial (M, up) and caudal (C, right) are labeled on directional arrows. The Bar is 1mm.

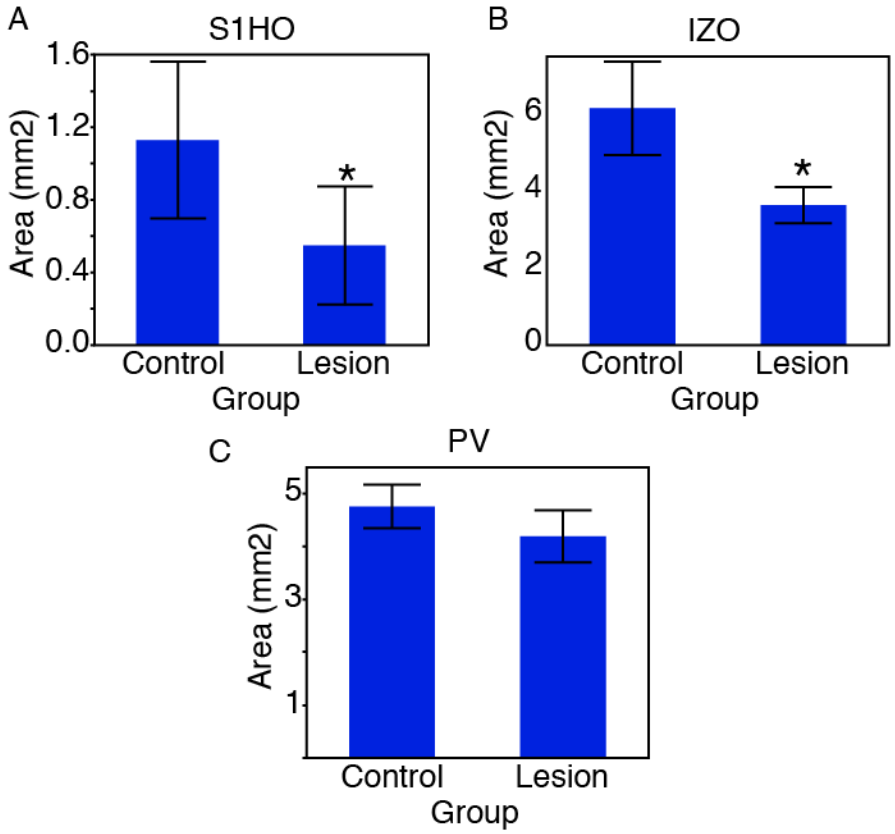
A
S1HO
Area (mm2)
1.6
1.2
0.8
0.4
0.0
*
Control
Lesion
Group
B
IZO
Area (mm2)
6
4
2
0
*
Control
Lesion
Group
C
PV
Area (mm2)
5
3
1
Control
Lesion
Group

Fig. 5 Histograms showing change in the area of regions between control and lesion groups. A significant decrease ($p < 0.05$) in area was identified for both S1HO and IZO of lesion animals when compared to control animals using ANOVA. Area (mm^2) means ± SEM (box and whisker) are plotted versus group for regions S1HO (**A**), IZO (**B**), and PV (**C**). Significance difference ($p < 0.05$) between control and lesion groups is designated by "*".

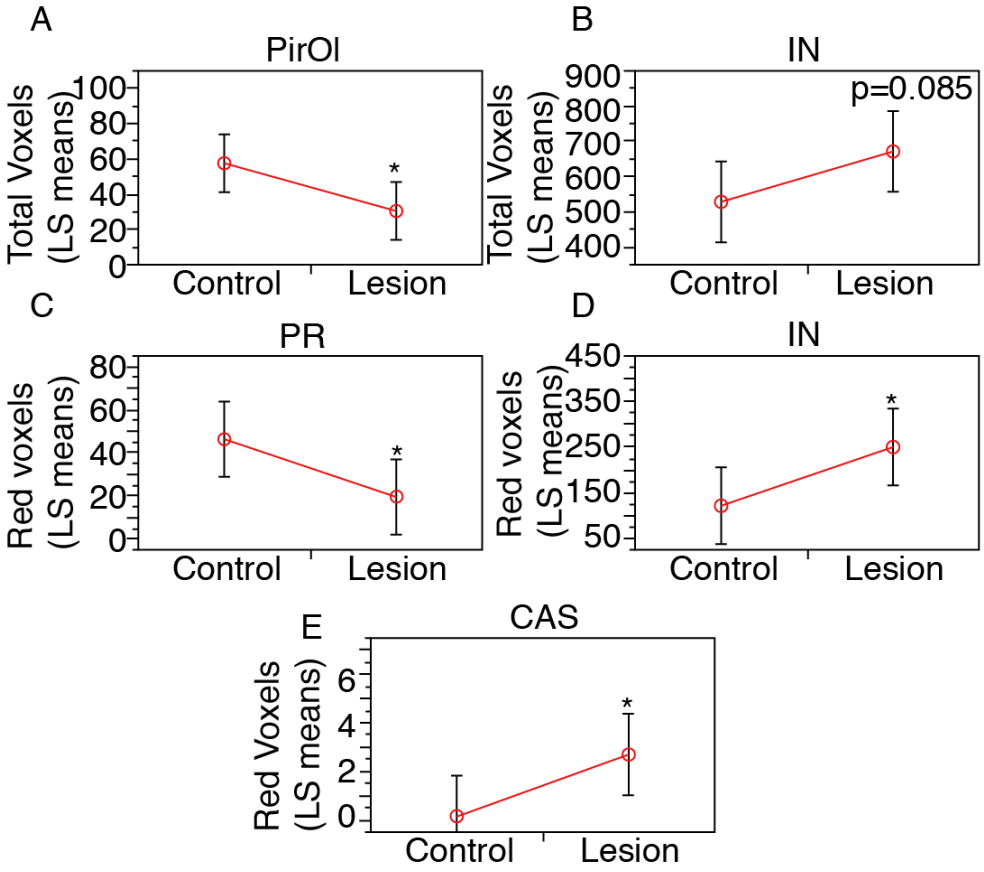
A
PirOl
Total Voxels (LS means)
100
80
60
40
20
0
*
Control
Lesion
B
IN
p=0.085
Total Voxels (LS means)
900
800
700
600
500
400
Control
Lesion
C
PR
Red voxels (LS means)
80
60
40
20
0
*
Control
Lesion
D
IN
Red voxels (LS means)
450
350
250
150
50
*
Control
Lesion
E
CAS
Red Voxels (LS means)
6
4
2
0
*
Control
Lesion

Fig. 6 Point and whisker plots showing voxel counts differences within cortical regions in lesion animals. Voxels counts, least square mean ± SEM (point and whisker), are plotted versus group. A significant difference ($p < 0.05$) between control and lesion group least squared means was identified with ANCOVA using area of the region as covariate. Total voxels within PirOl (**A**) were significantly decreased, red voxels within PR (**C**) were significantly reduced, red voxels were significantly increased within IN (**D**), and red voxels were significantly increased within CAS (**E**) after lesion. There was a trend towards increase in total voxels within IN (**B**), $p = 0.085$. Significant difference ($p < 0.05$) between control and lesion groups is designated by "*".

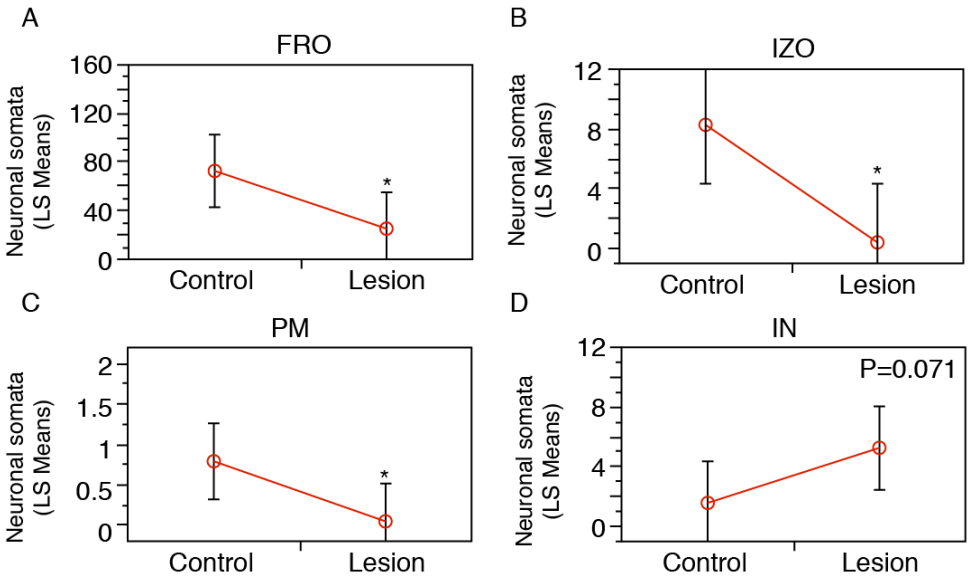
A
FRO
Neuronal somata (LS Means)
160
120
80
40
0
Control
Lesion
*
B
IZO
Neuronal somata (LS Means)
12
8
4
0
Control
Lesion
*
C
PM
Neuronal somata (LS Means)
2
1.5
1
0.5
0
Control
Lesion
*
D
IN
P=0.071
Neuronal somata (LS Means)
12
8
4
0
Control
Lesion

Fig. 7 Point and whisker plots showing differences in neuronal somata counts within cortical regions in lesion animals. Neuronal somata counts, least square mean ± SEM (point and whisker), are plotted versus group. A significant difference ($p < 0.05$) between control and lesion group least squared means was identified with ANCOVA, using the regions' area as covariate. Neuronal somata were significantly decreased within FRO (**A**), IZO (**B**), and PM (**C**) after lesion. There was a trend towards increase in neuronal somata within IN (**D**), $p = 0.071$. Significant difference ($p < 0.05$) between control and lesion groups is designated by "*".

Discussion

The current study demonstrated a significant difference in RFA connectivity in animals with primary motor cortex ischemic infarct compared to control animals. There is a significant ($p=0.05$) reduction in total voxels with labeled terminal boutons within PirOl, red voxels within PR, and increase in red voxels within both CAS and IN, a trend towards a decrease ($p=0.071$) within PR, and a trend towards increase ($p=0.071$) in total voxels within IN in animals with ischemic infarct compared to control animals. There is also significant decrease ($p=0.05$) in neuronal somata within FRO, IZO and PM, and a trend toward increase ($p=0.071$) within IN in animals with ischemic infarct compared to control animals. This study provides evidence that anatomical connectivity from the RFA changes after ischemic infarct to the motor cortex in specific regions of the adult rat brain, while remaining stable in most cortical regions. These changes may provide an anatomical substrate for recovery of function after ischemic infarct.

Comparison of Rat and Primate Premotor Reorganization After Primary Motor Lesion

The connectivity patterns of PMv in primate and RFA in rat are remarkably similar. Dancause investigated the corticocortical connectivity patterns of PMv in Squirrel Monkey (Dancause N *et al.* 2006b). First, the regions projected to are

similar, PMv connected to M1, other frontal areas rostral to PMV, posterior operculum/inferior parietal cortex, S1, and posterior parietal regions. These regions have counterparts in the rodent and the RFA connects to each of them. Second, the density of connectivity to these regions is similar. PMv has major connections to M1, and frontal area rostral to PMv. This pattern is very similar to the pattern found to RFA with dense connectivity to FRO, and M1. Also, PMv has increased connectivity to the rostro-lateral M1, found in rats as dense connectivity to the rostral half of FIA, while the caudal half of FIA receives moderate connectivity. Further, PMv has only minor connectivity to S1, and so does RFA, as it sends sparse and negligible connectivity to GZO, PMBSF, and S1HO.

The notable differences between RFA and PMv connectivity occur in regards to regions that do not exist in both species. There are several other premotor regions that exist in the primate and have moderate connectivity, but not in the rodent (Dum RP and PL Strick 2002). PMv has moderate connectivity to CMA and PMD, (Dancause N *et al.* 2006a) (see their summary Figure 11). Also, the IZ/IZO of the rodent does not have an exact correlate in the primate, although it may be homologous to region 3a (Krubitzer L *et al.* 2011).

RFA and PMv similarities led the authors to hypothesize that ischemic infarct to primary motor cortex in rat would result in similar connectivity pattern changes as was shown after ischemic infarct in primate M1. In squirrel monkey, ischemic infarct in M1 hand area resulted in significant increase in PMv

connectivity to a subregion of the primary somatosensory cortex, within the hand representation of area 1/2 (Dancause N *et al.* 2005). In the current study, connectivity to S1HO or CFAOv was not significantly different after ischemic injury.

Despite the similarities in healthy animals, the difference in connectivity changes between RFA and PMv after ischemic infarct may be explained by several reasons. M1 of the primate connects to S1 area 1/2, but the PMv does not. Sensory information is necessary for proper motor control. Movement deficits result after lesioning the sensory cortex, without lesioning motor cortex. Since PMv does not connect directly to S1, connections from S1 to PMv would be indirect through other brain regions. The new connectivity patterns found after ischemic infarct of PMv, may represent the reintegration of the PMv with sensory information, thereby increasing the recovery of motor function.

This plausible line of reasoning would not be valid in the rat, and may account for the difference between species. The RFA connects to S1, as well as the CFA (our FIA). Rouiller determined that both RFA and CFA connect to the S1 to a similar extent (Rouiller EM *et al.* 1993). The connectivity pattern change after ischemic infarct in primate M1 may represent the reintegration of premotor cortex with somatosensory cortex, but the RFA maintains its connection to the somatosensory cortex after ischemic stroke (no significant difference in connectivity between stroke and control animals). The conditions and possible pressures inducing reintegration in primate may not be produced in the rat due to

this stable connectivity with S1. Therefore, the patterns of RFA connectivity did not change in a similar fashion as PMv.

Significance of Changes Within Brain Regions After Ischemic Infarct

Connectivity Changes

After cortical injury, RFA connectivity changes within several regions (Fig. 8). In general, this change may be beneficial, detrimental or epiphenomenal. We side with the beneficial interpretation of anatomical connectivity changes, because studies involving treatments to increase connectivity changes after injury showed increase in functional recovery (Zai L *et al.* 2009; Liu Z et al. 2010). Although we did not assess function in the current study, a model used in previous study showed recovery of function after ischemic infarct of the motor cortex with or without intervention (Fang PC *et al.* 2010). As such, the increased connectivity to certain regions in the current study may represent the unenhanced reorganization responsible for spontaneous recovery.

There is a possibility that such change represents exuberant sprouting after infarct. However, one would expect a significant increase in connectivity within most regions, if the infarct instigated unguided exuberant sprouting. This explanation of increased connectivity is less likely, as most regions show no significant change after infarct.

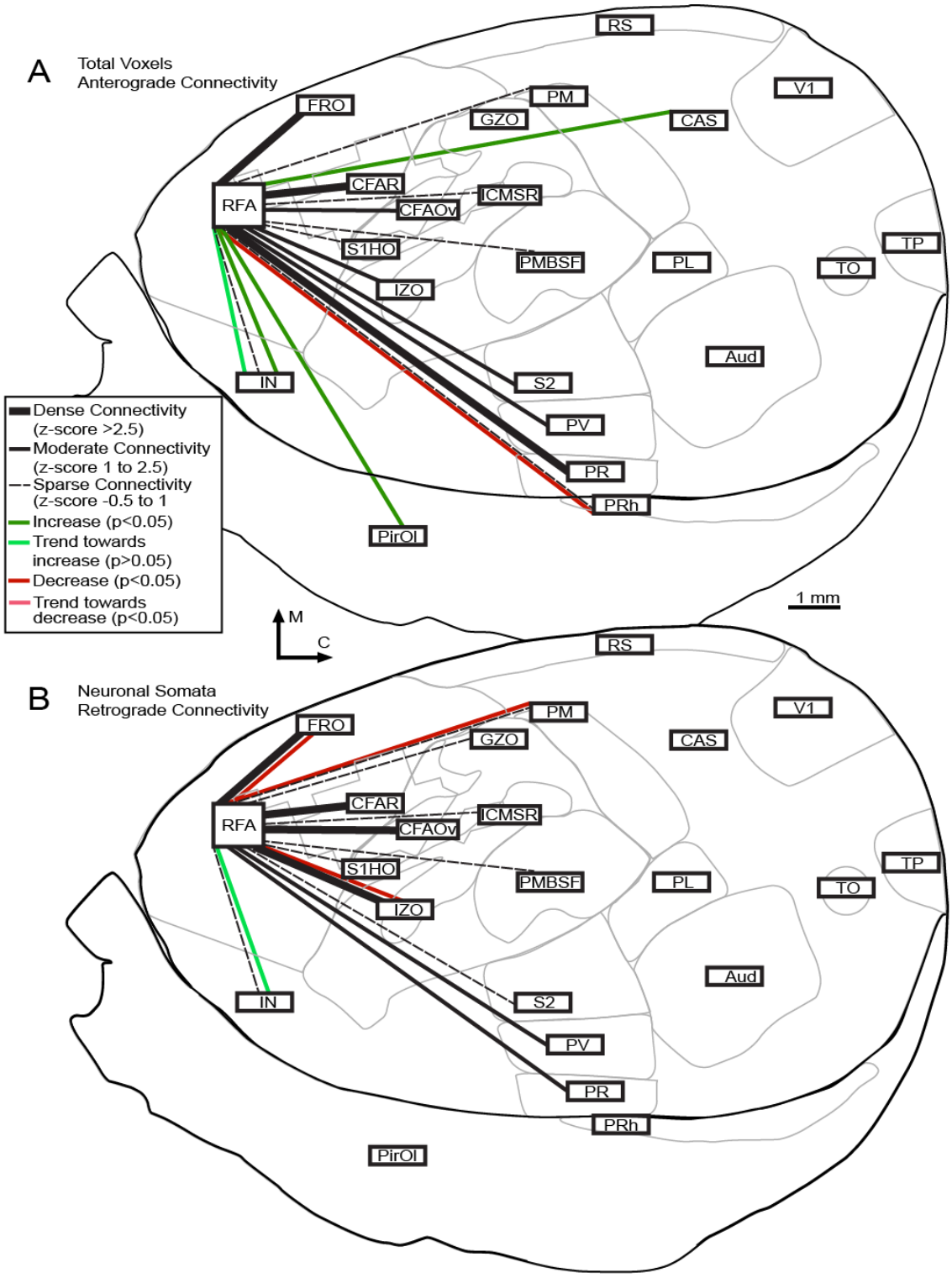
A
Total Voxels
Anterograde Connectivity
RS
V1
PM
FRO
GZO
CAS
CFAR
RFA
ICMSR
CFAOv
S1HO
PMBSF
PL
TP
TO
IZO
Aud
IN
S2
PV
PR
PRh
PirOl
Dense Connectivity (z-score >2.5)
Moderate Connectivity (z-score 1 to 2.5)
Sparse Connectivity (z-score -0.5 to 1
Increase (p<0.05)
Trend towards increase (p>0.05)
Decrease (p<0.05)
Trend towards decrease (p<0.05)
M
C
1 mm
B
Neuronal Somata
Retrograde Connectivity
RS
V1
PM
FRO
GZO
CAS
CFAR
RFA
ICMSR
CFAOv
S1HO
PMBSF
PL
TP
TO
IZO
Aud
IN
S2
PV
PR
PRh
PirOl

Fig. 8 Line drawings demonstrating the connectivity changes after ischemic infarct. Anterograde (**A**) and retrograde (**B**) connectivity changes overlaid on outlines of the flattened cortex (thin black line) and regions (grey outlines). Connectivity to regions in control animals is marked for dense (thick black line, z-score > 2.5), moderate (medium black line, z-score 1 to 2.5), and sparse (dotted black line, z-score -0.5 to 1). Connectivity changes to regions after infarct are marked as significantly increased ($p < 0.05$, green), trend towards increase ($p > 0.05$, light green), significantly decreased ($p < 0.05$, red), and trend towards decrease ($p > 0.05$, pink). The medial (M) and caudal (C) directions are labeled. Figure adjusted from (Urban et al., in process). Bar is 1mm.

Anterograde Connectivity Changes after Stroke

Increased connectivity to IN after infarct is an interesting finding. The current study found connectivity differences to IN after infarct. Connectivity significantly increased in red voxels with a trend towards increase (p=0.071) for total voxels and a trend towards increase (p=0.071) for neuronal somata. This increase is interesting in that regions with increased connectivity after stroke, if beneficial, suggest a restoration of lost integration between regions. RFA projections to IN have been previously reported (Rouiller EM *et al.* 1993) as a major difference between the primary motor and premotor cortex. The RFA is already heavily interconnected to the insular cortex, while the primary motor cortex is not (Rouiller EM *et al.* 1993). After FIA infarct, increased connectivity from RFA to IN would not represent reintegration, but a further strengthening of differential connectivity that was present before the lesion.

Increase to IN may not represent a reintegration of lost circuitry, but may be beneficial in other ways. IN contains visceral sensory, gustatory and aversive behavior functions. It has somatosensory, autonomic, visceral and limbic connections (Saper CB 1982). The IN has been suggested to be involved in both the consolidation and expression phases, but not the acquisition of fear memory (Alves FH et al. 2013). It may be that our experimental injury is such a strong aversive stimulus that the brain is rewiring to increase behavior to avoid noxious stimulus involving the forelimb in the future.

An increase in connectivity to CAS may also be beneficial. The current study found a significant increase in red voxels within CAS after infarct. The CAS, identified by exclusion, is a region in the caudal half of the brain of association cortex that could not be differentiated well with the current methods. It does not include any of the special sensory cortex of sight (Vis), or hearing (Aud). This region contains Te2, Te3, Oc2L, Oc2ML, and Oc2MM of Zilles (Zilles K 1990), and has been shown to be responsive to polysensory stimulation (Barth DS et al. 1995). Polysensory areas decrease reaction time to multimodal stimulation (Hirokawa J et al. 2008).

The current study found a decrease in connectivity to PR. Red voxels were significantly decreased, while neuronal somata displayed a trend for decrease. This region has been described in rats (Koralek K-A *et al.* 1990) and squirrel (Krubitzer LA *et al.* 1986). PR has been suggested to be a higher order processing center based on its connectivity to other somatosensory areas (Krubitzer LA *et al.* 1986). This decrease in connectivity may indicate a limit to reorganization. As only a finite number of neurons exist within RFA, there is only so much reorganization that can be produced. Connectivity to other areas may reorganize first, and the RFA's reorganization capacity may be reached. Connectivity to PR may have been withdrawn to supply other closer or more needy areas.

Retrograde Connectivity Changes after Stroke

Several of the regions (FRO, IZO and PM) have a significant decrease in neuronal somata when compared to control animals. While this could be an indication of the death of neurons or layer specificity, it could also be an indication of reorganization involving neurons projecting to the RFA. Neuronal cell death takes place through anterograde excitotoxicity. As the lesion progresses, neurons within the lesion core undergo anoxic depolarization. The process instigates release of neurotransmitters possibly resulting in overstimulation and excitotoxic cell death of neurons receiving anterograde signal. These three regions are interconnected with M1 as well as RFA, raising the possibility of this phenomenon. This explanation is less likely as similar models of small cortical infarct in areas with comparably high interconnectivity showed cell death only within the ischemic core and a thin layer of adjacent tissue (Katsman D *et al.* 2003).

The most parsimonious explanation of decreased connectivity would be disruption of the axons due to the lesion itself, concomitantly decreasing connectivity from both IZO and PM. The FIA, and therefore the lesion, is geographically directly between RFA and both the IZO and PM on the cortical surface. The most direct path for axons to travel from either region to RFA is directly through the FIA. If retraction of axons from a region produced a decrease in connectivity, then one would expect a similar axonal retraction with any axon coursing through the lesion territory. In such a case, both anterograde and retrograde connectivity would be reduced, but the results show anterograde

connectivity is not changed. This suggests that regions connecting to the RFA are undergoing reorganization. One could make the point that lower numbers of somata compared to voxels could be skewing this interpretation. Lower numbers of somata in each region could turn the absence of even one or two neurons into a significant difference, while large reductions in voxels are required to produce significant differences.

Alternatively, it is reasonable that decreased somata number indicates possible reorganization within these areas. It is unknown whether neurons located in distant regions that undergo reorganization are the same neurons connected to the lesion area. It is possible that distant regions reorganize by disconnecting from other regions not affected by the lesion. Neurons from the FRO, IZO and PM regions connected to RFA could have been induced to reorganize by retracting from RFA. Whether these neurons reconnect with another region after disconnecting from RFA is unknown with the current methods. This indicates that neurons directly connected to a lesion may not be the only neurons that reorganize after lesion. Neurons within uninjured regions and connected to uninjured regions may also participate in reorganization after ischemic infarct.

Changes in Area of Regions

Changes in the area of regions after stroke may represent important aspects of post infarct reorganization. We found a significant decrease in both

IZO and S1HO area after infarct compared to control animals. The most parsimonious explanation is that the lesion encroached upon both of these areas, and they were simply smaller in size after cavitation of the lesion. This is a less likely explanation, as other similarly affected regions did not show a similar decrease in area. The S1H is adjacent to the lesion along with the S1HO, but did not show a similar decrease. An alternative explanation is that some aspect of region has changed to actually shrink its size. Dendrites may have decreased with post-stroke pruning as was shown in contralateral cortex after ischemic infarct (Jones TA and T Schallert 1992). It may also be related to the movement of resident glia and inflammatory cells within these regions (Weston RM et al. 2007). This particular aspect of post stroke morphology may warrant further study.

Reorganization Without Considering Forepaw Dominance

Some may question the relevance of the current study, as it did not take into account forepaw preference. The current study lesioned the right hemisphere without determining the individual rat's dominant hemisphere. Studies in non-human primates carefully document hand preference and study the effect of lesion on the dominant hand.

There is some evidence to support that CNS lesion recovery is similar without considering hand preference. Whishaw showed that regardless of initial

forepaw preference on a reaching task, rats recovered similarly after lesion, even if the non-preferred forepaw was trained for the task that was tested (Whishaw IQ 1992). In other words, initial forepaw preference for a task did not change the recovery characteristics. This suggests, that unlike the lateralized non-human primate, the more quadruped rat displays less lateralization.

Reorganization Without Training

There has been much suggested about the essential role of experience to drive plasticity. Future work focused on differences after ischemic infarct with and without training will be an important next step, but the current study was to establish the general principle of corticocortical anatomical reorganization in this model of ischemic infarct. While the role of experience-driven reorganization is beyond the scope of the current study, it will be important in the future to understand how experience drives anatomical changes that occur spontaneously after cortical infarct.

Chapter 4

Gene Expression Changes After Stroke

Abstract (Urban ET, 3rd *et al.* 2012)

After cortical injury resulting from stroke, some recovery can occur and may involve spared areas of the cerebral cortex reorganizing to assume functions previously controlled by the damaged cortical areas. No studies have specifically assessed gene expression changes in remote neurons with axonal processes that terminate in the infarcted tissue, i.e., the subset of neurons most likely to be involved in regenerative processes. By physiologically identifying the primary motor area controlling forelimb function in adult rats (caudal forelimb area = CFA), and injecting a retrograde tract-tracer, we labeled neurons within the non-primary motor cortex (rostral forelimb area = RFA) that project to CFA. Then, 7 days after a CFA infarct (n=6), we used laser capture microdissection techniques to harvest labeled neurons in RFA. Healthy, uninjured rats served as controls (n=6). Biological interactions and functions of gene profiling were investigated by Affymetrix Microarray, and Ingenuity Pathway Analysis. A total of 143 up- and 128 down-regulated genes showed significant changes (fold change ≥±1.3 and $p < 0.05$). The canonical pathway, "Axonal Guidance Signaling," was overrepresented (p-value = 0.002). Significantly overrepresented functions included: branching of neurites, organization of cytoskeleton, dendritic growth and branching, organization of cytoplasm, guidance of neurites, development of cellular protrusions, density of dendritic spines, and shape change (p = 0.000151 to 0.0487). As previous studies have shown that spared motor areas are important in recovery following injury to the primary motor area, the results

suggest that these gene expression changes in remote, interconnected neurons may underlie reorganization and recovery mechanisms.

Abbreviations

CFA	Caudal Forelimb Area
RFA	Rostral Forelimb Area
PMv	Ventral Premotor Area
S1	Primary Sensory Area
M1	Primary Motor Area
ICMS	Intracortical Microstimulation
CTB647	Cholera Toxin Beta Subunit Conjugated to AlexaFluor 647
LCM	Laser Capture Microdissection
IPA	Ingenuity Pathway Analysis
IM	Intramuscular
IP	Intraperitoneal
RIN	RNA Integrity Number
IVT	In Vitro Transcription
RMA	Robust Multi-array Averaging
NeuN	Neuronal Nuclei

Introduction

Stroke affects 795,000 individuals in the US, and over 15 million individuals worldwide each year, making stroke one of the major causes of adult disability (MMWR 2001; Roger VL et al. 2011). Some recovery can occur and may be related to plasticity in spared areas of the brain, presumably to assume functions that were previously controlled by the destroyed areas, a process known as vicariation. Evidence for functional plasticity in spared cortical areas has been found in peri-infarct cortex in both sensory and motor cortex in humans(Cramer SC et al. 1997), monkeys (Nudo RJ and GW Milliken 1996b; Frost SB et al. 2003), and rodents (Carmichael ST *et al.* 2001; Jablonka JA et al. 2010). It is widely recognized that plasticity in spared brain areas is correlated with behavioral improvement after cortical infarct, but the underlying mechanisms are still unclear (Nudo RJ 2006).

Gene expression changes have been reported in tissue homogenate and sprouting neurons within the peri-infarct region (Carmichael ST *et al.* 2005; Li S et al. 2010). A cortical infarct induces sequential waves of growth-inhibitory and growth-promoting genes associated with neuron-, glia- and extracellular matrix-associated molecules over a period lasting at least a month (Carmichael ST *et al.* 2001). This pattern involves decreases in some inhibitory molecules, and increases in growth-associated genes suggested to support the anatomical reorganization (Carmichael ST 2006). Thus, peri-infarct tissue is likely to be a locus for regenerative processes, and it is now clear that neurophysiological

reorganization in peri-infarct cortex is directly related to behavioral recovery (Nudo RJ *et al.* 1996c).

While most studies of gene expression changes after ischemic injury have focused on the peri-infarct cortex, it is now known that neurophysiological and neuroanatomical plasticity occurs in many regions of the cortex that are spared by the ischemic injury, but remote from it. In particular, intact cortical areas that are functionally related to the area of injury, and anatomically connected to it via axonal connections, are altered. For example, after motor cortex injury in the rat, the motor cortex in the spared hemisphere undergoes a time-dependent process of dendritic arborization and synaptogenesis (Jones TA and T Schallert 1994). Gene expression studies in the contralateral (intact) hemisphere have been limited to a single study of tissue homogenates and neurons connected to spinal cord (not the cortical lesion) (Keyvani K et al. 2002; Zai L *et al.* 2009). These studies demonstrated molecular changes that were suggested to be supportive of anatomical reorganization.

It has also been suggested that functionally related areas that are spared by the ischemic injury within the injured hemisphere and that have anatomical connections with the injury zone also undergo neurophysiological and anatomical plasticity. For example, after injury to motor cortex, premotor cortex, although remote from the direct damage of the ischemic infarct and penumbra, can also undergo neuroanatomical and neurophysiological plasticity. In human stroke survivors, finger movements of the impaired limb are associated with increased

blood flow in premotor areas (Chollet F et al. 1991). Further, after an infarct in primary motor cortex in non-human primates, the ventral premotor cortex (PMv), an area whose principal output target is the primary motor cortex, undergoes neurophysiological reorganization that is correlated with behavioral recovery (Frost SB *et al.* 2003). The PMv also undergoes neuroanatomical reorganization, sending new axonal terminations into the parietal cortex (Dancause N *et al.* 2005). In addition, neurons in PMv undergo molecular changes as demonstrated by immunohistochemical studies (Stowe AM et al. 2007; Stowe AM et al. 2008). In both mice and rats, anatomical reorganization in spared areas distant from the lesion has been well documented (Zai L *et al.* 2009; Li S *et al.* 2010). There is indirect evidence that functional recovery may be mediated by plasticity in spared areas, since treatments that increase sprouting improve behavioral outcomes (Zai L *et al.* 2009; Liu Z *et al.* 2010).

Though functionally related and neuroanatomically interconnected areas likely play a role in recovery of function, little is known about the concomitant molecular program that occurs in spared, remote, neuronal populations that may trigger and orchestrate axonal sprouting and neurophysiological reorganization. The present study is unique in that it selectively identifies and characterizes the gene expression changes in neurons that send axonal connections to a focal infarct core in a remote area of cortex. We have developed a model of ischemic injury in rats that specifically targets the primary motor cortex, sparing the premotor cortex that normally has reciprocal connections with primary motor cortex (Rouiller EM

et al. 1993). In rodents, the homolog of the primate primary motor cortex is the caudal forelimb area (CFA), while the premotor equivalent is the rostral forelimb area (RFA). RFA is important for recovery, as secondary lesions to the RFA after CFA lesions reinstate behavioral deficits after recovery (Conner JM *et al.* 2005).

The goals of the present study were accomplished by physiologically identifying the forelimb representation in the CFA of adult rats, then labeling neuronal somata projecting to the CFA by injection of a retrograde tracer, next creating an ischemic lesion in the CFA, then finally, harvesting labeled neurons within the RFA 7 days after the infarct using laser capture microdissection. The 7-day post-infarct time point represents the onset of an "initiation phase" in which growth-promoting molecules are thought to be initially increased (Carmichael ST *et al.* 2005). Gene expression patterns were then determined using Affymetrix Microarray analysis. Ingenuity Pathway Analysis software was used to further understand the biological significance. The resulting expression changes are consistent with the hypothesis that neurons in the RFA undergo neuroanatomical reorganization by involvement of specific genes associated with axonal growth, and guidance. These data help to elucidate the genetic response to infarct in interconnected neurons, and may eventually provide potential targets for regenerative therapy.

Materials and Methods

Subjects

Male Long-Evans hooded rats (n=14; 270-470g; 3-6 months of age; Harlan, Indianapolis, IN) were singly housed in a temperature-controlled room on a 12 hr:12 hr light:dark cycle, with *ad libitum* access to food and water. Animal use was approved by the Institutional Animal Care and Use Committee of the University of Kansas Medical Center. Animals were randomly assigned to lesion (n=6) and control (n=6) groups.

Surgical Procedure I: Neurophysiological Identification of CFA and Retrograde Tracer Injection

Surgical Preparation

After sedation with isoflurane, each rat was anesthetized with ketamine (100-80mg/kg IM) and xylazine (30mg/kg IP). The rat was placed in a stereotaxic frame, a local anesthetic (Bupivacaine, 2.5mg) was applied to the scalp. The scalp was incised and reflected, muscles attached to the temporal ridge and occipital ridge were released. The dura overlying the cisterna magna was incised to relieve cerebrospinal fluid pressure, and a craniotomy performed using a hand drill with a burr bit from +5 to -4 mm relative to bregma and from 1mm lateral of the sagittal suture to the temporal ridge. Anesthesia was maintained with

supplemental doses of ketamine (20 mg/kg IM), as needed, and temperature held constant with a homeothermic blanket system at physiological normal. Core temperature was monitored with a rectal probe. The dura was reflected and warm, sterile silicone oil was applied to the craniotomy to aid in visualization and to prevent desiccation of the cortex.

Neurophysiologial Mapping Procedure

The CFA was identified in each animal by intracortical microstimulation (ICMS) mapping techniques as described in previous publications (Nishibe M *et al.* 2010). A magnified digital image of the cortical surface vasculature was obtained and a grid pattern (250μm) overlaid with image processing software (Canvas, Deneba Software, Miami, FL). The microelectrode, a tapered and beveled glass micropipette (20μm outside diameter at the tip) filled with concentrated saline NaCl solution (3.5M), was advanced perpendicular to the cortical surface (1725μm subpial depth) with the aid of a hydraulic microdrive (650 Micropositioner, David Kopf Instruments, Tujunga, CA) at sites corresponding to every other grid intersection (500μm resolution), or when necessary, every grid intersection (250μm resolution), to accurately delineate the CFA/RFA boarder. The stimulus consisted of a 40msec duration train of 13 monophasic cathodal pulses (200μsec duration) at 350Hz delivered one per second from an electrically isolated, charge-balanced, constant-current stimulation circuit (BSI-2, Bak Electronics Inc, Mount Airy, MD). The current was

increased from 0-80μA until a movement was just visible from at least 50% of the train bursts, then movement type and minimum current required to evoke the movement were recorded. The site was recorded as "nonresponsive" if no movement was elicited before reaching the maximum current level (80μA). The 500μm resolution grid used in these experiments was adequate to delineate the borders of the CFA for defining the location for the tracer injection and the extent of the intended lesion (see Surgical Procedure II below).

Retrograde Tracer Injection

After delineating the CFA borders, the rostral half of CFA was injected with a retrograde neuronal tracer, cholera toxin beta subunit conjugated to AlexaFluor 647 (CTB-647, 5μg/μL in 0.9% sterile saline, C34778, Invitrogen, Grand Island, NY). CTB-647 leaves a residual blue mark on the cortical surface that is identifiable upon reopening. Preliminary experiments determined that the synaptic terminal field from RFA was most dense in this subregion (unpublished observations and see (Rouiller EM *et al.* 1993)). The tracer was delivered by pressure injection from a tapered glass micropipette (70μm outside diameter) secured with wax to a 1μL Hamilton syringe (80100, Hamilton Company, Reno, NV). The syringe plunger was actuated by a microinjector (Micro4, World Precision Instruments, Sarasota, FL) clamped to a hydraulic microdrive on a stereotaxic arm. Each animal received injections at 2 sites 1mm apart within the CFA. At each site, 75nL (5nL/sec) of tracer was injected at each of two depths

(1500μm and 1250μm below the pial surface), for a total of 150nL at each site.

Surgical Closing and Recovery

Following the procedures described above, the craniotomy was rinsed with sterile saline. A silicone sheet was placed over the craniotomy followed by gel-foam and dental acrylic to form a protective cap. The scalp was sutured, followed by Bupivacaine (2.5mg, topical), and Vetropolylycine gel (topical antibiotic). Animals were monitored until alert and active, and then returned to their home cage.

Surgical Procedure II: Cortical Infarct

Animals in the lesion group underwent a second surgical procedure 14 days after Surgical Procedure I (ICMS and tracer injection). The 14-day interval allowed sufficient time for the tracer to be retrogradely transported to the parent somata in RFA, where it remains for later identification. Animals in the control group did not undergo a second procedure. General surgical procedures discussed above were followed, except that the cortex was re-exposed by removing the protective cap from the first procedure without the need for further craniotomy. After re-exposing the cortex, a tapered glass micropipette (160μm outside diameter) was secured with wax to a 2μL Hamilton syringe filled with the vasoconstrictor, endothelin-1 (ET-1, 0.33mg/mL 0.9% sterile saline, H-6995,

Bachem Americas, Inc, Torrance, CA), and attached to a microinjector clamped to a microdrive on a stereotaxic arm. The residual blue mark of the tracer injections (visible on the cortex) and blood vessel patterns photographed from Procedure I were used to guide injection placement. The majority of the CFA representation was targeted for ischemic injury. The size of the CFA determined the number of ET-1 injection sites (2 to 5). The micropipette tip was lowered to 1500μm below the pial surface, perpendicular to the cortex. At each injection site, ET-1 was delivered at 5nL/sec in three 110nL boluses with a 1min delay between boluses, and a 5min delay before tip extraction. During the injections and delay times, the craniotomy was flushed constantly with sterile saline to prevent non-specific spread of ET-1. At the conclusion of the ET-1 injections, rats underwent the *Surgical closing and recovery* procedure described above.

Tissue Harvest and Laser Capture Microdissection (LCM)

Seven days after Surgical Procedure II (or an equivalent time period in control rats), rats were anesthetized with isoflurane and ketamine (45mg IP), then decapitated by guillotine in accordance with American Veterinary Medicine Association Guidelines on Euthanasia. The brain was extracted and flash frozen for 30sec in heptane (on dry ice for 5min) and stored in a -80C freezer until sectioning. After a 30min equilibration time, brains were sectioned in the coronal plane on a cryostat at 14um. Sections were cut rostral to caudal beginning at the

rostral pole until the tracer injection cores in the CFA were contacted. At 7 days post-lesion the CTB647 injection cores were still visible to the unaided eye within the translucent lesion of lesion animals, or opaque tissue of the control animals. Then, after a series of 7 sections were cut, 4 sections were thaw mounted to charged slides and 3 sections discarded. Four sections per slide proved to be the optimal number of sections for LCM collection (Arcturus Veritas, Applied Biosystems, Carlsbad, CA). In lesion animals, in order to obtain an accurate measure of the lesion volume, 2 serial sections were taken at 504 μm intervals (every 36 sections) throughout the extent of the lesion. Slides were returned to dry ice within 20sec of thaw mounting to preserve RNA integrity, and stored in a -80C freezer until the LCM procedure.

Given the time dependent nature of RNA degradation, only one slide at a time was processed for LCM. Each slide at the level of the RFA was removed from dry ice and dehydrated by an increasing alcohol gradient and xylenes for clearing. The procedure was slightly modified from protocols available from Arcturus (Applied Biosystems). Briefly, each slide was exposed to 75% ethanol (30s), water (30s), 75% ethanol (30s), 95% ethanol (30s), 100% ethanol (2x2 min) and xylene (5min). The slide was placed in the LCM along with Macro collection caps (Arcturus, Applied Biosystems). Sections were viewed under fluorescent illumination to identify retrogradely labeled somata at the level of the RFA (Rouiller EM *et al.* 1993; Nishibe M *et al.* 2010). After test firing, the infrared laser settings were adjusted to produce a collection spot of 32μm in diameter.

Standard laser settings were used, but power varied from 35-90 mW as needed to produce a collection spot of 30μm. Within 2 hours of dehydration, 100 to 500 cells were collected per cap to prevent overloading. The cap was inserted into a microcentrifuge tube and exposed to PicoPure RNA extraction buffer (30min at 42C, Arcturus, Applied Biosystems). This process was repeated with as many slides as was necessary until 28 ng of purified RNA (~ 1900 cells) was collected from each animal. Extracted RNA was stored at -80°C until RNA isolation.

RNA Sample Preparation and Affymetrix Microarray Procedures

A PicoPure (Arcturus, Applied Biosystems) on-column RNA isolation kit was used per manufacturer's instructions, along with the DNase I (Qiagen, Valencia, CA,) treatment to eliminate DNA contamination, and RNA quality was assessed by Agilent 2100 Bioanalyzer with a RNA 6000 Pico LabChip kit (Agilent Technologies, Santa Clara, CA). Only samples with RNA Integrity Numbers (RIN's) of 7 or above were considered of acceptable quality for microarray assay. RIN is calculated with a proprietary algorithm (www.chem.agilent.com), which takes into account the entire electrophoretic trace of the Pico LabChip. Total RNA (~35ng, 1500 cells) from each animal was amplified twice according to Affymetrix Small Sample Labeling protocol: reverse transcription with Superscript II (SuperScript Choice System, Invitrogen), in vitro transcription (IVT) with MEGAscript T7 kit (Ambion, Invitrogen) including T7(dT)24 primer

(5'GGCCAGTGAATTGTAATACGACTCACTATAGGGAGGCGGTTTTTTTTTTTT TTTTTTTTTTTT-3') for 1st and random primers for 2nd round IVT, cDNA cleanup through ethanol precipitation, cRNA cleanup with Qiagen RNeasy columns, and GeneChip Expression 3'-Amplification IVT Labeling kit (Affymetrix, Santa Clara, CA) for the last round of IVT and biotin labeling. Biotinylated-cRNA was fragmented (buffer: 200mM Tris-Acetate, pH 8.1, 500mM potassium acetate, 150mM magnesium acetate), and average fragment length was assessed by RNA 6000 Nano LabChip kit (Agilent). Affymetrix GeneChip Rat Genome 230 2.0 Arrays (Affymetrix Cat. No.: 900506) were hybridized, washed and stained using GeneChip Fluidics Station 450 (Affymetrix) under the Standard Array Format. The automated scanning process (Affymetrix GeneChip Scanner 3000 7G with autoloader) completed 1 scan for each array using standard settings for pixel value (3um), and wavelength (570nm). Absolute and comparison analysis was performed with the target signal scaled to 500 with a normalization factor of 1 (no normalization).

Microarray Data And Gene Pathway Analysis

Probe intensities from microarrays were background corrected, quantile normalized and summarized using Robust Multi-array Averaging (RMA, Partek Genomic Suite 6.4, Partek Incorporated, St Louis, MO)(Irizarry RA et al. 2003). The resulting log (base2) transformed intensity values were used for quality control and further analysis. Probe level fold changes were obtained by taking the

exponentiation of the linear contrast between the least square means of the 7 day control and 7 day lesion samples. The significance of these fold-changes was calculated using a 2-way mixed model ANOVA. Apart from the treatment effect; the day each array was hybridized was included as a random effect in the ANOVA model.

Interaction networks, functions and canonical pathways were developed using Ingenuity Pathway Analysis (IPA, version 7.6, Ingenuity Systems, Redwood City, CA), an online software that uses a curated database of genes, proteins, chemicals, drugs, and molecular relationships to build biological models. The significance of the interaction networks, functions and canonical pathways were determined by the right-tailed Fisher's Exact test which measures the significance of the number of genes common to both the input gene set and the particular network, function or canonical pathway. The significance p-values of networks were adjusted for multiple hypothesis testing using the Benjamani-Hochberg correction procedure.

Lesion Volume Estimation

At 504 μm intervals during "Tissue Harvest," described above, 2 coronal sections (14μm) were thaw mounted to charged slides for lesion volume estimation. The following procedure occurred on slides with a hydrophobic barrier created by PAP pen (SuperHT, Research Products International Corp.,

Mount Prospect, IL). After washing in tris-buffered saline (TBS), sections were incubated overnight at 4ºC, and slowly agitated in 0.05M TBS containing 5% Donor Goat Serum (Equitech-Bio, Inc, Kerrville, TX), 0.4% Triton X-100, and 1:1000 dilution of biotinylated mouse monoclonal anti-Neuronal Nuclei (NeuN) antibody (MAB377B, Chemicon, Temecula, CA). Sections were rinsed in 0.05M TBS, incubated for 3 hr at room temperature in Avidin-Biotin Complex solution (ABC, PK-6100, Vector Laboratories, Burlingame, CA), rinsed in 0.05M TBS, and incubated in Vector SG Substrate Solution (SK-4700, Vector Laboratories) until visually acceptable background was evident (2-7min). Sections were rinsed in 0.05M TBS, then dried, dehydrated, and coverslipped with DPX mounting medium (Sigma-Aldrich, St Louis, MO). An Axioplan 2 microscope (Zeiss, Thornwood, NY) was used with Stereo Investigator software (Microbrightfield, Williston, VT) and Cavalieri probe to estimate the lesion size in 4 animals. Cortical areas (dorsal to the corpus callosum on coronal sections) containing presumed neurons (NeuN-positive cells) were selected as normal tissue, while cortical areas containing light or no NeuN staining were selected as infarcted tissue. Although the lesion was complete at 7 days post-infarct, the cortical tissue was not cavitated, allowing for the lesion to be traced and calculated directly. Every 36th section (504μm apart) was analyzed and only sections with a visible lesion were included in the probe. Lesion area from each section was multiplied by section thickness and distance between sections to calculate the lesion volume. Mean and standard error of the mean for lesion volume were

calculated for 4 animals (SPSS, IBM, Armonk, NY).

Results

Description of Lesion

Based on ICMS results (Fig. 1B), the CFA was found in a location similar to that of previous reports (Rouiller EM *et al.* 1993). The lesion was similar in size compared with previous results using identical Endothelin-1 infarct procedures (Fang PC *et al.* 2010). The ET-1 injections resulted in a continuous area of neuronal death, as judged by NeuN staining, and extended through all 6 cortical layers throughout the CFA. There was no evidence of damage to the corpus callosum or underlying subcortical structures. As expected, no cavitation was observed at this 7 day post-lesion time point, so lesion volume was calculated directly by measuring the area of the lesion on coronal sections at 500μm intervals and multiplying by the section thickness and section interval (Cavalieri Probe, Microbrightfield. The lesion volume was 12mm^3 ± 1.7mm^3 (mean ± SEM; n=4 brains available for lesion volume estimation).

Neuronal Harvesting

Fourteen animals received surgical procedures. Of these, one, 1 control animal was found to have cortical damage and one 1 lesion animal was found to have subcortical damage, and were excluded from the study. *In vivo* labeling of neurons with CTB-647 allowed for identification of neuronal somata that terminated in the infarcted area, as described in Methods. Approximately 1900 somata per animal were targeted for collection during the LCM procedure (Fig. 2A-D).

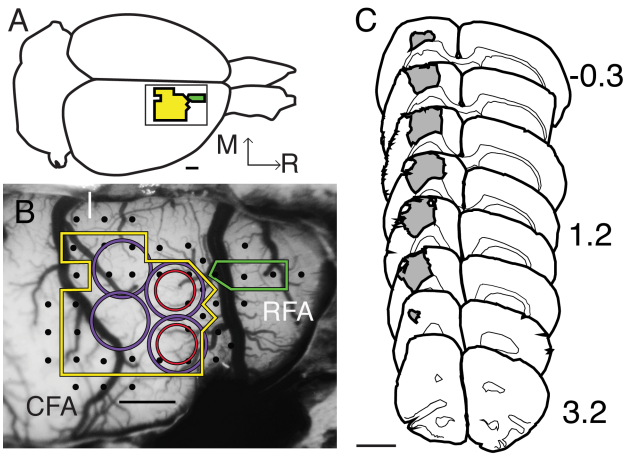
A
M
R
B
RFA
CFA
C
-0.3
1.2
3.2

Fig. 1 Physiological identification of cortical areas and lesion volume. **a** Illustration of the rat brain labeled with CFA (yellow) and RFA (green). Inset shows same area as **b**. Bar is 1mm. **b** Photomicrograph of exposed rat cortex taken through surgical microscope optics (18x magnification) and overlaid with a 250 x 250um grid (grid is removed for clarity) in image processing software (Canvas; ACDSee, Victoria, British Columbia, Canada). The ICMS electrode was inserted at grid intersections, stimulation elicited movements (black dots) of the forelimb, and non-forelimb defined the borders of CFA (yellow line) and caudal portion of RFA (green line), and allow for accurate placement of CTB647 (red circle). Blood vessel patterns, ICMS data recorded on the surgical photograph and visible blue of dye core guided placement of ET-1 injection (purple circle) 2 weeks after ICMS/tracer procedure, completely overlapping the CTB647 injection. Medial (M) and rostral (R) directions are the same in **a-b**. Bar is 1mm. **c** Coronal section tracing series (drawn at 5x magnification) of lesion size and location (gray). Lesion volume per ET-1 injection ($12mm^3 \pm 1.7mm^3$ SEM) was determined using Stereoinvestigator (Microbrightfield) on coronal sections labeled with biotinylated NeuN immunohistochemistry, numbers represent section distance from Bregma (Paxinos G and C Watson 1986). Bar is 3mm

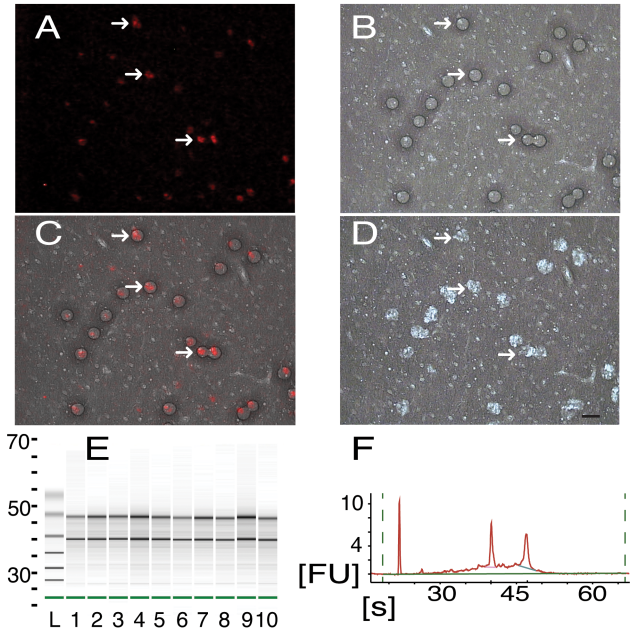
A
B
C
D
E
70
50
30
L 1 2 3 4 5 6 7 8 9 10
F
10
4
[FU]
30
45
60
[s]

Fig. 2 LCM collection and RNA quality verification. **a** Cortical neurons (red), retrogradely-labeled in vivo with CTB-647 during the 1st procedure, viewed through the LCM optics at 40x magnification (same for **a-d**). White arrows point to the same neurons in **a-d**. **b** Brightfield illumination of the same section as **a** after laser fire showing wetted spots (dark circles) of photoreactive polymer. **c** Overlap of **a** and **b** showing accuracy of wetted spot placement over labeled neurons. **d** Same section as **a** after removal of collection cap showing removal of selected tissue (holes appear white). 1,900 neurons were collected from 14µm-thick sections at the level of the RFA. Frames **a** and **c** were adjusted for contrast and brightness for easier viewing. Bar is 20μm (same for **a-d**). **e** Electropherogram in gel format of isolated RNA of 5 samples run in duplicate (1-5, 6-10) plotted vs run time (s, seconds), standard ladder (L) is included. **f** Electropherogram of lane 2 from **e** in native format, run time (s) is plotted vs fluorescence units (FU). Well-defined bands of 18S and 28S rRNA (**e** black lines, **f** sharp peaks) are present in high quality samples

RNA Quality Analysis

After RNA extraction and isolation from each section, purity was assayed with RNA 6000 Nano LabChip kit, and only samples with RIN's of 7 or above were used for further analysis (Fig. 2E-F). The entire electropherogram was taken into account in the proprietary RIN calculation (Agilent), although with high quality samples, the characteristic sharp bands of 18s and 28s can be seen (Fig. 2E-F).

RNA from neurons collected from a single animal was run on its own microarray (n=12). After background correction, quantile normalization and summarization with RMA analysis (Partek Genomic Suite 6.4), log (base2) expression values were compared between microarrays to assess quality (Irizarry RA *et al.* 2003). It is generally assumed that expression changes between groups are a small percentage of those assayed, and most gene expression remains the same. The quality control assessment showed gene expression similarity between chips: the frequency histogram shows overlap, and log probe cell intensity and log expression signal graphs show similarity of mean and quartile signal characteristics of control (red) and lesion (blue) microarrays. The Pearson's correlation, shows a correlation of > 0.883 for all arrays (Fig. 3) after MAS5 analysis (Partek).

Differential gene expression at 7 days post-infarct compared with controls was determined by mixed model ANOVA after RMA analysis. A total of 237 genes were significantly up-regulated and 357 genes were significantly down-

regulated ($p < 0.05$). Of the 271 genes whose expression changed $\geq \pm 1.3$ fold and $p < 0.05$, 143 were up-regulated and 128 were down-regulated. These genes included ion channels (Clic3, Glrb), receptors (Trem2, Oprk1), enzymes (Gpam, Neu2), and transcription regulators (Creg1, Pou3f1) (Table 1 and 2).

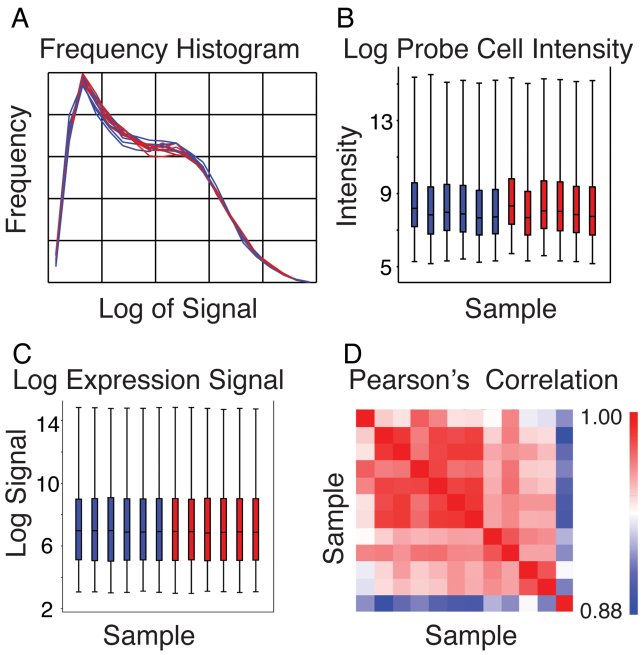
A
Frequency Histogram
Frequency
Log of Signal
B
Log Probe Cell Intensity
Intensity
13
9
5
Sample
C
Log Expression Signal
Log Signal
14
10
6
2
Sample
D
Pearson's Correlation
Sample
1.00
0.88
Sample

Fig. 3 Quality control assessment of microarrays. **a** Frequency histogram of signal following RMA analysis, plotted as frequency of signal vs log of the signal for all lesion (blue) and control (red) arrays. **b** Box-and-whisker plots showing the log of probe cell intensity, and **c** the log of the expression signal for each of the arrays (Sample 1-12) following RMA analysis plotted as sample number vs log of the probe cell intensity or log of the expression signal, respectively. Lesion (blue) and control (red) plots are divided into 100, 75, 50 and 0^{th} percentile (same for **b** and **c**). **d** Pearson's correlation for signal after MAS5 analysis is greater than 0.883 for all arrays, plotted as Sample 1-12 vs Sample 1-12 (red boxes in diagonal line are identity). The indicator to the right displays higher (red) to lower (blue) correlation

Table 1 List of upregulated genes 7 days post-infarct

Symbol	Entrez Gene Name	Fold Change	p-Value	Location	Type
Rgs5	regulator of G-protein signaling 5	3.45	0.0117	Plasma Membrane	other
Fbln2	fibulin 2	2.26	0.0176	Extracellular Space	other
Aqp4	aquaporin 4	2.15	0.0116	Plasma Membrane	transporter
NnaT	neuronatin	2.15	0.0153	Plasma Membrane	transporter
Dennd4c	DENN/MADD domain containing 4C	2.08	0.0004	Unknown	other
Omd	osteomodulin	2.02	0.0213	Extracellular Space	other
Tubb2c	tubulin, beta 2C	2.00	0.0243	Cytoplasm	other
Creg1	cellular repressor of E1A-stimulated genes 1	1.97	0.0169	Nucleus	transcription regulator
Clic2	chloride intracellular channel 2	1.91	0.0021	Unknown	ion channel
Cd44	CD44 molecule (Indian blood group)	1.89	0.0445	Plasma Membrane	other
Timp3	TIMP metallopeptidase inhibitor 3	1.87	0.0429	Extracellular Space	other
Gng11	guanine nucleotide binding protein (G protein), gamma 11	1.81	0.0486	Plasma Membrane	enzyme
Flnc	filamin C, gamma	1.79	0.0433	Cytoplasm	other
Hist2h4 (includes others)	histone cluster 2, H4	1.78	0.0455	Nucleus	other
Huwe1	hypothetical protein LOC501546	1.77	0.0316	Nucleus	enzyme
Klhl5	kelch-like 5 (Drosophila)	1.75	0.0056	Unknown	other
Nars2	asparaginyl-tRNA synthetase 2, mitochondrial (putative)	1.74	0.0258	Cytoplasm	enzyme
Pabpc4	poly(A) binding protein, cytoplasmic 4 (inducible form)	1.72	0.0070	Cytoplasm	other
Klhdc3	kelch domain containing 3	1.71	0.0047	Cytoplasm	other
Mpp6	membrane protein, palmitoylated 6 (MAGUK p55 subfamily member 6)	1.69	0.0303	Plasma Membrane	kinase
Clic3	chloride intracellular channel 3	1.66	0.0170	Nucleus	ion channel
Plin2	perilipin 2	1.64	0.0272	Plasma Membrane	other
Plod2	procollagen-lysine, 2-oxoglutarate 5-dioxygenase 2	1.63	0.0240	Cytoplasm	enzyme
Sox4	SRY (sex determining region Y)-box 4	1.62	0.0164	Nucleus	transcription regulator
Cotl1	coactosin-like 1 (Dictyostelium)	1.62	0.0341	Cytoplasm	other
Pdlim4	PDZ and LIM domain 4	1.58	0.0226	Cytoplasm	other
Asf1b	ASF1 anti-silencing function 1 homolog B (S. cerevisiae)	1.58	0.0172	Nucleus	other
Prpf4b	PRP4 pre-mRNA processing factor 4 homolog B (yeast)	1.58	0.0408	Nucleus	kinase
Trem2	triggering receptor expressed on myeloid cells 2	1.57	0.0474	Plasma Membrane	transmembrane receptor
Ahi1	Abelson helper integration site 1	1.56	0.0092	Cytoplasm	other
Map3k1	mitogen-activated protein kinase kinase kinase 1	1.55	0.0397	Cytoplasm	kinase
Elmo2	engulfment and cell motility 2	1.55	0.0058	Cytoplasm	other
Gpam	glycerol-3-phosphate acyltransferase, mitochondrial	1.55	0.0065	Cytoplasm	enzyme
Cyp26b1	cytochrome P450, family 26, subfamily B, polypeptide 1	1.54	0.0126	Cytoplasm	enzyme
Ldb3	LIM domain binding 3	1.54	0.0307	Cytoplasm	transporter
Pnisr	PNN-interacting serine/arginine-rich protein	1.54	0.0233	Nucleus	other
Sema4b	sema domain, immunoglobulin domain (Ig), transmembrane domain (TM) and short cytoplasmic domain, (semaphorin) 4B	1.54	0.0143	Plasma Membrane	other
Chrdl1	chordin-like 1	1.53	0.0048	Extracellular Space	other

Table 2 List of down regulated genes 7 days post-infarct

Symbol	Entrez Gene Name	Fold Change	p-Value	Location	Type
Clca1	chloride channel accessory 1	-2.69	0.0044	Plasma Membrane	ion channel
Ermn	ermin, ERM-like protein	-2.40	0.0132	Extracellular Space	other
Mobp	myelin-associated oligodendrocyte basic protein	-1.98	0.0054	Cytoplasm	other
Lypd6b	LY6/PLAUR domain containing 6B	-1.76	0.0291	Unknown	other
Oprk1	opioid receptor, kappa 1	-1.76	0.0214	Plasma Membrane	G-protein coupled receptor
Scn4b	sodium channel, voltage-gated, type IV, beta	-1.72	0.0233	Plasma Membrane	ion channel
Mycbp2	MYC binding protein 2	-1.64	0.0375	Nucleus	enzyme
Glrb	glycine receptor, beta	-1.64	0.0426	Plasma Membrane	ion channel
Neu2	sialidase 2 (cytosolic sialidase)	-1.60	0.0192	Cytoplasm	enzyme
Fdft1	farnesyl-diphosphate farnesyltransferase 1	-1.58	0.0348	Cytoplasm	enzyme
Rpusd2	RNA pseudouridylate synthase domain containing 2	-1.56	0.0266	Unknown	enzyme
Gypc	glycophorin C (Gerbich blood group)	-1.55	0.0342	Plasma Membrane	other
Etv1	ets variant 1	-1.55	0.0045	Nucleus	transcription regulator
Pou3f1	POU class 3 homeobox 1	-1.55	0.0057	Nucleus	transcription regulator
Xkr4	XK, Kell blood group complex subunit-related family, member 4	-1.54	0.0163	Unknown	other
Hrasls	HRAS-like suppressor	-1.53	0.0152	Cytoplasm	other
Chodl	chondrolectin	-1.51	0.0298	Plasma Membrane	other
Bbs5	Bardet-Biedl syndrome 5	-1.51	0.0452	Cytoplasm	other
Pcdhb6	protocadherin beta 6	-1.51	0.0055	Plasma Membrane	other
Trim54	tripartite motif containing 54	-1.50	0.0172	Cytoplasm	other
Skp2	S-phase kinase-associated protein 2 (p45)	-1.50	0.0038	Nucleus	other
Kcns3	potassium voltage-gated channel, delayed-rectifier, subfamily S, member 3	-1.49	0.0156	Plasma Membrane	ion channel
Cadps2	Ca++-dependent secretion activator 2	-1.48	0.0475	Plasma Membrane	other
Slc5a7	solute carrier family 5 (choline transporter), member 7	-1.48	0.0170	Plasma Membrane	transporter
Plxdc1	plexin domain containing 1	-1.48	0.0032	Plasma Membrane	other
Grem1	gremlin 1	-1.48	0.0134	Extracellular Space	other
Lemd3	LEM domain containing 3	-1.47	0.0397	Nucleus	other
Nefm	neurofilament, medium polypeptide	-1.47	0.0238	Cytoplasm	other
Stard4	StAR-related lipid transfer (START) domain containing 4	-1.46	0.0070	Cytoplasm	transporter
Kcns1	potassium voltage-gated channel, delayed-rectifier, subfamily S, member 1	-1.46	0.0296	Plasma Membrane	ion channel
Znf385b	zinc finger protein 385B	-1.46	0.0283	Nucleus	other
Nxph1	neurexophilin 1	-1.46	0.0095	Extracellular Space	other
40794	septin 8	-1.45	0.0088	Extracellular Space	other
Ttc39a	tetratricopeptide repeat domain 39A	-1.45	0.0080	Unknown	other
Sstr2	somatostatin receptor 2	-1.45	0.0293	Plasma Membrane	G-protein coupled receptor
Znf654	zinc finger protein 654	-1.44	0.0354	Unknown	other
Spock3	sparc/osteonectin, cwcv and kazal-like domains proteoglycan (testican) 3	-1.44	0.0064	Extracellular Space	other
C3orf67	chromosome 3 open reading frame 67	-1.44	0.0238	Unknown	other
Nefl	neurofilament, light polypeptide	-1.44	0.0269	Cytoplasm	other
B3galt5	UDP-Gal:betaGlcNAc beta 1,3-galactosyltransferase, polypeptide 5	-1.43	0.0453	Cytoplasm	enzyme
Pdyn	prodynorphin	-1.43	0.0399	Extracellular Space	transporter
Nefh	neurofilament, heavy polypeptide	-1.43	0.0375	Cytoplasm	other

Table 3 List of regulated genes involved in the Axonal Guidance Signaling pathway

Symbol	Entrez Gene Name	Fold Change	p-Value	Location	Type
Actr2	ARP2 actin-related protein 2 homolog (yeast)	1.40	0.0499	Plasma Membrane	other
Bmp1	bone morphogenetic protein 1	1.46	0.0196	Extracellular Space	peptidase
Bmp4	bone morphogenetic protein 4	1.51	0.0303	Extracellular Space	growth factor
Gng11	guanine nucleotide binding protein (G protein), gamma 11	1.81	0.0486	Plasma Membrane	enzyme
Ntng1	netrin G1	-1.41	0.0047	Extracellular Space	other
Ntrk2	neurotrophic tyrosine kinase, receptor, type 2	1.35	0.0468	Plasma Membrane	kinase
Pak1	p21 protein (Cdc42/Rac)-activated kinase 1	-1.38	0.0269	Cytoplasm	kinase
Ppp3r1	protein phosphatase 3, regulatory subunit B, alpha	-1.32	0.0367	Cytoplasm	phosphatase
Pxn	paxillin	1.36	0.0394	Cytoplasm	other
Rock2	Rho-associated, coiled-coil containing protein kinase 2	1.33	0.0347	Cytoplasm	kinase
Rras	related RAS viral (r-ras) oncogene homolog	1.41	0.0310	Cytoplasm	enzyme
Sema4b	sema domain, immunoglobulin domain (Ig), transmembrane domain (TM) and short cytoplasmic domain, (semaphorin) 4B	1.54	0.0143	Plasma Membrane	other
Tubb2c	tubulin, beta 2C	2.00	0.0243	Cytoplasm	other
Wnt9a	wingless-type MMTV integration site family, member 9A	-1.32	0.0051	Extracellular Space	other

Canonical Pathways Analysis

Differentially expressed gene products ($p < 0.05$, $\geq \pm 1.3$ fold change) were fit to known "canonical" pathways developed with a curated gene database (IPA analysis software). Significance of overrepresentation was determined by right-tailed Fisher's Exact test. The canonical pathway, "Axonal Guidance Signaling," was differentially regulated (-log(p-value) = 2.68). The pathway involved 14 significantly regulated genes from the current data set. The differentially regulated genes were: Actr2, Pxn, Bmp4, Rras, Wnt9a, Rock2, Ntng1, Pak1, Tubb2c, Gng11, Ntrk2, Ppp3r1, Sema4b, and Bmp1 (Table 3).

Gene Function Analysis

Genes with significant differential regulation ($p < 0.05$, $\geq \pm 1.3$ fold change) were also overrepresented in several biological processes, determined with the right-tailed Fisher's exact test with a Benjamini-Hochberg correction (IPA analysis software). Although some genes were included in multiple categories, 220 unique genes were fit to overrepresented functional categories, which were reduced to 186 after the Benjamini-Hochberg correction. "Neurological Disease," "Cell-to-cell Signaling and Interaction," and "Nervous System Development and Function" were among the top categories dysregulated (Fig. 4). Within the categories, the functions "Branching of Neurites", "Organization of Cytoskeleton",

“Dendritic Growth and Branching”, “Organization of Cytoplasm”, “Guidance of Neurites”, “Development of Cellular Protrusions”, “Density of Dendritic Spines”, and “Shape Change” (p = 0.000151 to 0.0487) involved 50 genes. The functions, “Development of Nervous Tissue”, “Neurogenesis”, “Development of Neurons”, and “Organization of Nervous Tissue” (p=0.0322 to 0.0495), involved 30 genes. There were 13 genes involved in the function, “Synaptic Transmission” (p=0.0229). The function of “Synaptic Transmission” (p = 0.0229) included: ApoE, Cd24, Chrm3, Gabrd, Glrb, Kcnd2, Nlgn2, Npy5r, Oprk1, Pcdhb6, Rasd2, Slc1a3, and Slc5a7. Interestingly, the function, “Rheumatic Disease” was overrepresented with 50 differentially expressed genes (p = 0.0113), and included the up-regulated genes, Rgs5, Tubb2c, Timp3, Klhl5, Ahi1, Bmp4, Tcf12 and Hla-Dqa1, and the down regulated genes Lypd6b, Oprk1, Scn4b, Mycbp2, Kcns3 and Znf385b.

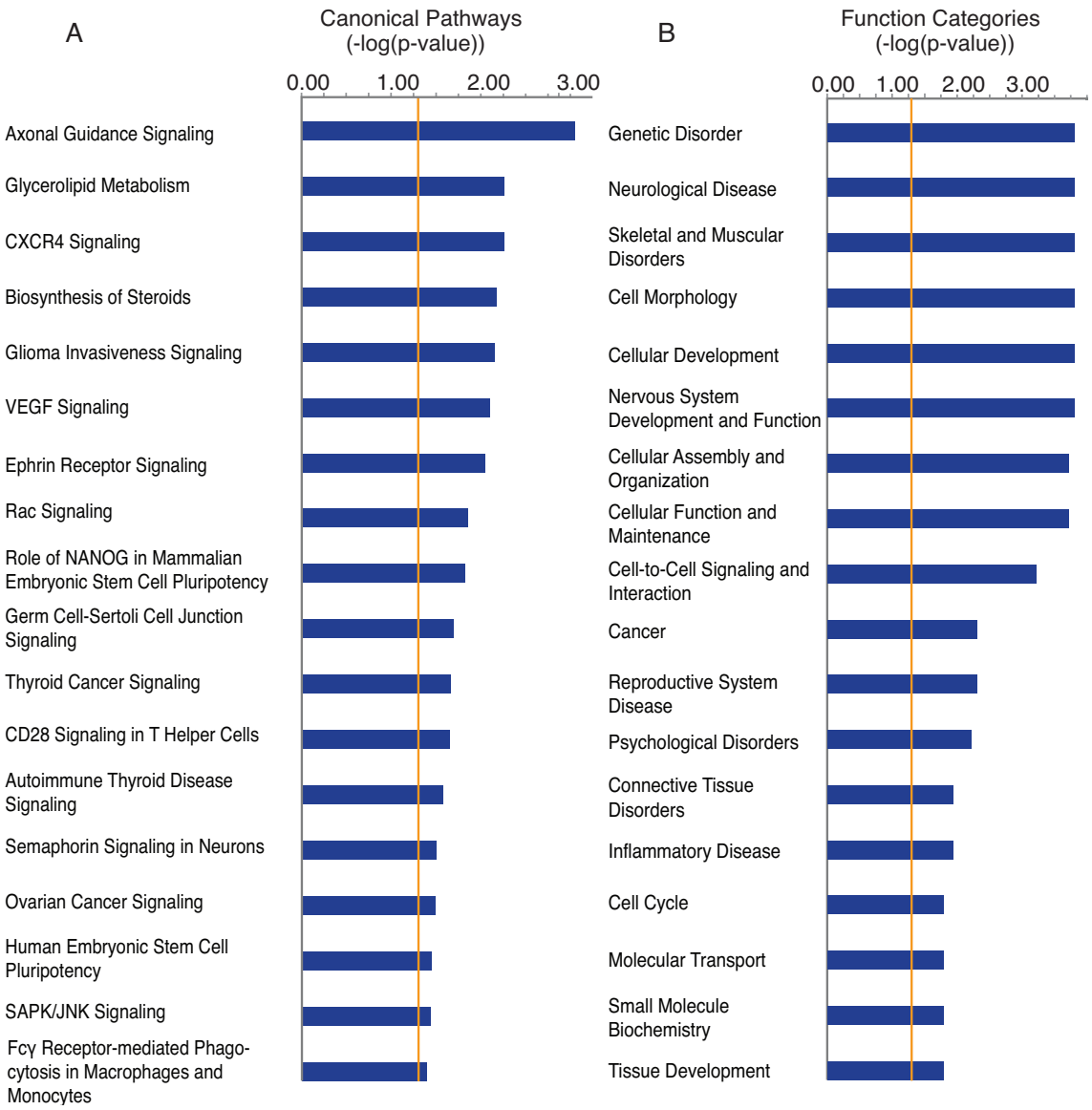
A
Canonical Pathways
(-log(p-value))
0.00
1.00
2.00
3.00
Axonal Guidance Signaling
Glycerolipid Metabolism
CXCR4 Signaling
Biosynthesis of Steroids
Glioma Invasiveness Signaling
VEGF Signaling
Ephrin Receptor Signaling
Rac Signaling
Role of NANOG in Mammalian Embryonic Stem Cell Pluripotency
Germ Cell-Sertoli Cell Junction Signaling
Thyroid Cancer Signaling
CD28 Signaling in T Helper Cells
Autoimmune Thyroid Disease Signaling
Semaphorin Signaling in Neurons
Ovarian Cancer Signaling
Human Embryonic Stem Cell Pluripotency
SAPK/JNK Signaling
Fcγ Receptor-mediated Phagocytosis in Macrophages and Monocytes
B
Function Categories
(-log(p-value))
0.00
1.00
2.00
3.00
Genetic Disorder
Neurological Disease
Skeletal and Muscular Disorders
Cell Morphology
Cellular Development
Nervous System Development and Function
Cellular Assembly and Organization
Cellular Function and Maintenance
Cell-to-Cell Signaling and Interaction
Cancer
Reproductive System Disease
Psychological Disorders
Connective Tissue Disorders
Inflammatory Disease
Cell Cycle
Molecular Transport
Small Molecule Biochemistry
Tissue Development

Fig. 4 Canonical pathways and function categories involving significantly regulated genes from interconnected neurons 7 days post-infarct. **a** Significantly regulated genes ($p < 0.05$ and above $\geq \pm 1.3$ fold change) were analyzed for interaction of their gene products and fit to canonical pathways developed with a curated gene database using Fisher's Exact test (IPA software) to determine the probability of the same result when choosing genes at random. The length for each canonical pathway or function (blue box) is the negative log of the p-value, and is significant if it extends to the right of the orange threshold line ($-\log(p \leq 0.05)$). Fisher's Exact test accounts for the number of uploaded genes, genes in the reference set, genes in the pathway and uploaded genes in the pathway. "Axonal Guidance Singnaling", has a $-\log(p) = 2.86$. **b** Significantly regulated genes ($p < 0.05$ and above $\geq \pm 1.3$ fold change) were analyzed for overrepresented biological functions involving their gene products in accordance with a curated gene database using Fisher's Exact test (IPA software) to determine the probability of the function being overrepresented when choosing genes at random. Box length and threshold line are the same as in **a**

Gene-Gene Interactions Network Analysis

Genes up- or down-regulated (≥ 1.3x and $p < 0.05$) were further analyzed for gene product interactions. The most dysregulated genes were used as "seed" molecules and other molecules with known interactions were added to form networks of interaction, in accordance with a curated gene database (IPA). Significance was determined with right-tailed Fisher's Exact test, and adjusted with Bonferonni correction to determine the probability that the same network would be developed, if choosing genes at random. Significant networks involved 260 differentially expressed genes. The top 3 interaction networks (Fig. 5) had p values ranging from 2.5×10^{-37} to 2.5×10^{-22}, and involved 124 differentially expressed genes.

Differentially regulated molecules appearing as nodes in the first 6 networks (Fig. 5) were: FBLN2 2.26, TIMP3 1.874, AQP4 2.146, RGS5 3.446, FLNC 1.793, OMD 2.021, TUBB2C 1.996, CD44 1.894, CREG11 1.966, GNG11 1.813, NNAT 2.145, ERMIN -2.398, and OPRK1 -1.760 (symbol and fold change, respectively).

Those genes in the "Axonal Guidance Signaling" pathway with ≥±1.5 fold changes and p-value< 0.05 were further analyzed for interactions. IPA software identified several potential interactions using the significant genes involved in the pathway and genes from its curated knowledge base. Network 4 (Fig. 5D) shows GNG11 interacting with BMP4 through RGS19 and TUBB2C through NOTCH1.

TUBB2C can also interact with GNG11 through TUBA1A, and BMP4 though MYD88, SMURF1, and BMP receptors 1A or1B. SEMA4B can interact with TBB2C through DLG4 and SYT1, and BMP4 through DLG4 and EZH2.

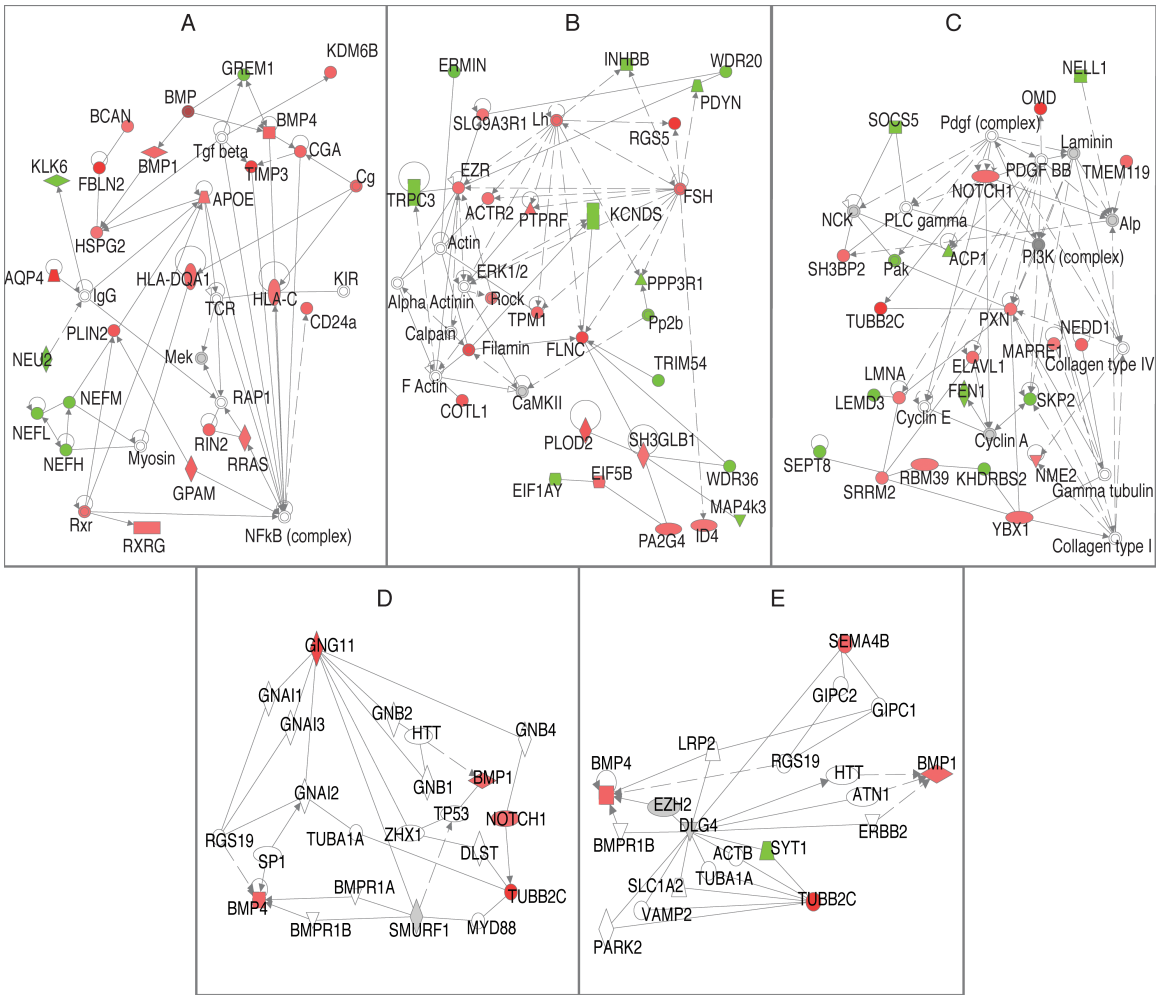
A
KDM6B
GREM1
BMP
BCAN
BMP4
Tgf beta
CGA
KLK6
BMP1
TIMP3
Cg
FBLN2
APOE
HSPG2
AQP4
HLA-DQA1
KIR
IgG
TCR
HLA-C
CD24a
PLIN2
NEU2
Mek
NEFM
RAP1
NEFL
RIN2
Myosin
RRAS
NEFH
GPAM
Rxr
RXRG
NFkB (complex)
B
ERMIN
INHBB
WDR20
PDYN
SLG9A3R1
Lh
RGS5
EZR
TRPC3
FSH
ACTR2
PTPRF
KCNDS
Actin
ERK1/2
PPP3R1
Alpha Actinin
Rock
TPM1
Pp2b
Calpain
Filamin
FLNC
TRIM54
F Actin
COTL1
CaMKII
PLOD2
SH3GLB1
EIF5B
WDR36
EIF1AY
MAP4k3
PA2G4
ID4
C
NELL1
OMD
SOCS5
Pdgf (complex)
Laminin
PDGF BB
TMEM119
NOTCH1
NCK
PLC gamma
Alp
SH3BP2
Pak
ACP1
PI3K (complex)
TUBB2C
PXN
NEDD1
MAPRE1
ELAVL1
Collagen type IV
LMNA
FEN1
SKP2
LEMD3
Cyclin E
Cyclin A
SEPT8
RBM39
KHDRBS2
NME2
SRRM2
Gamma tubulin
YBX1
Collagen type I
D
GNG11
GNAI1
GNB2
GNAI3
HTT
GNB4
BMP1
GNB1
GNAI2
TP53
NOTCH1
RGS19
TUBA1A
ZHX1
DLST
SP1
BMPR1A
TUBB2C
BMP4
BMPR1B
SMURF1
MYD88
E
SEMA4B
GIPC2
GIPC1
LRP2
BMP4
RGS19
HTT
BMP1
ATN1
EZH2
DLG4
ERBB2
BMPR1B
ACTB
SYT1
SLC1A2
TUBA1A
TUBB2C
VAMP2
PARK2

Fig. 5 Interaction networks of significantly regulated genes from interconnected neurons 7 days post-infarct. **a-c** Significantly regulated genes ($p < 0.05$ and above $\geq \pm 1.3$ fold change) were analyzed for interactions of their gene products using Fisher's Exact test (IPA software) to determine the probability of the same interaction network occurring after choosing genes at random, interactions significant at $p < 0.05$. **d-e** Show the reanalysis to detect interactions between genes in the "Axonal Guidance Signaling" pathway, which have $\geq \pm 1.5$ fold change and p-value< 0.05. **a-e** Upregulated (red) and downregulated (green) genes interact directly (solid line) or indirectly (dotted line). Genes ($p < 0.05$) not meeting the fold change cutoff (gray), and genes not present in the uploaded gene set (white) were only included in the interaction networks, if the gene was required as a necessary intermediary between two significant genes

Discussion

The injured brain is no longer seen as an uninjured brain with a missing puzzle piece (Nudo RJ 2006). An ischemic infarct instigates an array of molecular, physiologic and anatomical changes in spared areas of the adult CNS (Dancause N *et al.* 2005; Stowe AM *et al.* 2008; Li S *et al.* 2010). Surviving areas play a role in recovery from CNS damage, but little has been done to understand the mechanisms underlying neural plasticity at the level of gene expression. While hypoxia in the ischemic territory and surrounding penumbra undoubtedly results in gene-associated changes in a host of cell types, including neurons, glia, astrocytes and endothelial cells, the signaling pathways may be very different in remote tissue that is far removed from the hypoxic zone. Neuronal somata located in remote areas, in particular, may be triggered to initiate growth processes, since many of them send axonal arbors into the ischemic territories, where they normally form synaptic connections. This study was designed to isolate such remote neurons that have known terminations in an ischemic territory, and determine their differential gene expression changes.

The results demonstrated that 143 genes were up-regulated and 128 genes were down-regulated at 7 days post-infarct. IPA analysis revealed potential biological interactions of gene products from significant genes and found several canonical pathways that were overrepresented in the dataset with “Axonal Guidance Signaling” being the most overrepresented. IPA also identified the

overrepresented functions of “Branching of Neurites”, “Organization of Cytoskeleton”, “Dendritic Growth and Branching”, “Organization of Cytoplasm”, “Guidance of Neurites”, “Development of Cellular Protrusions”, “Density of Dendritic Spines”, and “Shape Change,” which involved 50 genes. Putative networks of interaction were also developed with IPA involving highly dysregulated genes as nodes. Those genes in the “Axonal Guidance Signaling” pathway with ≥±1.5 fold change and p-value< 0.05 were included in a second analysis and fit to their own interaction networks. These analyses add to the known functions of the current study’s significant genes, showing possible biological relevance. Taken together, these data add credence to the idea that neurons in remote areas that are anatomically connected to an ischemic territory may initiate growth and guidance signaling pathways, presumably in an attempt to reorganize. This process appears to be in place at 7 days after infarct.

Relevance of the Current Model

Our lesion model is the first to study gene expression in a neuronal population located in an anatomically identified premotor area after a primary motor cortex injury. After Neafsey and Sievert identified the RFA as a non-primary motor area, Rouiller further defined its general pattern of connectivity and its relationship to the primary motor, subcortical and sensory areas (Neafsey EJ and C Sievert 1982; Rouiller EM *et al.* 1993). The rodent RFA is a premotor

area, as classically defined, since it contains a forelimb representation distinct from the primary motor cortex (CFA), its principal target of efferent fibers in the cortex is to the primary motor cortex, and it contains neurons that project directly to the spinal cord via the corticospinal tract. Both CFA and RFA are involved in function of the forelimb in intact animals, and both can be identified *in vivo* by the presence of movements evoked by ICMS at low current levels.

The RFA is important to behavioral recovery when CFA is injured. After a lesion to CFA and subsequent functional recovery over a period of 5 weeks, a secondary lesion in RFA leads to reinstatement of the deficits, even though a lesion to RFA in otherwise normal rats does not induce significant impairments (Conner JM *et al.* 2005). In different rat models of cortical infarct, increased recovery of function has been correlated with treatments that increase anatomical sprouting (Zai L *et al.* 2009; Liu Z *et al.* 2010). Also, after a primary motor cortex lesion in non-human primates, the ventral premotor area (PMv), which shares structural and functional similarities to RFA, undergoes physiological reorganization that is proportional to the size of the lesion (Frost SB *et al.* 2003). In addition, neurons in PMv undergo axonal reorganization that results in trajectory alteration and formation of synaptic contacts in completely new territories in the parietal lobe (Dancause N *et al.* 2005).

The current study adds to earlier findings by identifying a specific neuronal population that is connected to an infarcted area. LCM was used to provide a more specific picture of the gene expression changes in identified neurons from

this area after ischemia compared to neurons from non-infarcted animals. While LCM is not completely selective, and closely apposed cell fragments and neuropil are also collected, the collected RNA is concentrated with neuronal signal. This is the first model to selectively acquire neurons interconnected to an area that is destined for infarction. Though Li et al. used LCM and double retrograde labeling to selectively acquire sprouting neurons in peri-infarct cortex, the study was focused on a specific population of neurons that sprouted after the infarct, rather than a more remote population of neurons that were connected to the infarct core prior to injury, as in the present study (Li S *et al.* 2010). It is possible that the harvested neurons in the Li et al. study displayed somewhat different expression patterns since they were likely within a hypoxic territory. By identifying the areas targeted for infarct physiologically with ICMS, retrogradely labeling the RFA neurons, and employing LCM at the level of the RFA, we have produced a more specific picture of gene expression changes in RFA neurons after CFA ischemic infarct.

Relevance of Gene Expression Changes after Brain Injury

Although initially thought to be a recapitulation of developmental gene expression, the brain's response to injury, such as occurs in stroke, is now seen in a broader context, including regulation of a similar set of genes to those involved in development, as well as genes specific to neuronal response to injury

(Benowitz LI and ST Carmichael 2010). Studies in peri-infarct cortex show up- and down-regulation of both developmentally and non-developmentally associated genes that are both neuronal and non-neuronal in origin (Carmichael ST *et al.* 2005). Extensions of this work found gene expression differences specifically in sprouting neurons that were not strictly developmental in nature. Notably, these studies revealed changes in the expression of some novel genes not known to be associated with axonal sprouting after ischemic infarct (Li S *et al.* 2010).

Likewise, the present study, which examined specific neuronal populations well outside of the peri-infarct, and presumably hypoxic, territory, found up- and down-regulation of both developmentally and non-developmentally associated genes. While gene expression changes were characterized at a single time point after infarct (7 days), it important to note that there is a complex temporal profile of gene regulation over time (Carmichael ST *et al.* 2005). Seven days was chosen in this study because it represents the beginning of an initiation phase of growth promotion. However, future studies will be important to address other time points to establish a more complete temporal profile of neuron-specific gene expression during trigger, initiation, maintenance and termination phases.

The importance of understanding the temporal profile of gene expression changes after brain injury is related to the potential for identifying specific targets for therapeutic development. It may be possible to induce adaptive changes in neuronal connections by triggering one or more of the identified pathways at

specific time points after injury. Likewise, in the future, it will be critical to understand how various rehabilitative therapies affect both growth-promoting and growth-inhibiting molecules. Such neuron-specific gene expression studies may be used for the development of surrogate markers of recovery.

Genes Regulated in Current Study

The genes most differentially regulated in the current study can be grouped into several categories, based on their presumed function, including nervous system development, neuroprotection, apoptosis, axonal growth and guidance, and several genes that have not been associated with ischemia previously. There were also genes with expression profiles that were counterintuitive to expectations.

Development

Regulation of developmentally-associated genes after focal cortical infarct is consistent with the findings of other studies involving neuronal gene expression *in vivo*. Northern blot analysis of E13 and newborn mice showed increased expression of fibulin 2 (Fbln2, +2.26 fold change in the current study) in certain ganglia and embryonic spinal cord, suggesting a role in motor neuron development (Zhang HY et al. 1996). Tripartite motif containing 54 (Trim54, -1.503 fold change in the current experiment) an E3 ubiquitin ligase is not

significantly expressed before birth, and knockdown perturbs tubulin dynamics and disrupts ordered Z and M bands in cardiac development (Perera S et al. 2011). Chondrolectin (Chodl, -1.533 fold change in the current experiment) a type I transmembrane protein is important in development, proliferation and differentiation of a myoblastic cell line and maturation of T-cells in mice (Weng L, DR Van Bockstaele, et al. 2003; Claessens A et al. 2008). Chodl was also localized to cholinergic, fast motor neurons in spinal cord with *in situ* hybridization and in the brain of adult mice with southern blot (Weng L, R Hubner, et al. 2003; Enjin A et al. 2010). Cellular repressor of E1A-stimulated genes 1 (Creg1, +1.96 fold change in the current study), a secreted glycoprotein, is suggested to have a role in development of the mouse brain, due to its differential gene expression and protein concentration pattern (Yang G et al. 2011). CREG1 enhances differentiation, reduces proliferation, and its RNA is present in adult mouse brain (Veal E et al. 2000).

Other genes are also involved in neuronal development. Nnat is an imprinted gene important in hindbrain development (Sowpati DT et al. 2008). Oprk1 is involved in EGF-stimulated spinal cord development (Tsai NP et al. 2010). Mycbp2 is involved in retinocollicular targeting (Vo BQ et al. 2011), while thyroid hormone partially regulates brain development through Cd44 (Dong H et al. 2009). Finally, Sema4b is important for the developing cerebellum (Maier V et al. 2011), and Bmp1 (Ge G and DS Greenspan 2006) and Bmp4 (Mehler MF et al. 1997) are involved in dorsal/ventral patterning of the embryo. These genes

are differentially expressed during neuronal development and are differentially expressed in the same direction after CNS injury in adult rat, consistent with a return to a previous developmental state.

Carmichael et al found that although developmentally related genes in peri-infarct tissue were differentially expressed after cortical infarct, the expression pattern included genes not reported with development and the authors suggested that regeneration exhibits a unique pattern of expression (Carmichael ST *et al.* 2005). Likewise, the current study found genes not typically associated with development, but involved in regeneration. For example, Tubb2c increases neurite sprouting (Lewis GP et al. 1998; Mandal N et al. 2011), while Gng11 regulates senescence (Hossain MN et al. 2006). Scn4b up-regulation increases neuroblastoma cell neurite extension and dendritic spine density in hippocampal primary neuron cultures (Oyama F et al. 2006), while Dennd4c is a guanine exchange factor (Sano H et al. 2011). The differential regulation of genes in the current study associated with neuronal development as well as unique regenerative genes may suggest axonal regeneration is taking place in RFA neurons.

Neuroprotection

Regulation of a gene thought to be involved in neuroprotection was also found. Knockdown of sodium channel, voltage-gated, type IV, beta, (Scn4b, -1.72 fold change in the current study) has been shown to decrease the resurgent

firing in cultured cerebellar granule neurons (Bant JS and IM Raman 2010). Preventing resurgent firing may provide protection from excitotoxic injury in neurons reciprocally connected to an area undergoing anoxic depolarizations, as in our model; thus, its down regulation in the current model may be neuroprotective. Its role in development has yet to be investigated (Brackenbury WJ and LL Isom 2011)

Apoptosis

Apoptosis related gene expression changes also were detected in the current study. In a model of middle cerebral artery (MCA) occlusion, intracortical ET-1 injection near the MCA led to hypoperfusion of the cortex for 16-22 hours (Biernaskie J et al. 2001). After 2 hr of transient or permanent MCA occlusion, cell death in the penumbra and ischemic core was similar for 2 hr of transient or permanent MCA occlusion (Zhang RL et al. 1994). Although the time course of apoptosis and necrosis is unknown in our model, the potentially long lasting effects of ET-1 make more probable the comparison between our model and other focal lesions. Neuronal apoptosis and necrosis during a ligation model of focal ischemic cortical infarct peak at 1 day post-infarct, and are minimal by 5 days post-infarct, as shown by caspase 3 activation, and 8-Hydroxy-2-deoxy guanosine (8-OH-dG) and TUNEL staining (Katsman D *et al.* 2003). This time frame is consistent with the observation that 24 hr after ischemia ~80% of neurons in the ischemic core in focal ischemia have apoptosed (Lipton P 1999).

In the current study, the RFA is outside the lesion core and penumbra, and therefore outside of the area of known apoptosis. Further, neuronal harvesting was conducted 7 days after the infarct, at a time when further cell death was minimal anywhere in the cortex. Therefore, neurons undergoing apoptosis would have already done so, and not been collected in the LCM process. In addition to the previously stated role for CREG1, CREG1 upregulation inhibits apoptosis of cultured vascular smooth muscle cells, and was inversely correlated with caspace-3 activation (Han Y et al. 2010). Apoptotic and anti-apoptotic related gene changes in the current study were relatively few, but those present may be enough to instigate apoptosis in surviving cortical neurons. The presence of both apoptotic and anti-apoptotic related genes may indicate different populations of interconnected neurons undergoing stages of apoptosis, neuroprotection, or are still within the decision process of whether to enter apoptosis or not.

Axonal Growth and Guidance

Several genes were related to sprouting or axonal growth, but not included in the canonical IPA pathway of "Axonal Guidance Signaling". A decrease of MYC binding protein 2 (MycBp2, -1.69 fold change in the current study) was shown to increase axonal regeneration in adult c. elegans after axotomy (Nix P et al. 2011). CD44 molecule (Indian blood group) (Cd44, +1.894 fold change in the current study) a cell-adhesion molecule involved in extracellular matrix changes can influence cell growth, survival and differentiation (Ponta H et al. 2003). CD44

acts as a repulsive signal for retinal ganglionic cell axons entering the embryonic diencephalon that will become the optic chiasm and has been reported to decrease neurite length of retinal neuron explants in vitro (Sretavan DW et al. 1994). The increase in CD44 in the current experiment may play a role in decreasing axon length.

Novel Gene Not Previously Reported with Stroke

Genes not previously reported in ischemia, were also differentially expressed in the present study. While the novelty of these findings may be related to the specific time point chosen for analysis in various studies, it may represent novel findings important to the specific roles of interconnected neurons after injury. DENN/MADD domain containing 4C (Dennd4c, +2.081 in the current study) is a guanine nucleotide exchange factor for RAB10. Activation of RAB10 by DENND4C leads to increased trafficking of glucose transporter, GLUT4, to the cell membrane in adipocyte cultures and an increase of glucose influx (Sano H *et al.* 2011). *In situ* hybridization has shown that Glut4 mRNA is localized to neurons within the rat motor cortex (El Messari S et al. 2002).

Genes with Presumably Paradoxical Expression

There were several genes that did not fit with expected expression patterns. It has been shown that Artemin treatment (3 hrs) of adult rat DRG neurons increased total neurite length, branching and synaptic vesicle clustering,

and decreased neuronatin (Park S and YW Hong 2006). The increase in Neuronatin in the current study (Nnat, +2.145 fold change) would seem to hinder neurite extension, and is contrary to expectations. Down-regulation of opioid receptor, kappa 1 in the current study (Oprk1, -1.76 fold change) also is paradoxical, in that agonism during ischemia has been shown to be neuroprotective (Zhang Z et al. 2003) and knockdown or inhibition leads to less EGF-stimulated growth in cultured neurons (Tsai NP *et al.* 2010). A decrease in opioid receptor would seemingly increase neuronal death and decrease sprouting. It is possible this could be indicative of a balance between maintaining enough activity to induce and guide sprouting, and decreasing activity, so as not to induce excitotoxicity. GABA disinhibition and NMDA receptor increase has been noted in areas interconnected to an infarct (Chen R et al. 2002). Growth associated protein of 43 kDa (Gap43) was not found to be differentially regulated in the current experiment, even though it is found at this time point (7 days post-infarct) in neuronal sprouting studies in similar distances from the cortex, and is seen as a paradigmatic growth cone marker (Stroemer RP et al. 1993; Carmichael ST *et al.* 2005). This suggests that some or all of the collected neurons are not sprouting, or that they do sprout but do not employ Gap43 up-regulation. However, interconnected neurons could instead be serving as a relay station, signaling and instigating reorganization in nearby neurons, instead of the interconnected neurons themselves sprouting. As size and type of lesion is also important during reorganization, this lesion may not be of a sufficient size or type

to instigate sprouting (Carmichael ST and MF Chesselet 2002; Dancause N *et al.* 2006b).

Biological Context Revealed by IPA

In the current study, IPA software was used to give broader biological implications beyond what would be concluded by the identification of single genes significantly regulated. Gene product functions, pathways, and interactions are based on the Ingenuity Knowledge Base, a curated database of literature findings. IPA is well accepted by the scientific community and a PubMed search reveals 473 articles involving the software, as well as 13 reviews, since the year 2005.

Select functions found to be overrepresented were “Branching of Neurites”, “Organization of Cytoskeleton”, “Dendritic Growth and Branching”, “Organization of Cytoplasm”, “Guidance of Neurites”, “Development of Cellular Protrusions”, “Density of Dendritic Spines”, and “Shape Change,” and involved 50 genes. These functions involve morphological changes, and are consistent with collected neuron reorganization.

IPA identified genes ($\geq \pm 1.3$ fold change and $p < 0.05$) that were overrepresented in several canonical pathways: “Axonal Guidance Signaling”, “Actin-based Motility by Rho”, and “Actin Cytoskeleton Signaling”. IPA also identified the functional categories of cytoplasmic restructuring, and cytoskeletal

reorganization. Genes changed within these pathways and functional categories are consistent with other studies of reorganization. These genetic changes show that 7 days after CFA infarct, RFA neurons activate gene expression conducive to sprouting and reorganization. This suggests axonal sprouting is part of the response to ischemic infarct in axons connected to an infarct.

Those genes in the "Axonal Guidance Signaling" pathway of ≥±1.5 fold changed and p-value< 0.05 are further discussed below. They were also reanalyzed to determine interactions beyond the canonical pathway. Interactions were found that are different than those in the canonical pathway, and these interactions may be important in this model.

Relevance for the Most Regulated Genes of the "Axonal Guidance Signaling" Pathway

Sema4B

Semaphorins were originally characterized as negative guidance cues of axonal growth cones, are both soluble and membrane bound ligands, and can act as receptors themselves. They have both long and short range effects on the morphology of various cell types (Tran TS et al. 2007). As such, Semaphorins are repulsive signaling proteins involved in axonal guidance and dendritic structure (Tran TS *et al.* 2007). Semaphorin 4b (Sema4b, +1.54 fold change in the current study), primarily localized to Bergman glia and astrocytes in postnatal

mice, may be important in granule cell migration and proper formation of the cerebellum (Maier V *et al.* 2011). By knocking down Sema4b and staining for synapsin 1 and PSD-95 in in vitro cultures of E18 hippocampal neurons, Paradis et al. found Sema4b was necessary for gluatamatergic synapse formation (Paradis S et al. 2007). RNA in situ hybridization experiments detected Sema4B in neurons (with low level signal in chondrocytes) from E14-E19 in Sprague-Dawley rats. It was absent in adults, but increased in olfactory epithelium neurons 2 weeks after olfactory bulbectomy. The authors suggested Sema4b's presence in the adult bulbectomy model instigated a growth pause in regenerating axons because the axons lacked the target of the bulb (Williams-Hogarth LC et al. 2000).

Tubb2c

Microtubules are cytoskeletal proteins involved in diverse processes from signaling to mitosis, and are formed from heterodimers of alpha and beta-tubulin. Beta-tubulin 2c (Tubb2c, +2.00 fold change in the current study), one of several isoforms identified, is ubiquitous in human tissues (Leandro-Garcia LJ et al. 2010). Lewis et al, used adult cats to show neurite outgrowth from neurons whose cell bodies reside in the inner nuclear layer after retinal detachment (Lewis GP *et al.* 1998). The inner nuclear layer was later shown to have an increase in TUBB2C protein 7 days after retinal detachment in rabbits (Mandal N *et al.* 2011). This increase in TUBB2C points to its possible role in sprouting.

Bmp1

Bone morphogenetic protein 1 (Bmp1, +1.46 fold change in the current study) is the prototype of a highly conserved family of metalloproteinase involved in dorso-ventral patterning in the vertebrate embryo through activation of BMP2 and 4 (Ge G and DS Greenspan 2006). Originally thought to activate the other BMP's with which it was co-purified, it was later found to have procollagen C-proteinase activity. Its role in development may come from formation of extracellular matrix and activity of growth factors (Hopkins DR et al. 2007). Also, mRNA of the Aplysia homolog to Bmp1 (Aplysia tolloid/BMP-1-like protein, apTBL-1) was increased after long term training in Aplysia and was suggested to play a role in synaptic plasticity between sensory and motor neurons (Liu QR et al. 1997).

Bmp4

Bone morphogenetic protein 4 (Bmp4, +1.51 fold change in the current study) is part of the transforming growth factor beta (TGF-b) superfamily localized to the extracellular space. BMP2 and BMP4-7 are involved in dorsal patterning in the embryo, while sonic hedgehog (SHH) is responsible for the ventral. Intracisternal injection of BMP7, which activates similar receptors as does BMP4 (Mehler MF *et al.* 1997), increased behavioral recovery in rats after MCAO, without decreasing the lesion size (Kawamata T et al. 1998). It was suggested

that the behavioral improvements were related to the BMP7's known instigation of dendrite growth and development (Withers GS et al. 2000). BMP4 is also present during neural tube closing and is suggested to have autocrine or paracrine activity during development (Mehler MF *et al.* 1997). Injection of an Adeno-associated virus encoding Bmp4 into the dorsal root ganglia increased the ability of severed axons to regenerate after spinal cord injury (complete dorsal column transection) in adult mice. Regeneration was increased even if injection occurred 15 min after transection (Parikh P et al. 2011).

Gng11

Guanine nucleotide binding protein (G protein) gamma 11 (Gng11, +1.81 fold change in the current study), a membrane bound G-protein subunit that can translocate to the Golgi apparatus and alter its structure, may have a role in increasing cell senescence (Cho JH et al. 2011). Gng11 down-regulation by antisense cDNA increased longevity of human fibroblasts and oxidative stress induced its transcription. Over expression leads to activation of ERK1/2 but not RAS (Hossain MN *et al.* 2006). GNG11 was not found in normal retina or brain tissue (Balcueva EA et al. 2000). The gamma11 subunit has differential A1 adenosine receptor, M1 muscarinic receptor and phospholipase C-beta activation depending on beta subunit pairings (McIntire WE et al. 2006). Gamma11 was not found in rat brain by immunoblot but expression was abundant in blood cells and may explain its presence at 7 days (Morishita R et al. 1998). As GNG11

increase leads to senescence, this may represent a paradoxical expression pattern.

Summary

In summary, stroke induces a unique set of gene expression patterns in spared interconnected corticocortical neurons 7 days after ischemic infarct. The gene expression patterns display up- and down regulation associated with nervous system development, apoptosis, and axonal growth. Several have not been reported previously in ischemia models. Canonical pathways and interaction networks developed with IPA suggest gene product interactions. Though RFA neurons display some aspects of reorganization, they may serve to instigate other cortical neurons to reorganize, or simply survive. Future experiments will be necessary to further investigate the purpose of this unique genetic program.

Acknowledgements

We would like to thank S. Thomas Carmichael for his consultation and Diane Durham and Doug Wright and their lab members for advice and equipment usage. We would also like to thank Don Warn, Yafen Niu, Clark Bloomer, Stan Svojanovsky and Sumedha Gunewardena. This work was supported by NIH

grant R37 NS030853, NICHD HD02528, and the Landon Center on Aging. The Microarray Facility is supported by the Kansas University-School of Medicine, KUMC Biotechnology Support Facility, the Smith Intellectual and Developmental Disabilities Research Center (HD02528), and the Kansas IDeA Network of Biomedical Research Excellence (RR016475).

Chapter 5

Discussion

Summarization of Results

This series of experiments has shown the cortical connectivity of RFA (Ch. 2), the connectivity changes four weeks after an ischemic infarct to the primary motor cortex (Ch. 3), and the gene expression changes 7-days post-infarct that may be the substrate for the anatomical reorganization (Ch. 4).

The second chapter shows a clear picture of the corticocortical connectivity of RFA. The RFA does not connect homogeneously throughout the cortex. It preferentially connects to other motor regions, multisensory regions, and higher order processing regions. This work confirms the work of others, but adds specificity that was not previously present. It also provides evidence that RFA shares a cortical connectivity pattern similar to the PMv of primates, and strengthens the argument for homology of these regions.

The third chapter provides evidence of corticocortical reorganization of the RFA four weeks after motor cortex ischemic infarct. Although other models in rats show corticocortical reorganization is possible in the somatosensory and spinal column after various cortical lesions, this study is the first to specifically target changes in the premotor cortex of the rat after specific motor cortex lesion.

The fourth chapter identifies gene expression changes, which may represent the substrate for anatomical changes discussed in the third chapter. These gene expression changes occur 7-days post-infarct. This time frame is consistent with the instigation phase of expression changes, thought to be

responsible for anatomical reorganization found in other models. The fourth chapter provides further evidence that post-infarct reorganization requires differential gene expression.

Together, these studies increase the field of knowledge concerning the premotor cortex in the rat and its response to injury of an interconnected region.

Methodological Details

There are several methodological decisions that aided in the success of this set of studies. From lesion choice to tract tracer, and even model animal, the decisions affect the generalizability of any findings.

Choice of Lesion Type

The lesion type itself is important to the resulting reorganization or lack thereof. Aspiration lesions did not produce reorganization, even though they were of the same size and location as thermal-ischemic lesions (Carmichael ST and MF Chesselet 2002). An ischemic infarct is also more closely related to the natural process of stroke in other species, unlike mechanical or thermal injury produced in some models.

The vasoconstrictor Endothelin 1 (Et-1), was used to create the current ischemic model. Et-1 is an endogenous compound in mammals. In other models, injecting the cortex near the large middle cerebral artery created

hypoperfusion for 16-22 hours (Biernaskie J *et al.* 2001), which was enough to cause permanent ischemia. The ability to constrict arteries by diffusion through tissue was exploited in the current model. This method has been shown to create complete lesions throughout the cortical layers with little involvement of the corpus callosum (Fang PC *et al.* 2010).

BDA Tract Tracer

Considering the properties of neuroanatomical tracers is paramount to a successful study. Biotinylated dextran amine (BDA) has been used extensively for its non-toxic, fixable, anterograde and retrograde tracing properties. Anterograde tracing is favored with the 3,000 molecular weight polymer and shorter in vivo incubation times, while retrograde tracing is favored with the 10,000 molecular weight polymer and longer in vivo incubation times. Both molecular weight polymers will label in the reverse direction less effectively. Streptavidin conjugated to peroxidase can be easily attached and reacted with diamobenzidine to create an indelible brown product that is visible in light or electron microscopy. Axons, dendrites, spines, boutons, and soma can be completely labeled for long periods of time. BDA signal is not degraded over long periods within animal neurons. It is stable both before and after tissue harvest. Within squirrel monkey, detection up to 7 weeks of in vivo has been reported without distinguishable loss of signal for BDA reacted with DAB elite kit

(Brandt HM and AV Apkarian 1992). The length of time required to quantify connectivity mandates a stable label.

The label-filled boutons have also been shown to be the light microscopic equivalent of synapses. Electron microscopy of BDA labeled cortico-cortical axons show 1.7 synapses per bouton when synapsing on spines, dendrites and somata of other neurons and some boutons were large enough to envelope the spine head (Anderson JC et al. 1998). As this is a study of connectivity, such identification is necessary.

Though biotinylated dextran amine is an anatomical study stalwart, it is not without its considerations. Biotinylated dextran amine can be carried in both anterograde and retrograde directions, having the effect of filling a cell and all of its projections, if given enough time (Chen S and G Aston-Jones 1998). One can imagine a situation in which a retrogradely labeled axon with labeled-filled collaterals appears to be an anterogradely labeled axon from the area of interest. Even a retrogradely axon could have anterograde transport that would fill the axon and give the appearance of boutons on an anterogradely labeled axon. As there is no way to eliminate such labeling, boutons of such a nature would certainly be counted as anterogradely labeled from the area of interest.

CTB tracer

The use of cholera toxin beta subunit has special considerations as well. There is evidence of uptake in fibers of passage and both anterograde and

retrograde transport (Chen S and G Aston-Jones 1995). In the current gene expression study using CTB, the collection process targeted cell bodies, so any anterograde transport would not have interfered with proper identification and extraction of labeled neurons. Labeling fibers of passage is a more problematic issue, in that one could imagine a situation in which a corticocortical axon was labeled because it passed through the injection core but did not maintain synapses with the CFA. The lesion overlapped the CTB injection core. Any fibers passing through the CTB injection core would necessarily also pass through the lesion core. Fibers passing though the lesion, regardless of final target would be subjected to an environment that instigates retraction and degeneration in cultured neurons; therefore, even soma labeled from fibers of passage would be collected from the RFA, and be de-efferented neurons, just like the other RFA neurons which projected to the newly lesioned CFA. In the current experiment of connectivity, the CTB647 was used as a fiducial marker only, negating any effect in tract tracing.

Contralesional Cortex Relevance in Stroke

The contralesional cortex has been studied in the same ways as ipsilateral cortex. Contralateral hemisphere activity is important during stroke, as overactivity of the uninjured side after lesion is thought to contribute to diaschisis. The contralesional and ipsilesional cortex hyperexcitably up to days after photothrombic stroke in rat has also been suggested to contribute to

reorganization (Buchkremer-Ratzmann I et al. 1996). After pyramidal tract lesion (pyramidotomy) and treatment with a neutralizing antibody to a myelin-associated neurite growth inhibitor, corticorubral and corticopontine sprouting from the uninjured side was identified, and was correlated with improved function on pellet retrieval, rope climbing and grid walking tasks (Z'Graggen WJ et al. 1998). These other pathways might play a role in recovery after CNS injury in rats.

Although the contralateral cortex activity increases after stroke, it seems to be related with larger lesions that do not leave enough tissue on the ipsilateral cortex to take over function. In fMRI studies, contralateral tissue activation is associated with worse functional outcomes (Carey JR et al. 2002). Studies which train the unaffected arm after stroke show increased dendritic arborization, but this is correlated with decrease in function of the injured arm (Luke LM et al. 2004; Allred RP and TA Jones 2008). As the ultimate goal is to increase function for stroke survivors, a paradigm that is detrimental to the injured cortex is not as useful and brings doubt into the contralateral cortex's role in behavioral recovery after stroke.

Ipsilateral connections from the contralesional side might also play a role in functional recovery after unilateral stroke. Ipsilateral connections do exist and can be stimulated during ICMS of the motor cortex. It has been suggested that strengthening of ipsilateral may play a role in recovery of function. Without treatments to increase the effectiveness of corticospinal signal, this affect seems to require the influence of the intact homotopic cortical area. No ipsilateral

movements were found in rats after deactivation of the homotypic motor cortex or contralateral pyramid laceration (Brus-Ramer M et al. 2009). Reliance on an intact contralateral side may limit any models role in the recovery process.

Use of Laser Capture Microdissection

The extraction of RNA from specific cells in the brain for analysis is difficult. Digestion of neonatal rat brain has been described, followed by flow cytometry to separate pre-labeled cells. Although RNA can be isolated successfully after flow cytometry, the adult rat brain is not conducive to current digestion protocols (Barrett MT et al. 2002). Therefore, LCM was chosen as the best method of neuron extraction.

Significance of Results

Anatomical Reorganization

Some lesion models that involve recovery of function do not include physiological reorganization. In one study, contusion, ablation and undercut lesions involving the hind limb motor cortex, did not produce reorganization of motor map representation (Boyeson MG et al. 1991). The rats receiving the ablation recovered function (Boyeson MG *et al.* 1991), even though ablation injury has not instigated anatomical reorganization in same cortex that will anatomically reorganize if given ischemic injury (Carmichael ST and MF

Chesselet 2002). Such examples represent the main argument against the relationship between recovery of function and reorganization. If recovery can occur without anatomical or physiological reorganization, there may be some other location or mechanism to underlie recovery in the rat.

Though this is a consideration, the current studies (Ch. 3 in specific) show evidence of reorganization in a region, which is important for recovery of function. RFA was shown to increase connectivity to IN, 28 days post-infarct. A similar model in rats produced a lesion in the primary motor cortex, allowed for recovery, and then produced a lesion in the RFA. The recovered function was destroyed with RFA destruction (Conner JM *et al.* 2005), providing evidence for the importance of the RFA in recovery after lesion. Taken together with the current studies, which provide evidence of anatomical change to an uninjured region's connectivity patterns and genetic expression changes occurring during a critical time point involving genes (Ch. 4) likely supportive of said anatomical reorganization, and the question is not a foregone conclusion.

Lesion Size Dependence of Physiological Reorganization

A possible size limitation exists, with larger cortical lesions or spinal cord hemisection (effectively disconnecting hemispheres from spinal cord) leading to more involvement of the uninjured hemisphere. After hemisection in rat, projections from the intact hemisphere can recross the spinal cord and re-innervate the denervated side. It was also found that the intact hemisphere was

responsive to ipsilateral hind limb stimulation through voltage sensitive dyes and IOS imaging (Ghosh A et al. 2009). The size dependent nature of lesion specific reorganization was also highlighted by work done by the Biernaskie lab (Biernaskie J et al. 2005). Rats were given large and small infarcts and trained on a retrieval task. After 4 weeks of recovery and rehabilitation, the intact hemisphere was deactivated with lidocaine injection, and rats were tested on the retrieval task again. Rats with large lesions had significantly impaired performance after deactivation of the uninjured hemisphere, but those with small lesions were not significantly impaired. This suggests that with large lesions, the uninjured hemisphere is relied upon for regaining function, while during a small lesion, the remaining cortex in the injured hemisphere may be sufficient to reorganize and regain the lost function. The current results (Ch 3) seem to be consistent with this size dependence, as the cortical lesion produced in the current studies are small and the reorganization occurred in the ipsilesional cortex.

Generalizability of Results

Some differences in rat and higher mammals' brain function do exist. The striatum is used more often in rat movement. This non-cortical area can take over functions that would be solely cortical in primates. Some studies suggest that although the striatum is utilized during stereotyped movements, both

excitatory and inhibitory cortical neurons are active during skilled reaching task (Hyland B 1998). Having cortical involvement during movements makes the results more generalizable.

Monosynaptic corticomotor connections are thought to exist in primates, but not rat and underlie the primate's increased hand dexterity over the rat. There is some evidence that minor components of the corticospinal tract make monosynaptic connections in rodents (Bareyre FM et al. 2005). In order to show connectivity corticospinal axons and synapses must be labeled in an anterograde direction from the cortex. The cell bodies of motor neurons within the spinal cord must be retrogradely labeled from the muscle itself. If labeled synapses form, they can only come from a direct corticomotor connection. Such direct connection was observed in one model using stable expression of yellow fluorescent protein (YFP) in mice layer V corticospinal neurons and synaptic vesicle (SV2) immunofluorescence and retrograde label from hind limb muscle for motor neuron location. The other nuclei sending projections to the spinal cord did not contain YFP+ neurons. Thus aberrant YFP expression in the red nucleus, superior colliculus, and reticular formation could not account for synaptic connections. This adds to the similarities between rodent and primate models (Bareyre FM *et al.* 2005). In a rat model, ICMS was used to find physiologically defined cortical regions and the specific muscle groups activated, then anterograde tracer was injected into cortex and retrograde tracer was injected into the muscle group. Under light microscopy, contacts were made between

corticospinal projections and motor neurons (Liang FY et al. 1991). Though this is minimal evidence for monosynaptic corticospinal connections, it does show that some corticomotor connectivity may be present in the rat similar to that found in the primate.

Translating animal research results into primates and possibly one-day humans is problematic. Although amphetamine was mostly successful in improvement of function of rat and cat, the human trials were not as effective (Barbay S and RJ Nudo 2009). On the other hand, parietal cortex lesions in the rat produce similar deficits as human and non-human primate lesions of the parietal cortex, namely visual-spatial and attentional deficits (DiMattia BV and RP Kesner 1988). The frontal pole has a role in maintaining attention in the rat and bilateral frontoparietal area lesions create deficits in reaction time to visual cue for food reward (Baunez C *et al.* 1998). In human children stroke survivors during the subacute phase (5-30 days) and in rat pups 1 week after ischemia, X-linked inhibitor of apoptosis protein (XIAP) is increased and may be neuroprotective (Askalan R et al. 2009). These examples show that at least some brain regions and processes have good correlation between species.

Environmental factors may be important in translation. Plasticity is active in nonlesioned animals, and this has implications for animal models of stroke. Human stroke survivors invariably experience an enriched environment compared to the Spartan accommodations of a singly housed animal, therefore

animal studies would seem more translational if the manipulation of interest was performed against a backdrop of enriched environments (Xerri C *et al.* 1996).

Different locations of stroke may make translation more difficult. Although specific location of stroke is less studied in human research as location is random in survivors, some evidence shows the brain reacts differently to different stroke locations. Activation patterns determined by fMRI during elbow flexion were different between survivors of sensorimotor cortex plus subcortical lesions and subcortical lesions only (Luft AR et al. 2004). The subcortical survivors activated areas more similar to normal activation patterns (contralateral motor, ipsilateral cerebellum, bilateral mesial (MSA, cingulate) and perisylvian), but the cortical survivors activated much different areas (ipsilateral postcentral mesial and peri-infarct.) This suggests the brain is employing different strategies for recovery depending on location of lesion despite similar behavior deficits.

The Future of Stroke Research: Unanswered Questions

What are the factors that direct neural sprouting after injury?

The relationship of exogenous guidance cues to in vivo sprouting after injury is still an open question. Semaphorins act as both attractive and repellant cues for axon guidance during development. Embryonic neurons had binding sites for neuropilin-1 and neuropilin-2 (semaphorin receptor components) during periods of development when corticofugal projections are forming (Bagnard D et

al. 1998). Neurotrophin 3 was overexpressed in specific areas of the brain stem, and after spinal cord injury the in vivo gradient not only led to regenerating axons extending into the lesion site and past the lesion site, but it also led to regenerating axons re-innervating both a physiologically appropriate (nucleus gracilis) site, as well as researcher designated site (reticular formation). Although synapses were not confirmed to be functional, the axons formed morphologically correct axodendritic synapses (Alto LT et al. 2009). In this case, the guidance cue was overexpressed by experimentation, but it is an effective example of the important role endogenous guidance cues may be playing after injury. More studies involving guidance cues would be warranted.

Are new connections beneficial?

There is still the question of exuberant projections. Cortical neurons, primed by the ischemic injury to change gene expression, may send out a multitude of projections, which connect at random to a receptive environment. Connections forming in such a process could range from beneficial to simply unbeneficial to detrimental to the organism. The evidence presented in Ch. 3 suggests a more focused process, but more study is necessary.

What could the far-off future hold?

Successful therapeutic interventions for stroke have been few in number and wrought with problems. The advent of tissue plasminogen activator (tPA)

treatment was amazingly affective, but has been restricted severely by a tight treatment period after the stroke. This “clot-buster” reduces ischemia and necrosis by removing the blockage within the vascular system. Only a small percentage of stroke victims seek treatment within the effective treatment period. Though education is increasing regarding the symptoms of stroke and the need for quick response to take advantage of this small treatment window, there will always be those that do not receive the treatment. The 15% of strokes yearly that are hemorrhagic are not candidates for tPA and some comorbidities are contraindicated (Roger VL *et al.* 2011). Hence, there will always be a need for studies of the brain’s response to ischemia. Studies showing increased anatomical reorganization leads to increased recovery of function are the most exciting (Zai L *et al.* 2009). Future studies should be geared to confirm the beneficial nature of reorganization. If reorganization is proven beneficial, work could be done to discover the best way to guide reorganization, and understand which brain regions are the most important for recovery after lesion of specific cortical areas. In the far-off future, it may be a possibility to guide reorganization in vivo to the most advantageous regions in order to maximize any functional recovery needed.

References

http://www.stroke.org/site/PageServer?pagename=REHABT
http://www.heart.org/HEARTORG/General/Heart-and-Stroke-Association-Statistics_UCM_319064_SubHomePage.jsp
Adkins DL, Hsu JE, Jones TA. 2008. Motor cortical stimulation promotes synaptic plasticity and behavioral improvements following sensorimotor cortex lesions. Exp Neurol. 212:14-28.

Allred RP, Jones TA. 2008. Maladaptive effects of learning with the less-affected forelimb after focal cortical infarcts in rats. Exp Neurol. 210:172-181.

Alto LT, Havton LA, Conner JM, Hollis Ii ER, Blesch A, Tuszynski MH. 2009. Chemotropic guidance facilitates axonal regeneration and synapse formation after spinal cord injury. Nat Neurosci. 12:1106-1113.

Alves FH, Gomes FV, Reis DG, Crestani CC, Correa FM, Guimaraes FS, Resstel LB. 2013. Involvement of the insular cortex in the consolidation and expression of contextual fear conditioning. Eur J Neurosci.

Anderson JC, Binzegger T, Martin KA, Rockland KS. 1998. The connection from cortical area V1 to V5: a light and electron microscopic study. J Neurosci. 18:10525-10540.

Arvidsson A, Collin T, Kirik D, Kokaia Z, Lindvall O. 2002. Neuronal replacement from endogenous precursors in the adult brain after stroke. Nat Med. 8:963-970.

Askalan R, Salweski R, Tuor UI, Hutchison J, Hawkins C. 2009. X-linked inhibitor of apoptosis protein expression after ischemic injury in the human and rat developing brain. Pediatr Res. 65:21-26.

Astrup J, Siesjo BK, Symon L. 1981. Thresholds in cerebral ischemia - the ischemic penumbra. Stroke. 12:723-725.

Astrup J, Symon L, Branston NM, Lassen NA. 1977. Cortical evoked potential and extracellular K+ and H+ at critical levels of brain ischemia. Stroke. 8:51-57.
Back T. 1998. Pathophysiology of the ischemic penumbra--revision of a concept. Cell Mol Neurobiol. 18:621-638.

Bagnard D, Lohrum M, Uziel D, Puschel AW, Bolz J. 1998. Semaphorins act as attractive and repulsive guidance signals during the development of cortical projections. Development. 125:5043-5053.

Balcueva EA, Wang Q, Hughes H, Kunsch C, Yu Z, Robishaw JD. 2000. Human G protein gamma(11) and gamma(14) subtypes define a new functional subclass. Exp Cell Res. 257:310-319.

Balestrino M. 1995. Pathophysiology of anoxic depolarization: new findings and a working hypothesis. J Neurosci Methods. 59:99-103.

Bant JS, Raman IM. 2010. Control of transient, resurgent, and persistent current by open-channel block by Na channel beta4 in cultured cerebellar granule neurons. Proc Natl Acad Sci U S A. 107:12357-12362.

Barbay S, Nudo RJ. 2009. The effects of amphetamine on recovery of function in animal models of cerebral injury: a critical appraisal. NeuroRehabilitation. 25:5-17.

Bareyre FM, Kerschensteiner M, Misgeld T, Sanes JR. 2005. Transgenic labeling of the corticospinal tract for monitoring axonal responses to spinal cord injury. Nat Med. 11:1355-1360.

Barrett MT, Glogovac J, Prevo LJ, Reid BJ, Porter P, Rabinovitch PS. 2002. High-quality RNA and DNA from flow cytometrically sorted human epithelial cells and tissues. Biotechniques. 32:888-890, 892, 894, 896.

Barth DS, Goldberg N, Brett B, Di S. 1995. The spatiotemporal organization of auditory, visual, and auditory-visual evoked potentials in rat cortex. Brain Res. 678:177-190.

Baunez C, Salin P, Nieoullon A, Amalric M. 1998. Impaired performance in a conditioned reaction time task after thermocoagulatory lesions of the fronto-parietal cortex in rats. Cerebral Cortex. 8:301-309.

Becker T, Bernhardt RR, Reinhard E, Wullimann MF, Tongiorgi E, Schachner M. 1998. Readiness of zebrafish brain neurons to regenerate a spinal axon correlates with differential expression of specific cell recognition molecules. J Neurosci. 18:5789-5803.

Benowitz LI, Carmichael ST. 2010. Promoting axonal rewiring to improve outcome after stroke. Neurobiol Dis. 37:259-266.

Bernier PJ, Vinet J, Cossette M, Parent A. 2000. Characterization of the subventricular zone of the adult human brain: evidence for the involvement of Bcl-2. Neurosci Res. 37:67-78.

Biernaskie J, Corbett D, Peeling J, Wells J, Lei H. 2001. A serial MR study of cerebral blood flow changes and lesion development following endothelin-1-induced ischemia in rats. Magn Reson Med. 46:827-830.

Biernaskie J, Szymanska A, Windle V, Corbett D. 2005. Bi-hemispheric contribution to functional motor recovery of the affected forelimb following focal ischemic brain injury in rats. Eur J Neurosci. 21:989-999.

Boyeson MG, Feeney DM, Dail WG. 1991. Cortical microstimulation thresholds adjacent to sensorimotor cortex injury. J Neurotrauma. 8:205-217.

Brackenbury WJ, Isom LL. 2011. Na Channel beta Subunits: Overachievers of the Ion Channel Family. Front Pharmacol. 2:53.

Brandt HM, Apkarian AV. 1992. Biotin-dextran: a sensitive anterograde tracer for neuroanatomic studies in rat and monkey. J Neurosci Methods. 45:35-40.

Brecht M, Krauss A, Muhammad S, Sinai-Esfahani L, Bellanca S, Margrie TW. 2004. Organization of rat vibrissa motor cortex and adjacent areas according to cytoarchitectonics, microstimulation, and intracellular stimulation of identified cells. The Journal of Comparative Neurology. 479:360-373.

Brett-Green B, Fifkova E, Larue DT, Winer JA, Barth DS. 2003. A multisensory zone in rat parietotemporal cortex: intra- and extracellular physiology and thalamocortical connections. J Comp Neurol. 460:223-237.

Brett-Green BA, Chen-Bee CH, Frostig RD. 2001. Comparing the Functional Representations of Central and Border Whiskers in Rat Primary Somatosensory Cortex. The Journal of Neuroscience. 21:9944-9954.

Brown CE, Aminoltejari K, Erb H, Winship IR, Murphy TH. 2009a. In vivo voltage-sensitive dye imaging in adult mice reveals that somatosensory maps lost to stroke are replaced over weeks by new structural and functional circuits with prolonged modes of activation within both the peri-infarct zone and distant sites. J Neurosci. 29:1719-1734.

Brus-Ramer M, Carmel JB, Martin JH. 2009. Motor cortex bilateral motor representation depends on subcortical and interhemispheric interactions. J Neurosci. 29:6196-6206.

Buchkremer-Ratzmann I, August M, Hagemann G, Witte OW. 1996. Electrophysiological transcortical diaschisis after cortical photothrombosis in rat brain. Stroke. 27:1105-1109; discussion 1109-1111.

Burwell RD, Amaral DG. 1998. Cortical afferents of the perirhinal, postrhinal, and entorhinal cortices of the rat. The Journal of Comparative Neurology. 398:179-205.

Calautti C, Baron JC. 2003. Functional neuroimaging studies of motor recovery after stroke in adults: a review. Stroke. 34:1553-1566.

Campi KL, Krubitzer L. 2010. Comparative studies of diurnal and nocturnal rodents: differences in lifestyle result in alterations in cortical field size and number. J Comp Neurol. 518:4491-4512.

Carey JR, Kimberley TJ, Lewis SM, Auerbach EJ, Dorsey L, Rundquist P, Ugurbil K. 2002. Analysis of fMRI and finger tracking training in subjects with chronic stroke. Brain. 125:773-788.

Carmichael ST. 2006. Cellular and molecular mechanisms of neural repair after stroke: making waves. Ann Neurol. 59:735-742.

Carmichael ST, Archibeque I, Luke L, Nolan T, Momiy J, Li S. 2005. Growth-associated gene expression after stroke: evidence for a growth-promoting region in peri-infarct cortex. Exp Neurol. 193:291-311.

Carmichael ST, Chesselet MF. 2002. Synchronous neuronal activity is a signal for axonal sprouting after cortical lesions in the adult. J Neurosci. 22:6062-6070.

Carmichael ST, Tatsukawa K, Katsman D, Tsuyuguchi N, Kornblum HI. 2004. Evolution of diaschisis in a focal stroke model. Stroke. 35:758-763.

Carmichael ST, Wei L, Rovainen CM, Woolsey TA. 2001. New patterns of intracortical projections after focal cortical stroke. Neurobiol Dis. 8:910-922.

Castro-Alamancos MA, Borrel J. 1995. Functional recovery of forelimb response capacity after forelimb primary motor cortex damage in the rat is due to the reorganization of adjacent areas of cortex. Neuroscience. 68:793-805.

Cechetto DF, Saper CB. 1987. Evidence for a viscerotopic sensory representation in the cortex and thalamus in the rat. J Comp Neurol. 262:27-45.

Chapin JK, Lin C-S. 1984. Mapping the body representation in the SI cortex of anesthetized and awake rats. The Journal of Comparative Neurology. 229:199-213.

Chapin JK, Sadeq M, Guise JL. 1987. Corticocortical connections within the primary somatosensory cortex of the rat. J Comp Neurol. 263:326-346.

Chapin JK, Woodward DJ. 1986. Distribution of somatic sensory and active-movement neuronal discharge properties in the MI-SI cortical border area in the rat. Exp Neurol. 91:502-523.

Chen R, Cohen LG, Hallett M. 2002. Nervous system reorganization following injury. Neuroscience. 111:761-773.

Chen S, Aston-Jones G. 1995. Evidence that cholera toxin B subunit (CTb) can be avidly taken up and transported by fibers of passage. Brain Res. 674:107-111.

Chen S, Aston-Jones G. 1998. Axonal collateral-collateral transport of tract tracers in brain neurons: false anterograde labelling and useful tool. Neuroscience. 82:1151-1163.

Cho JH, Saini DK, Karunarathne WK, Kalyanaraman V, Gautam N. 2011. Alteration of Golgi structure in senescent cells and its regulation by a G protein gamma subunit. Cell Signal. 23:785-793.

Chollet F, DiPiero V, Wise RJ, Brooks DJ, Dolan RJ, Frackowiak RS. 1991. The functional anatomy of motor recovery after stroke in humans: a study with positron emission tomography. Ann Neurol. 29:63-71.

Claessens A, Weyn C, Merregaert J. 2008. The cytoplasmic domain of chondrolectin interacts with the beta-subunit of Rab geranylgeranyl transferase. Cell Mol Biol Lett. 13:250-259.

Conner JM, Chiba AA, Tuszynski MH. 2005. The basal forebrain cholinergic system is essential for cortical plasticity and functional recovery following brain injury. Neuron. 46:173-179.

Cooke DF, Padberg J, Zahner T, Krubitzer L. 2011. The Functional Organization and Cortical Connections of Motor Cortex in Squirrels. Cerebral Cortex.

Cramer SC, Nelles G, Benson RR, Kaplan JD, Parker RA, Kwong KK, Kennedy DN, Finklestein SP, Rosen BR. 1997. A functional MRI study of subjects recovered from hemiparetic stroke. Stroke. 28:2518-2527.

Dancause N, Barbay S, Frost SB, Plautz EJ, Chen D, Zoubina EV, Stowe AM, Nudo RJ. 2005. Extensive cortical rewiring after brain injury. J Neurosci. 25:10167-10179.

Dancause N, Barbay S, Frost SB, Plautz EJ, Popescu M, Dixon PM, Stowe AM, Friel KM, Nudo RJ. 2006. Topographically divergent and convergent connectivity between premotor and primary motor cortex. Cereb Cortex. 16:1057-1068.

Dancause N, Barbay S, Frost SB, Plautz EJ, Stowe AM, Friel KM, Nudo RJ. 2006a. Ipsilateral connections of the ventral premotor cortex in a new world primate. J Comp Neurol. 495:374-390.

Dancause N, Barbay S, Frost SB, Zoubina EV, Plautz EJ, Mahnken JD, Nudo RJ. 2006b. Effects of small ischemic lesions in the primary motor cortex on neurophysiological organization in ventral premotor cortex. J Neurophysiol. 96:3506-3511.

Deacon TW, Eichenbaum H, Rosenberg P, Eckmann KW. 1983. Afferent connections of the perirhinal cortex in the rat. J Comp Neurol. 220:168-190.

DiMattia BV, Kesner RP. 1988. Role of the posterior parietal association cortex in the processing of spatial event information. Behav Neurosci. 102:397-403.

Dong H, Yauk CL, Rowan-Carroll A, You SH, Zoeller RT, Lambert I, Wade MG. 2009. Identification of thyroid hormone receptor binding sites and target genes using ChIP-on-chip in developing mouse cerebellum. PLoS One. 4:e4610.

Donoghue JP, Kerman KL, Ebner FF. 1979. Evidence for two organizational plans within the somatic sensory-motor cortex of the rat. The Journal of Comparative Neurology. 183:647-663.

Donoghue JP, Wise SP. 1982. The motor cortex of the rat: cytoarchitecture and microstimulation mapping. J Comp Neurol. 212:76-88.

Dum RP, Strick PL. 2002. Motor areas in the frontal lobe of the primate. Physiology & Behavior. 77:677-682.

El Messari S, Ait-Ikhlef A, Ambroise DH, Penicaud L, Arluison M. 2002. Expression of insulin-responsive glucose transporter GLUT4 mRNA in the rat brain and spinal cord: an in situ hybridization study. J Chem Neuroanat. 24:225-242.

Enjin A, Rabe N, Nakanishi ST, Vallstedt A, Gezelius H, Memic F, Lind M, Hjalt T, Tourtellotte WG, Bruder C, Eichele G, Whelan PJ, Kullander K. 2010.

Identification of novel spinal cholinergic genetic subtypes disclose Chodl and Pitx2 as markers for fast motor neurons and partition cells. J Comp Neurol. 518:2284-2304.

Fabri M, Burton H. 1991. Ipsilateral cortical connections of primary somatic sensory cortex in rats. J Comp Neurol. 311:405-424.

Fang PC, Barbay S, Plautz EJ, Hoover E, Strittmatter SM, Nudo RJ. 2010. Combination of NEP 1-40 treatment and motor training enhances behavioral recovery after a focal cortical infarct in rats. Stroke. 41:544-549.

Frappé I, Roger M, Gaillard A. 1999. Transplants of fetal frontal cortex grafted into the occipital cortex of newborn rats receive a substantial thalamic input from nuclei normally projecting to the frontal cortex. Neuroscience. 89:409-421.

Frost SB, Barbay S, Friel KM, Plautz EJ, Nudo RJ. 2003. Reorganization of remote cortical regions after ischemic brain injury: a potential substrate for stroke recovery. J Neurophysiol. 89:3205-3214.

Gaspar P, Stepniewska I, Kaas JH. 1992. Topography and collateralization of the dopaminergic projections to motor and lateral prefrontal cortex in owl monkeys. J Comp Neurol. 325:1-21.

Ge G, Greenspan DS. 2006. Developmental roles of the BMP1/TLD metalloproteinases. Birth Defects Res C Embryo Today. 78:47-68.

Ghosh A, Sydekum E, Haiss F, Peduzzi S, Zörner B, Schneider R, Baltes C, Rudin M, Weber B, Schwab ME. 2009. Functional and Anatomical Reorganization of the Sensory-Motor Cortex after Incomplete Spinal Cord Injury in Adult Rats. The Journal of Neuroscience. 29:12210-12219.

Hall RD, Lindholm EP. 1974. Organization of motor and somatosensory neocortex in the albino rat. Brain Research. 66:23-38.

Han Y, Wu G, Deng J, Tao J, Guo L, Tian X, Kang J, Zhang X, Yan C. 2010. Cellular repressor of E1A-stimulated genes inhibits human vascular smooth muscle cell apoptosis via blocking P38/JNK MAP kinase activation. J Mol Cell Cardiol. 48:1225-1235.

Harley CA, Bielajew CH. 1992. A comparison of glycogen phosphorylase a and cytochrome oxidase histochemical staining in rat brain. J Comp Neurol. 322:377-389.

Hirokawa J, Bosch M, Sakata S, Sakurai Y, Yamamori T. 2008. Functional role of the secondary visual cortex in multisensory facilitation in rats. Neuroscience. 153:1402-1417.

Hopkins DR, Keles S, Greenspan DS. 2007. The bone morphogenetic protein 1/Tolloid-like metalloproteinases. Matrix Biol. 26:508-523.

Hossain MN, Sakemura R, Fujii M, Ayusawa D. 2006. G-protein gamma subunit GNG11 strongly regulates cellular senescence. Biochem Biophys Res Commun. 351:645-650.

Hyland B. 1998. Neural activity related to reaching and grasping in rostral and caudal regions of rat motor cortex. Behavioural Brain Research. 94:255-269.

Irizarry RA, Hobbs B, Collin F, Beazer-Barclay YD, Antonellis KJ, Scherf U, Speed TP. 2003. Exploration, normalization, and summaries of high density oligonucleotide array probe level data. Biostatistics. 4:249-264.

Jablonka JA, Burnat K, Witte OW, Kossut M. 2010. Remapping of the somatosensory cortex after a photothrombotic stroke: dynamics of the compensatory reorganization. Neuroscience. 165:90-100.

Jones LL, Sajed D, Tuszynski MH. 2003. Axonal regeneration through regions of chondroitin sulfate proteoglycan deposition after spinal cord injury: a balance of permissiveness and inhibition. J Neurosci. 23:9276-9288.

Jones TA, Schallert T. 1992. Overgrowth and pruning of dendrites in adult rats recovering from neocortical damage. Brain Res. 581:156-160.

Jones TA, Schallert T. 1994. Use-dependent growth of pyramidal neurons after neocortical damage. J Neurosci. 14:2140-2152.

Jurgens U. 1984. The efferent and afferent connections of the supplementary motor area. Brain Res. 300:63-81.

Katsman D, Zheng J, Spinelli K, Carmichael ST. 2003. Tissue microenvironments within functional cortical subdivisions adjacent to focal stroke. J Cereb Blood Flow Metab. 23:997-1009.

Kawamata T, Ren J, Chan TC, Charette M, Finklestein SP. 1998. Intracisternal osteogenic protein-1 enhances functional recovery following focal stroke. Neuroreport. 9:1441-1445.

Keyvani K, Witte OW, Paulus W. 2002. Gene expression profiling in perilesional and contralateral areas after ischemia in rat brain. J Cereb Blood Flow Metab. 22:153-160.

Kissela B, Broderick J, Woo D, Kothari R, Miller R, Khoury J, Brott T, Pancioli A, Jauch E, Gebel J, Shukla R, Alwell K, Tomsick T. 2001. Greater Cincinnati/Northern Kentucky Stroke Study: volume of first-ever ischemic stroke among blacks in a population-based study. Stroke. 32:1285-1290.

Koralek K-A, Olavarria J, Kellackey HP. 1990. Areal and laminar organization of corticocortical projections in the rat somatosensory cortex. The Journal of Comparative Neurology. 299:133-150.

Krubitzer L, Campi KL, Cooke DF. 2011. All rodents are not the same: a modern synthesis of cortical organization. Brain Behav Evol. 78:51-93.

Krubitzer LA, Sesma MA, Kaas JH. 1986. Microelectrode maps, myeloarchitecture, and cortical connections of three somatotopically organized representations of the body surface in the parietal cortex of squirrels. J Comp Neurol. 250:403-430.

Kyuhou S-i, Gemba H. 2002. Projection from the perirhinal cortex to the frontal motor cortex in the rat. Brain Research. 929:101-104.

Kyuhou S-i, Matsuzaki R, Gemba H. 2003. Perirhinal cortex relays auditory information to the frontal motor cortices in the rat. Neuroscience Letters. 353:181-184.

Leandro-Garcia LJ, Leskela S, Landa I, Montero-Conde C, Lopez-Jimenez E, Leton R, Cascon A, Robledo M, Rodriguez-Antona C. 2010. Tumoral and tissue-specific expression of the major human beta-tubulin isotypes. Cytoskeleton (Hoboken). 67:214-223.

Lee T, Kim U. 2012. Descending projections from the dysgranular zone of rat primary somatosensory cortex processing deep somatic input. The Journal of Comparative Neurology. 520:1021-1046.

Lewis GP, Linberg KA, Fisher SK. 1998. Neurite outgrowth from bipolar and horizontal cells after experimental retinal detachment. Invest Ophthalmol Vis Sci. 39:424-434.

Li H, Crair MC. 2011. How do barrels form in somatosensory cortex? Ann N Y Acad Sci. 1225:119-129.

Li S, Overman JJ, Katsman D, Kozlov SV, Donnelly CJ, Twiss JL, Giger RJ, Coppola G, Geschwind DH, Carmichael ST. 2010. An age-related sprouting transcriptome provides molecular control of axonal sprouting after stroke. Nat Neurosci. 13:1496-1504.

Li X-G, Florence SL, Kaas JH. 1990. Areal Distributions of Cortical Neurons Projecting to Different Levels of the Caudal Brain Stem and Spinal Cord in Rats. Somatosensory & Motor Research. 7:315-335.

Liang FY, Moret V, Wiesendanger M, Rouiller EM. 1991. Corticomotoneuronal connections in the rat: evidence from double-labeling of motoneurons and corticospinal axon arborizations. J Comp Neurol. 311:356-366.

Lipton P. 1999. Ischemic cell death in brain neurons. Physiol Rev. 79:1431-1568.

Liu QR, Hattar S, Endo S, MacPhee K, Zhang H, Cleary LJ, Byrne JH, Eskin A. 1997. A developmental gene (Tolloid/BMP-1) is regulated in Aplysia neurons by treatments that induce long-term sensitization. J Neurosci. 17:755-764.

Liu Z, Li Y, Zhang ZG, Cui X, Cui Y, Lu M, Savant-Bhonsale S, Chopp M. 2010. Bone marrow stromal cells enhance inter- and intracortical axonal connections after ischemic stroke in adult rats. J Cereb Blood Flow Metab. 30:1288-1295.

Luft AR, Waller S, Forrester L, Smith GV, Whitall J, Macko RF, Schulz JB, Hanley DF. 2004. Lesion location alters brain activation in chronically impaired stroke survivors. Neuroimage. 21:924-935.

Luke LM, Allred RP, Jones TA. 2004. Unilateral ischemic sensorimotor cortical damage induces contralesional synaptogenesis and enhances skilled reaching with the ipsilateral forelimb in adult male rats. Synapse. 54:187-199.

Macas J, Nern C, Plate KH, Momma S. 2006. Increased generation of neuronal progenitors after ischemic injury in the aged adult human forebrain. J Neurosci. 26:13114-13119.

Maier V, Jolicoeur C, Rayburn H, Takegahara N, Kumanogoh A, Kikutani H, Tessier-Lavigne M, Wurst W, Friedel RH. 2011. Semaphorin 4C and 4G are ligands of Plexin-B2 required in cerebellar development. Mol Cell Neurosci. 46:419-431.

Mandal N, Lewis GP, Fisher SK, Heegaard S, Prause JU, la Cour M, Vorum H, Honore B. 2011. Protein changes in the retina following experimental retinal detachment in rabbits. Mol Vis. 17:2634-2648.

Matelli M, Camarda R, Glickstein M, Rizzolatti G. 1986. Afferent and efferent projections of the inferior area 6 in the macaque monkey. J Comp Neurol. 251:281-298.

McIntire WE, MacCleery G, Murphree LJ, Kerchner KR, Linden J, Garrison JC. 2006. Influence of differential stability of G protein betagamma dimers containing the gamma11 subunit on functional activity at the M1 muscarinic receptor, A1 adenosine receptor, and phospholipase C-beta. Biochemistry. 45:11616-11631.

McIntyre DC, Kelly ME, Staines WA. 1996. Efferent projections of the anterior perirhinal cortex in the rat. The Journal of Comparative Neurology. 369:302-318.

Mehler MF, Mabie PC, Zhang D, Kessler JA. 1997. Bone morphogenetic proteins in the nervous system. Trends Neurosci. 20:309-317.

Miller MW. 1987. The origin of corticospinal projection neurons in rat. Exp Brain Res. 67:339-351.

MMWR. 2001. Prevalence of disabilities and associated health conditions among adults--United States, 1999. MMWR Morb Mortal Wkly Rep. 50:120-125.

Morishita R, Ueda H, Kato K, Asano T. 1998. Identification of two forms of the gamma subunit of G protein, gamma10 and gamma11, in bovine lung and their tissue distribution in the rat. FEBS Lett. 428:85-88.

Mumby DG, Pinel JP. 1994. Rhinal cortex lesions and object recognition in rats. Behav Neurosci. 108:11-18.

Muntner P, Garrett E, Klag MJ, Coresh J. 2002. Trends in stroke prevalence between 1973 and 1991 in the US population 25 to 74 years of age. Stroke. 33:1209-1213.

Neafsey EJ. 1990. The Complete Ratunculus: Output Organization of Layer V of the Cerebral Cortex. In: Kolb B, Tees R, eds. The Cerebral Cortex of the Rat Cambridge, MA: MIT Press p 197-212.

Neafsey EJ, Bold EL, Haas G, Hurley-Gius KM, Quirk G, Sievert CF, Terreberry RR. 1986. The organization of the rat motor cortex: a microstimulation mapping study. Brain Res. 396:77-96.

Neafsey EJ, Sievert C. 1982. A second forelimb motor area exists in rat frontal cortex. Brain Res. 232:151-156.

Nishibe M, Barbay S, Guggenmos D, Nudo RJ. 2010. Reorganization of motor cortex after controlled cortical impact in rats and implications for functional recovery. J Neurotrauma. 27:2221-2232.

Nix P, Hisamoto N, Matsumoto K, Bastiani M. 2011. Axon regeneration requires coordinate activation of p38 and JNK MAPK pathways. Proc Natl Acad Sci U S A. 108:10738-10743.

Nudo RJ. 2006. Mechanisms for recovery of motor function following cortical damage. Curr Opin Neurobiol. 16:638-644.

Nudo RJ, Milliken GW. 1996b. Reorganization of movement representations in primary motor cortex following focal ischemic infarcts in adult squirrel monkeys. . J Neurophysiol. 75:2144-2149.

Nudo RJ, Wise BM, SiFuentes F, Milliken GW. 1996c. Neural substrates for the effects of rehabilitative training on motor recovery after ischemic infarct. Science. 272:1791-1794.

Oyama F, Miyazaki H, Sakamoto N, Becquet C, Machida Y, Kaneko K, Uchikawa C, Suzuki T, Kurosawa M, Ikeda T, Tamaoka A, Sakurai T, Nukina N. 2006. Sodium channel beta4 subunit: down-regulation and possible involvement in neuritic degeneration in Huntington's disease transgenic mice. J Neurochem. 98:518-529.

Paradis S, Harrar DB, Lin Y, Koon AC, Hauser JL, Griffith EC, Zhu L, Brass LF, Chen C, Greenberg ME. 2007. An RNAi-based approach identifies molecules required for glutamatergic and GABAergic synapse development. Neuron. 53:217-232.

Parikh P, Hao Y, Hosseinkhani M, Patil SB, Huntley GW, Tessier-Lavigne M, Zou H. 2011. Regeneration of axons in injured spinal cord by activation of bone morphogenetic protein/Smad1 signaling pathway in adult neurons. Proc Natl Acad Sci U S A. 108:E99-107.

Park S, Hong YW. 2006. Transcriptional regulation of artemin is related to neurite outgrowth and actin polymerization in mature DRG neurons. Neurosci Lett. 404:61-66.

Paxinos G, Watson C. 1986. The Rat Brain in Stereotaxic Coordinates. San Diego, CA: Academic Press Inc.

Perera S, Holt MR, Mankoo BS, Gautel M. 2011. Developmental regulation of MURF ubiquitin ligases and autophagy proteins nbr1, p62/SQSTM1 and LC3 during cardiac myofibril assembly and turnover. Dev Biol. 351:46-61.

Polley DB, Read HL, Storace DA, Merzenich MM. 2007. Multiparametric auditory receptive field organization across five cortical fields in the albino rat. J Neurophysiol. 97:3621-3638.

Ponta H, Sherman L, Herrlich PA. 2003. CD44: from adhesion molecules to signalling regulators. Nat Rev Mol Cell Biol. 4:33-45.

Reep RL, Corwin JV. 2009. Posterior parietal cortex as part of a neural network for directed attention in rats. Neurobiology of Learning and Memory. 91:104-113.

Reep RL, Corwin JV, Hashimoto A, Watson RT. 1987. Efferent connections of the rostral portion of medial agranular cortex in rats. Brain Res Bull. 19:203-221.

Remple MS, Henry EC, Catania KC. 2003. Organization of somatosensory cortex in the laboratory rat (Rattus norvegicus): Evidence for two lateral areas joined at the representation of the teeth. The Journal of Comparative Neurology. 467:105-118.

Rioult-Pedotti M-S, Friedman D, Donoghue JP. 2000. Learning-Induced LTP in Neocortex. Science. 290:533-536.

Rioult-Pedotti MS, Friedman D, Hess G, Donoghue JP. 1998. Strengthening of horizontal cortical connections following skill learning. Nat Neurosci. 1:230-234.

Roger VL, Go AS, Lloyd-Jones DM, Adams RJ, Berry JD, Brown TM, Carnethon MR, Dai S, de Simone G, Ford ES, Fox CS, Fullerton HJ, Gillespie C, Greenlund KJ, Hailpern SM, Heit JA, Ho PM, Howard VJ, Kissela BM, Kittner SJ, Lackland DT, Lichtman JH, Lisabeth LD, Makuc DM, Marcus GM, Marelli A, Matchar DB, McDermott MM, Meigs JB, Moy CS, Mozaffarian D, Mussolino ME, Nichol G, Paynter NP, Rosamond WD, Sorlie PD, Stafford RS, Turan TN, Turner MB, Wong ND, Wylie-Rosett J. 2011. Heart disease and stroke statistics--2011 update: a report from the American Heart Association. Circulation. 123:e18-e209.

Rossi F, Bravin M, Buffo A, Fronte M, Savio T, Strata P. 1997. Intrinsic properties and environmental factors in the regeneration of adult cerebellar axons. Prog Brain Res. 114:283-296.

Rossi F, Gianola S, Corvetti L. 2007. Regulation of intrinsic neuronal properties for axon growth and regeneration. Prog Neurobiol. 81:1-28.

Rouiller EM, Moret V, Liang F. 1993. Comparison of the connectional properties of the two forelimb areas of the rat sensorimotor cortex: support for the presence of a premotor or supplementary motor cortical area. Somatosens Mot Res. 10:269-289.

Sano H, Peck GR, Kettenbach AN, Gerber SA, Lienhard GE. 2011. Insulin-stimulated GLUT4 protein translocation in adipocytes requires the Rab10 guanine nucleotide exchange factor Dennd4C. J Biol Chem. 286:16541-16545.

Saper CB. 1982. Convergence of autonomic and limbic connections in the insular cortex of the rat. J Comp Neurol. 210:163-173.

Sievert CF, Neafsey EJ. 1986. A chronic unit study of the sensory properties of neurons in the forelimb areas of rat sensorimotor cortex. Brain Res. 381:15-23.

Sowpati DT, Thiagarajan D, Sharma S, Sultana H, John R, Surani A, Mishra RK, Khosla S. 2008. An intronic DNA sequence within the mouse Neuronatin gene exhibits biochemical characteristics of an ICR and acts as a transcriptional activator in Drosophila. Mech Dev. 125:963-973.

Sretavan DW, Feng L, Pure E, Reichardt LF. 1994. Embryonic neurons of the developing optic chiasm express L1 and CD44, cell surface molecules with opposing effects on retinal axon growth. Neuron. 12:957-975.

Stowe AM, Plautz EJ, Eisner-Janowicz I, Frost SB, Barbay S, Zoubina EV, Dancause N, Taylor MD, Nudo RJ. 2007. VEGF protein associates to neurons in remote regions following cortical infarct. J Cereb Blood Flow Metab. 27:76-85.

Stowe AM, Plautz EJ, Nguyen P, Frost SB, Eisner-Janowicz I, Barbay S, Dancause N, Sensarma A, Taylor MD, Zoubina EV, Nudo RJ. 2008. Neuronal HIF-1 alpha protein and VEGFR-2 immunoreactivity in functionally related motor areas following a focal M1 infarct. J Cereb Blood Flow Metab. 28:612-620.

Stroemer RP, Kent TA, Hulsebosch CE. 1993. Acute increase in expression of growth associated protein GAP-43 following cortical ischemia in rat. Neurosci Lett. 162:51-54.

Tran TS, Kolodkin AL, Bharadwaj R. 2007. Semaphorin regulation of cellular morphology. Annu Rev Cell Dev Biol. 23:263-292.

Tsai NP, Tsui YC, Pintar JE, Loh HH, Wei LN. 2010. Kappa opioid receptor contributes to EGF-stimulated neurite extension in development. Proc Natl Acad Sci U S A. 107:3216-3221.

Urban ET, 3rd, Bury SD, Barbay HS, Guggenmos DJ, Dong Y, Nudo RJ. 2012. Gene expression changes of interconnected spared cortical neurons 7 days after ischemic infarct of the primary motor cortex in the rat. Mol Cell Biochem. 369:267-286.

Veal E, Groisman R, Eisenstein M, Gill G. 2000. The secreted glycoprotein CREG enhances differentiation of NTERA-2 human embryonal carcinoma cells. Oncogene. 19:2120-2128.

Vo BQ, Bloom AJ, Culican SM. 2011. Phr1 is required for proper retinocollicular targeting of nasal-dorsal retinal ganglion cells. Vis Neurosci. 28:175-181.

Weng L, Hubner R, Claessens A, Smits P, Wauters J, Tylzanowski P, Van Marck E, Merregaert J. 2003. Isolation and characterization of chondrolectin (Chodl), a novel C-type lectin predominantly expressed in muscle cells. Gene. 308:21-29.

Weng L, Van Bockstaele DR, Wauters J, Van Marck E, Plum J, Berneman ZN, Merregaert J. 2003. A novel alternative spliced chondrolectin isoform lacking the transmembrane domain is expressed during T cell maturation. J Biol Chem. 278:19164-19170.

Weston RM, Jones NM, Jarrott B, Callaway JK. 2007. Inflammatory cell infiltration after endothelin-1-induced cerebral ischemia: histochemical and myeloperoxidase correlation with temporal changes in brain injury. J Cereb Blood Flow Metab. 27:100-114.

Whishaw IQ. 1992. Lateralization and reaching skill related: results and implications from a large sample of Long-Evans rats. Behav Brain Res. 52:45-48.

Whishaw IQ, Pellis SM, Gorny BP. 1992. Medial frontal cortex lesions impair the aiming component of rat reaching. Behavioural Brain Research. 50:93-104.

Wiesendanger M. 2006. Constantin von Monakow (1853–1930): A pioneer in interdisciplinary brain research and a humanist. Comptes Rendus Biologies. 329:406-418.

Williams-Hogarth LC, Puche AC, Torrey C, Cai X, Song I, Kolodkin AL, Shipley MT, Ronnett GV. 2000. Expression of semaphorins in developing and regenerating olfactory epithelium. J Comp Neurol. 423:565-578.

Withers GS, Higgins D, Charette M, Banker G. 2000. Bone morphogenetic protein-7 enhances dendritic growth and receptivity to innervation in cultured hippocampal neurons. Eur J Neurosci. 12:106-116.

Xerri C, Coq JO, Merzenich MM, Jenkins WM. 1996. Experience-induced plasticity of cutaneous maps in the primary somatosensory cortex of adult monkeys and rats. J Physiol Paris. 90:277-287.

Xerri C, Merzenich MM, Peterson BE, Jenkins W. 1998. Plasticity of primary somatosensory cortex paralleling sensorimotor skill recovery from stroke in adult monkeys. J Neurophysiol. 79:2119-2148.

Xie N, Yang Q, Chappell TD, Li CX, Waters RS. 2010. Prenatal alcohol exposure reduces the size of the forelimb representation in motor cortex in rat: an intracortical microstimulation (ICMS) mapping study. Alcohol. 44:185-194.

Yang G, Han Y, Tian X, Tao J, Sun M, Kang J, Yan C. 2011. Pattern of expression of the CREG gene and CREG protein in the mouse embryo. Mol Biol Rep. 38:2133-2140.

Z'Graggen WJ, Metz GAS, Kartje GL, Thallmair M, Schwab ME. 1998. Functional Recovery and Enhanced Corticofugal Plasticity after Unilateral Pyramidal Tract Lesion and Blockade of Myelin-Associated Neurite Growth Inhibitors in Adult Rats. The Journal of Neuroscience. 18:4744-4757.

Zai L, Ferrari C, Subbaiah S, Havton LA, Coppola G, Strittmatter S, Irwin N, Geschwind D, Benowitz LI. 2009. Inosine alters gene expression and axonal projections in neurons contralateral to a cortical infarct and improves skilled use of the impaired limb. J Neurosci. 29:8187-8197.

Zhang HY, Timpl R, Sasaki T, Chu ML, Ekblom P. 1996. Fibulin-1 and fibulin-2 expression during organogenesis in the developing mouse embryo. Dev Dyn. 205:348-364.

Zhang RL, Chopp M, Chen H, Garcia JH. 1994. Temporal profile of ischemic tissue damage, neutrophil response, and vascular plugging following permanent and transient (2H) middle cerebral artery occlusion in the rat. J Neurol Sci. 125:3-10.

Zhang Z, Chen TY, Kirsch JR, Toung TJ, Traystman RJ, Koehler RC, Hurn PD, Bhardwaj A. 2003. Kappa-opioid receptor selectivity for ischemic neuroprotection with BRL 52537 in rats. Anesth Analg. 97:1776-1783.

Zilles K. 1990. Anatomy of the Neocortex: Cytoarchitecture and Myeloarchitecture. In: Kolb B, Tees R, eds. The Cerebral Cortex of the Rat Cambridge, MA: MIT Press p 77-112.

Zilles KJ. 1985. The cortex of the rat: a stereotaxic atlas. New York: Springer-Verlag.